DISSERTATION

ROBUST CONTROL OF IRRIGATION CANALS

Submitted by

Omer Faruk Durdu

Department of Civil Engineering

In partial fulfillment of the requirements

For the Degree of Doctor of Philosophy

Colorado State University

Fort Collins, Colorado

Fall 2003

COLORADO STATE UNIVERSITY

May 22, 2003

WE HEREBY RECOMMEND THAT THE DISSERTATION PREPARED UNDER OUR SUPERVISION BY OMER FARUK DURDU ENTITLED ROBUST CONTROL OF IRRIGATION CANALS BE ACCEPTED AS FULLFILING IN PART REQUIREMENTS FOR THE DEGREE OF DOCTOR OF PHILOSOPHY.

Committee on Graduate Work

Adviser

Department Head

ABSTRACT OF DISSERTATION

ROBUST CONTROL OF IRRIGATION CANALS

The design of irrigation water delivery systems involves decisions about siting, dimensions, and characteristics of facilities for conveyance, regulation, monitoring, and diversion of flow. The characteristics of all there individual system components work together to determine the performance of the entire irrigation water delivery system. With the ever increasing demand for water due to population growth and competition from non-agricultural demands, there is an urgent need for efficient management of irrigation resources. Improvements in the operation and maintenance of an irrigation delivery system can translate into better overall management in an irrigation project, and automation of irrigation canals can be an effective way to achieve such improvements. Automation of irrigation distribution canals improves water-delivery service to farmers, reduce operating cost and improve distribution efficiency. The conveyance and distribution performance of irrigation canals can be improved to better meet the requirements of farmers by providing modern methods of canal control. Therefore, to avoid overflows and always be able to satisfy the demand, the irrigation canal system must be controlled and robust to maintain desired flow rates and water surface elevations. The goal of the canal controls is to match the actual flow in the canal to the required flow for that day while maintaining water surface elevations within allowable limits. Canal control systems must provide timely deliveries to customers with little or no waste use of water and power under predicted and unknown demands (perturbations). Because of that the design of highly accurate control systems in the presence of significant system uncertainty requires the designer to seek a robust control system. A robust control system

exhibits low sensitivities to unknown demands (disturbances) and is stable over a wide range of disturbance variations.

This research aims at strengthening the distribution link through the development of a robust control algorithm to provide for automatic control of a MIMO (multi-input, multi-output) water distribution system under unknown external perturbations. In the derivation, the canal between two gates is divided into N nodes, and the finite-difference forms of the continuity and the momentum equations are written for each node. The Taylor series is applied to linearize the equations around the initial steady state or equilibrium conditions. The Linear Quadratic Regulator (LQR) is designed to generate control input (optimal gate opening) $u(k)$. With a known control input, measured depth and density matrices, a Kalman filter is designed to provide an optimal estimate of the state vector, $x(k)$. The Separation Theorem is applied to combine LQR and Kalman filter as a Linear Quadratic Gaussian (LQG) controller. With combination of LQR and Kalman filter, there is some loss of robustness. To improve the robustness of the control algorithm, Loop Transfer Recovery (LTR) loop shaping technique is used. Loop shaping technique is an adjustment of the singular values of return ratio matrices to achieve desired closed-loop robustness and stability. To analyze the robustness of the controller, two robustness analysis methods are conducted: Singular Values and Bode Diagrams.

Omer Faruk Durdu
Department of Civil Engineering
Colorado State University
Fort Collins CO, 80521
Fall 2003

To my wife, Elanur, and my son, Emre.

ACKNOWLEDGEMENTS

I would like to thank my advisor Dr. Junna Mohan Reddy for his guidance and helpful suggestions throughout this research. He always had plenty of time for my questions. I also thank Dr. Albert Molinas, Dr. Darrell G. Fontane and Dr. Freeman M. Smith for accepting to be my graduate committee members without compromising the quality for their review. Appreciation is also extended to everybody in Civil Engineering Department for making the work atmosphere as pleasant as an ideal working environment could possibly be.

TABLE OF CONTENTS

LIST OF TABLES

LIST OF FIGURES

LIST OF SYMBOLS

Symbol	Definition	Dimensions
θ	Weighting coefficient	-
$\delta\hat{x}$	Estimated values of the state variables	-
A_b	Horizontal water surface area of the basin with	m
B	Width of the water surface	m
b_l	Width of outlet structure	m
C_d	Outlet discharge coefficient	-
D	Hydraulic depth	m
E_s	Sill elevation of head regulator	m
F(z)	z-transform of $f(kT)$	-
$F^*(s)$	Laplace transform of the ideally sampled signal	-
F_g	Gravitational force	
F_p	Pressure force	
F_s	Shear resistance	
g	Acceleration due to gravity	m/sec^2
G(z)	System transfer matrix	-
H	Output matrix	-
H(z)	Feedback controller matrix	-
H(z)G(z)	System return ratio	-
J	Cost function used in optimal control	-
I	Identity matrix of appropriate dimension	-
k	Numbers of sampling interval	-

$K(k)$	Controller gain matrix	-
K_∞	Number of sampling intervals considered to derive	-
L	Observer gain matrix	-
$M(\omega)$	Magnitude ratio	-
N_m	Number of measurements for full state feedback	-
Q	Discharge in the channel	m^3/sec
q	Discharge per unit length	m^2/sec
q_i	Lateral in or out flow	m^2/sec
S	Sensitivity function	-
S_∞	Solution of the discrete algebraic Riccati equation	-
S_f	Slope of energy line	-
S_o	Canal bottom slope	-
t	Time	sec
T	Top width of the canal	m
V	Mean velocity	m/sec
w_l	Height of gate opening of outlet structure	m
Δx	Length of subsurface	m
x	Length of the canal reach	m
y	Depth of water in the canal	m
$Y_d(z)$	Desired output of control system	-
z	Water level as referred to a horizontal datum	m
γ	Unit weight of water	lb/ft^3
Δ	Smallest structured perturbation	-

δq	Vector of system disturbances	m^3/sec
δu	Vector of system inputs (gate openings)	m
δy	Vector of system outputs	m
$\eta(k)$	Measurement noise inputs	-
ρ	Spectral density	-
σ_{min}	Smallest singular value	-
Φ	System transition matrix	-
Ψ	Disturbance distribution matrix	-
ω	Disturbance frequency	-
Γ	Control distribution matrix	-

CHAPTER 1

INTRODUCTION AND STATEMENT OF PROBLEM

1.1 Introduction

Water management in irrigated agriculture is now receiving more scrutiny than ever before. Irrigated agriculture generally uses large volumes of water compared to municipalities and industry, and competition for good quality water is at an all time high in many regions around the world. Thus it is recognized that improved water management practices in agriculture can lead to substantial benefits in terms of water availability for expanded agricultural activity and for other uses, and can directly address many environmental concerns. Irrigation water delivery systems are designed and managed to receive water from a source and distribute it among farms where it is used to meet agricultural demands. The design of these irrigation water delivery systems involves decisions about siting, dimensions, and characteristics of facilities for conveyance, regulation, monitoring, and diversion of flow. The characteristics of all these individual system components work together to determine the performance of an entire irrigation water delivery system. With the ever increasing demand for water, due to population growth and the competition from nonagricultural demands, there is an urgent need for efficient management of irrigation resources. Timely delivery of the required quantity of water is necessary for improved agricultural production. To utilize effectively the modern irrigation technology and other resources at the field level, flexibility in terms of water

delivery scheduling is of utmost importance. To perform their functions efficiently, irrigation and drainage canals must be managed appropriately; that is, the control structures need to be operated in such a way that canals execute their functions adequately. In most cases, this requirement can be translated in to water level control problem in irrigation canals. The main function of an irrigation canal is to deliver water in an accurate, timely and flexible manner. The water delivery is said to be accurate if the actual supply matches the intended supply, and it is said to be flexible if the delivery meets the changing water requirements of the users.

Water management improvement in irrigation canal systems is widely recognized as an important step in attaining better management at the farm level. Improvements in operation and maintenance of an irrigation delivery system can translate into better overall water management in an irrigation project, and automation of irrigation canal gate structures can be an effective way to achieve such improvements. Control of canals for irrigation water delivery is a complex task. This stems, in part, from hydraulic conditions that are hard to define. Control of irrigation structures is becoming increasingly popular because of the increasing demand for water, improved operational efficiency, improved water control, constant surveillance and reducing the costs of operation and maintenance. Automation of irrigation distribution canals improves water-delivery service to farmers, reduces operating costs and improves distribution efficiency. Introduction of automation in watering leads to their quicker recoupment, reduces the cost of agricultural produce, diminishes water consumption and labor.

Distribution of large volumes of water within irrigation projects in arid regions typically involves a network of canals. Control of distribution processes is executed by

means of inline canal gates and associated operational schedules whereby these canal gates are manipulated so as to meet control objectives. Such control is deemed acceptable to the extent that water is distributed among all water users in a timely, equitable, and efficient manner. The most essential attributes of the distribution process can be characterized in terms of the given water delivery frequency, rate and duration.

Conveyance and distribution performance of irrigation canals can be improved to better meet the requirements of farmers by providing modern methods of canal control. The demand for irrigation water varies with time among other factors, due to the variable weather conditions and crop growth characteristics. Therefore, to avoid overflows and always be able to satisfy the demand, the channel system must be controlled to maintain desired flow rates and water surface elevations. The use of flexible irrigation deliveries is necessary for efficient on-farm irrigation water management. Thus, the conversion from rigid to flexible delivery schedules will require better canal control to provide good uniform deliveries. The strategy of water delivery, the desired schedules, required communications (both digital and human), and the location of a variety of decision making must first be decided upon before the hardware is examined. The control strategy must be compatible with the flexibility of the ultimate water supply, and the social, political, geographical, and economic conditions under which it will be used. Furthermore, the control strategy used in automating canals for irrigation water delivery have important effects upon social development and the economic well-being of the irrigation project.

When the needs of farmers are more closely matched by canal deliveries, on-farm water management potentials are greater. Canal flows must match turnout demands and

water levels must remain high enough to supply all turnouts plus steady enough to maintain a constant delivery through gravity turnouts into open laterals. Additionally, canals must be operated to prevent rapid water level drawdown that can damage canal lining. The principal objectives of irrigation canal networks are to provide equitable and timely apportionment of water among irrigators and to do so in proper quantities (flow rate and duration). To accomplish these objectives, canals should be designed and operated to minimize flow rate and depth fluctuations in order to protect system structures, minimize required management activities, and reduce seepage and losses. The prerequisites for such operational efficiency include appropriate and properly maintained water conveyance and control structures, adequate water measurement and communication systems, and proper coordination of all operation and maintenance activities. The goal of canal operations is to match the actual flow in canals to the required flow for that day while maintaining water surface elevations within allowable limits. Many canal control systems must provide timely deliveries to customers with little or no wastage of water and power under predicted and unknown demands (perturbations). Confronting problems associated with the operation of canal networks is a necessary step for improving water management in an irrigation system as a whole.

For some years, writers like Merriam and Keller (1978) have stressed the importance of flexibility in flow rate, delivery frequency, and supply duration on efficiency and effectiveness of water use at farm level. In recent years, growing awareness of the importance of delivery reliability and distribution equity has focused attention on improving the operation of canal networks. When the water reserves are limited there is competition between the claims made upon them by the main consumers,

municipal authorities, industry and agriculture. Clemmens and Replogle (1988) have indicated that many irrigation projects which are facing increasing competition for water by outside sources will be forced to improve their control of water, if not for actual savings in water, then simply for accountability. Farmers require irrigation water supplies that are flexible in frequency, rate and duration to take full advantage of cropping and management options. For farmers receiving water from irrigation districts, this requirement translates to a need for a delivery scheduling policy that can accommodate farmers demand. In a scheduled delivery, once the schedule is established, however, the water-user association has the more difficult task of translating intentions into operational flexibility and precise delivery. Feedback or closed-loop control strategies can be used to regulate irrigation canal to minimize the magnitude and duration of the mismatch between the supply and the demand of water. Unknown disturbances in a feedback controlled irrigation canal can have a significant impact on the performance of the system. Canal control methods must handle the uncertainties in the canals. Because of that, the design of highly accurate control systems in the presence of significant system uncertainty requires the designer to seek a robust control system. A robust control system exhibits low sensitivities to disturbances (perturbations), such as unknown demands, and is stable over a wide range of disturbances variations.

This research is aimed at strengthening the distribution link through the development of a robust control algorithm to provide for automatic control of water distribution systems under unknown external disturbances. More specifically, this research addresses robust control of open-channel water distribution systems, where the accurate delivery of water to the customers depends on maintaining stable water surface

elevations within a canal. If a stable water surface is not maintained, either the customer does not receive the amount of water ordered or too much water is delivered resulting in either dissatisfied customers or a waste of water. In robust control, the aim is to control a system in such a way that model uncertainties and errors are accounted for. Robustness of a canal control system says nothing more than the stability of the system. Robustness of control systems to disturbances and uncertainties has always been the central issue in feedback control. Feedback would not be needed for most control systems if there were no disturbances and uncertainties. A control system is an elementary system in charge of operating canal regulating structures, based on information from the canal system. When designing a canal control system, we should be assured that a canal control design will function acceptably before committing to implementation. Such assurance can be obtained by analyzing canal control system stability and robustness with respect to a range of expected disturbances. This type of analysis is termed as robustness analysis.

1.2. Statement of Problem

There have been many successful canal automation projects and there have been many cases where canal control systems never lived up to expectations because of technical and non-technical reasons. Many problems have stemmed from a poor match between the engineered system and the personnel who operate it. Others can be traced to the lack of continuity: from design to installation, to operation and maintenance. More often than not, social issues have a major impact on the success of canal automation projects. The application of canal control technology is an increasingly valuable method to promote agricultural water conservation. On many water projects, canal automation is the single

option with the greatest potential for improvement in water system operations. Canal control technology has potential to yield agricultural benefits and environmental benefits at the same time: increased delivery flexibility and dependability will benefit farmers and canal operators while better system management reduces water waste, maintenance costs, and environmental impacts.

Significant research efforts in irrigation canal automation have been proposed in the literature. However, very few automatic control systems have actually been used (Rogers and Goussard 1998). During the last twenty years, the concept of optimal control theory have been applied for deriving feedback control algorithms for real-time control of irrigation canals. In particular, since it handles multivariable systems easily, optimal control was considered by Corriga et al. (1982a, b), Dora and Varga (1982), Burt (1983), Papageorgiou and Messmer (1985), Zimbelman (1987), Balogun et al. (1988), Reddy (1990), Chevereau (1991), Reddy et al. (1992), Savadogo (1992), Garcia (et al. 1992), Rodellar et al.(1993), Liu et al. (1995). However, most of these papers dealt with a single canal pool without robustness analysis. Extension of the optimal control concepts to multi-pool systems is more involved because of the interactions between the pools. Corriga et al. (1982), Balogun et al. (1988), Garcia et al. (1992), and Reddy (1995,1996) demonstrated application of optimal control concepts for derivation of global control algorithms for multi-pool canals. Reddy et al. (1992) considered unknown external perturbations and used a state observer.

A number of more modern downstream control algorithms have been proposed, but none have been adequately tested in the field. The canal control systems designed in the past did not consider the effect of unknown external disturbances on the robustness of

feedback control systems. The design of highly accurate canal control systems in the presence of significant uncertainty requires the designer to seek a robust system. Therefore, a robust canal control algorithm will be developed using the MATLAB computing language (The Mathworks Inc., 1997) to take care of the unknown perturbations (disturbances) acting on the canal. A robust control system provides stable, consistent performance as specified by the designer in spite of wide variation of system parameters and disturbances. It also provides a highly robust response to command inputs and a steady-state tracking error equal to zero. Designing highly accurate systems in the presence of significant system uncertainty is a classical feedback design problem. The theoretical bases for the solution of this problem date back to the works of Black and Bode in the early 1930s, when this problem was referred to as the sensitivities design problem. However, a significant amount of literature has been published since then regarding the design of systems subject to large system uncertainty. The designer seeks to obtain a system that performs adequately over a large range of uncertain parameters. A canal control system is said to be robust when it is durable, hardy, and resilient. A control system is robust when: (1) it has low sensitivities; (2) it is stable over the range of disturbance variations; and (3) the performance continues to meet the specifications in the presence of a set of changes in the disturbances. Robustness is the sensitivity to effects that are not considered in the analysis and design phase- for example, disturbances, measurements noise, and un-modeled dynamics. The system should be able to withstand these neglected effects when performing the tasks for which it was designed.

1.3. Objectives

The main purpose of this research is to develop a robust control algorithm that provides for the automatic control of an open-channel water distribution system under unknown perturbations acting in the canal. In order to guarantee that the water users' requirements are satisfied, especially those further downstream, as well as to avoid wasting large amounts of unused water at the canal end, it became indispensable to coordinate, to the greatest possible extent, the water amounts and relative times of releases at the upstream of the canal, with those drawn off by the users and the relative times of withdrawal, taking into account the position of the outlets along the canal. Implementation of this algorithm will facilitate the maintenance of stable water levels and consistent performance in spite of wide variation of unknown disturbances. The purpose of control algorithms is to increase water use efficiency of the system being controlled by minimizing over deliveries and to minimize the cost of resolving customer complaints of shortages by maintaining stable delivery rates. Specific objectives are as follows:

1. To provide stability of final storage in canal pools at the end of the forecast period, assuring of recovery of canal pool storage in the next operational cycle.
2. To maintain ideal target storage levels in each control pool under external perturbations;
3. To improve the robustness properties of the canal control system under unknown demands (perturbations).

CHAPTER 2

LITERATURE REVIEW

2.1. Canal Control and Automation Systems

Automation is a common engineering term. It is defined as: "A procedure or method used to regulate a system by mechanical or electronic equipment that takes place of human observation, effort, and decision; the condition of being automatically controlled. Thus canal automation is defined as: "The implementation of a control system that upgrades the conventional method of canal system operation. The water distribution system is one of the important elements of the overall water project. Basically it is constructed to convey water from one place to another. The basic types of water distribution systems can be classified as: a) Closed conduit, where the flow water is confined on all boundaries, i.e. pipe systems. b) Open channel, where the top flow boundary is free surface, i.e. canal systems.

Pipe systems have the capability to respond almost immediately to changes in downstream demand. A flow change in a pipe system occurs in the form of a pressure wave that travels through the pipe at high speed. Cost of constructing a pipe system is greater than for a canal system. The higher cost is prohibitive for most distribution systems that deliver large flow rates. Therefore, canal systems often constructed as the major conveyance features of water projects. Flow in a canal system is more difficult to regulate than in a pipe system. Flow changes in canals occur in the form of translatory wave fronts. The translatory wave travels at a relatively slow speed, about 200 times

slower than the pressure wave speed range is 10 to 20 feet per second (3 to 6 m/s); therefore, a canal system responds slower to changes in downstream demand than a pipe system does.

2.1.1. Canal System Control Methods

The term canal control describes those steps necessary to ensure the required pool water level and flow along the canal. These conditions are controlled by adjusting the volume of water pumped into the canal, adjusting the positions of check gates, and by regulating flow through the delivery turnouts. Canal conditions depend upon the adjustment of variables that effect control of the canal system. Some variables are easily adjusted while others are more complicated or cannot be adjusted. The variables easily adjusted are the gate positions, number of pumps supplying or diverting water, flow regulation of the pumps, and the diversion of water into and out of the canal system. Other variables such as weed growth, debris, siphons and the geometry of the canal cannot be readily controlled. A canal system can be controlled by the following methods:

1) Local manual: Control is onsite by a human operator (ditchrider). Local manual control is the conventional method of controlling a canal system. Labor saving devices and machines, such as a gate hoist motor, may be used onsite to assist the ditchrider when adjusting canal check gate opening. An experienced ditchrider can anticipate water arrival time within acceptable limits. This type of operation is greatly personalized (subjective). The ditchrider (in the field) must report canal data such as water levels and gate positions to the watermaster. The watermaster needs to know these data to implement the schedule upon the complete system. Successful operation depends in large

measure on the team's skill. 2) Local automatic: Control is onsite by control equipment without human intervention. Local automatic control allows unattended canal operation achieved through an arrangement of mechanical, electrical, and electronic components located onsite. The equipment monitors water depths and gate positions. The sensed information is interpreted by specially developed equations referred to as control algorithms. The algorithms designed to calculate adjustments required to position the canal check gates and to satisfy the actual operating needs. Required onsite human input is reduced to periodically monitoring the canal operation. Automatic control equipment does not require onsite manual adjustments by the ditchrider to achieve proper canal operation. However, an alarm system is required to notify central headquarters of abnormal conditions such as control equipment failure, high or low water levels, local power outages, and communication channel failures. Therefore a communication channel is necessary between each check gate controller and the headquarters to provide alarm information. The watermaster monitors the alarm information and promptly initiates corrective action based upon the abnormal condition. 3) Supervisory: Supervisory control is the operation of the canal system by the watermaster from a central location referred to as the headquarters or master station. The master station equipment performs the function of collecting data from remote sites in the canal system, analyzing the data, and presenting the data in a suitable format for further action by the watermaster. Each remote site, such as the canal check gate structure, requires a remote terminal unit (RTU). The RTU monitors data such as water levels, gate positions, and equipment status, and then transmits these data to the master station. The RTU also controls the remote site; it adjusts the gate position based upon the water master's instructions received from the

master station. Therefore, this type of operation requires a two-way communication system between each RTU at the remote sites and the master station. 4) Combined: Local manual, local automatic, and supervisory control systems are not mutually exclusive. In many water projects, the operation involves using a combination of two or perhaps all three types of control depend on the circumstances of use. For example, a gravity type turnout may require a local automatic controller to automatically maintain a constant delivery rate if the main canal water level changes frequently. The ditchrider is not always available to visit the site frequently enough to make the necessary gate opening adjustments to compensate for the water level variation and maintain a constant delivery rate. Each canal system control method has its own characteristics and advantages. The selection of the method that will upgrade a canal operation does not require knowledge of the associated control equipment.

2.1.2. Canal Automation

Generally, canal systems are constructed to convey water from a source to downstream diversion points in the most efficient and economical manner possible using the available resources. Usually, automation of canal systems upgrades and enhances to overall canal operations for increased crop yields to the farmers.

The primary purpose of canal system automation is to upgrade a canal operation. Upgrade a canal operation means to provide a better match between the canal system delivery capabilities and the water users' demands. Canal operation enhanced by installing a practical and modern control system to improve the water transfer efficiency. Many limitations inherent in the conventional method of operation can be overcome.

Conventional method means canal system control onsite by operations personnel (ditchrider and watermaster). Local automatic control, supervisory control, or combination control can provide the following advantages compared to the conventional method: a) Rapid transfer of water with frequent changes, b) achieve operational flexibility when simultaneous information in the entire system is known, c) adjustments in canal flow can be made to accommodate variances in canalside turnout diversions on a daily or an hourly basis, d) immediate response to sudden and unannounced variances in canalside diversion or to storm runoff flooding into the canal.

Advantages inherent in canal automation hold interest for canal operators. A control system can be designed to ensure coupling of the canalside turnout diversions and the canal inlet supply. An automated canal system can respond to abrupt and unscheduled changes in turnout diversion and immediately initiate corrective action. The action reduces the necessity for excess flow and minimizes the occurrences of shortages in the lower canal pools. A more optimum transfer of water can attained with an automated canal. The objective of canal system automation is to realize the benefits associated with implementing a practical control system. Some benefits of canal automation are: 1) Better service to the water user: Water users are the main beneficiaries. Water users receive a scheduled quantity of water at the time specified without the limitations imposed by the conventional method of operation. Water users should realize economic benefits and better service. By providing the water user with improved service the watermaster would certainly receive fewer complaints throughout the growing season. 2) Efficient transfer of water: Efficient transfer of water could result in an economic benefit if the canal system has a history of wasting water. Projects having to schedule power of relift pumping could

realize a substantial economic savings by not pumping surplus flow. 3) Reduction in operation costs: Significant savings could result from lower maintenance costs associated with canal lining and embankment failures. Efficient water transfer requires maintaining near steady-state water levels in the canal. The frequency of excessive pressure changes on the canal lining and recurrence of water levels above the canal freeboard can be greatly reduced. 4) Diversion minimization in wasteways: Minimizes water diversions into waste ways.

2.1.3. Canal Operation and Control Concept

The operation concept, established by the canal system operating criteria, determines the flow schedule. The control concept determines how the canal control structures are adjusted to satisfy the operation concept. Both operation and control concepts depend on upstream or downstream condition.

Downstream water demand or scheduled delivery determines the canal system flow schedule. Downstream operation concept applies to canal systems that are primarily demand-oriented and usually is associated with delivery systems as shown in Figure 2.1. Upstream water supply source or inflow determines the canal system flow schedule. Upstream operation concept applies to canal systems that are primarily supply-oriented and usually the concept is associated with collector systems. If we have a downstream control, canal control structure adjustments are based upon information from downstream. The required information could be measured by a sensor located downstream or be based upon the downstream water schedule established by the watermaster. Downstream control transfers the downstream canalside turnout demands to

the upstream water supply source and is compatible with the downstream operation concept. If we have an upstream control, control structure adjustments are based upon information from upstream as shown in Figure 2.2. The required information could be measured by a sensor located upstream or be based upon the upstream water schedule established by the watermaster. Upstream control transfers the upstream water supply downstream to points of diversion or to the end of the canal and is compatible with the upstream operation concepts.

The operation and control concepts must be compatible. It is impossible to operate supply-oriented canal system having an upstream operation concept using the downstream control concept. Additionally, it is impossible to apply both the downstream and upstream concepts to a canal system simultaneously. For most demand-oriented canal systems, using the downstream operation concept would be inefficient to apply the upstream control.

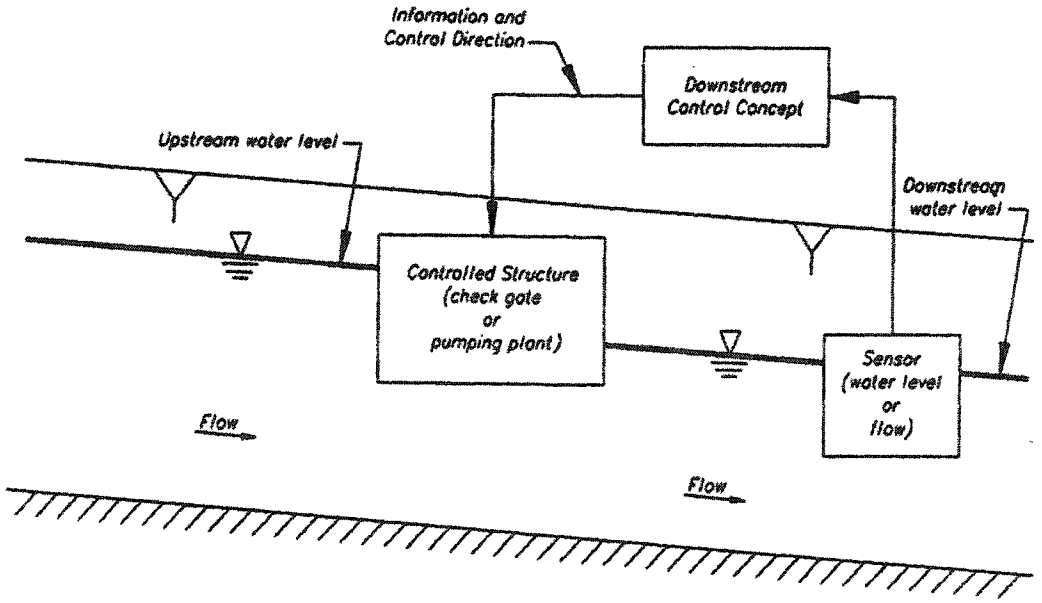

Figure 2.1. Downstream Control Concept.

2.2. Canal Pool Operations

Several methods are available which can be used to convey water downstream through a series of canal pools. The method of pool operation is based upon the location of the canal pool water surface pivot point. The pivot point is the location within a canal pool at which the depth remains constant while the water surface slope varies. The basic method of pool operation should be identified for a canal system before control alternatives are evaluated. The location of the pivot point is particularly important when selecting a control method, i.e., local manual, local automatic, or supervisory control.

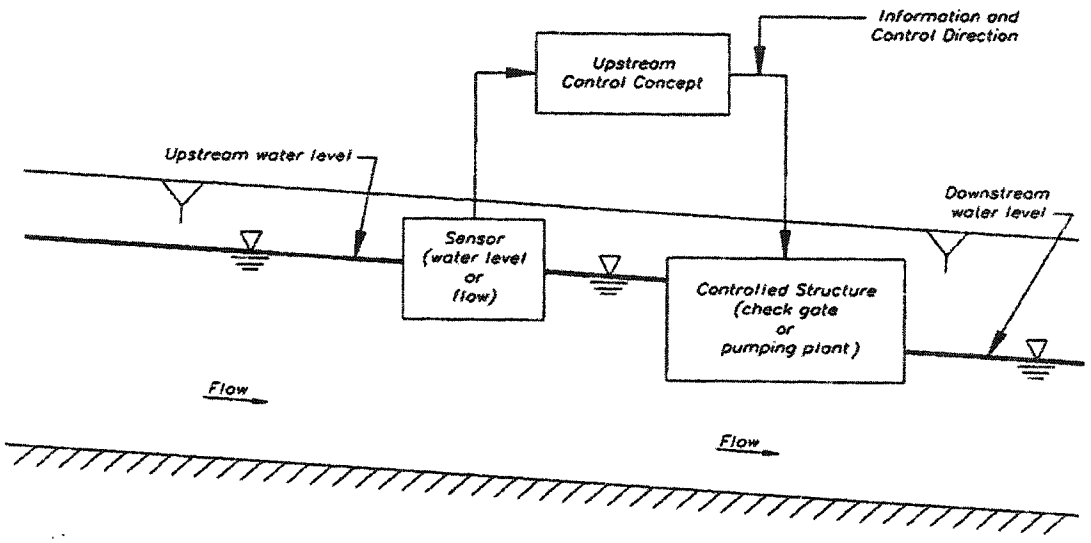

Figure 2.2. Upstream Control Concepts.

2.2.1 Constant Downstream Depth

Constant downstream depth method of operation- wherein the water depth at the downstream end of each canal pool remains relatively constant-is used in most canal systems. This method is associated with conventional operations and with local manual

control. With a constant downstream depth, major turnouts usually are located near the downstream end of the canal pools. This allows turnouts to be designed for a maximum and relatively constant depth in the canal, and also prevents problems in water delivery to users caused by low or fluctuating water depths. When a constant depth is maintained at the downstream end of canal pools, the water surface profile will essentially pivot about this point as the canal flow changes (Figure 2.3). Because of these storage considerations, the constant downstream depth method of operation is particularly effective when combined with the upstream operation concept having a supply oriented operation. A natural tendency exists for a flow change that originates at the upstream end of a pool to create the change in storage that is needed to keep the downstream pool depth constant.

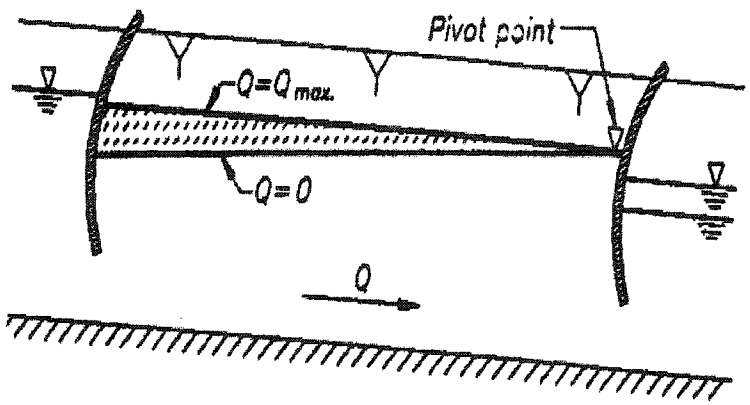

Figure 2.3. Constant Downstream Depth.

2.2.2 Constant Upstream Depth

With this method of operation, a constant upstream depth is maintained by pivoting the water surface at the upstream end of the canal pool as shown on Figure 2.4. The constant upstream depth of method is sometimes called level bank operation, because canal banks

must be horizontal to accommodate the zero-flow profile. The constant upstream depth method of operation is most effective when combined with the downstream operation concept (demand-oriented operation). Flow changes originating at the downstream end of the pool cause canal water depths to change in the direction needed to achieve new steady-state profiles. Level bank operation is inappropriate for supply-oriented canals. The operation would be inefficient and the additional expense for level bank construction would be unjustified.

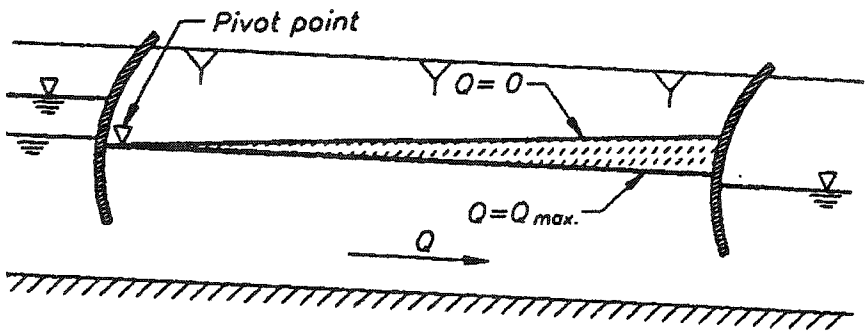

Figure 2.4. Constant Upstream Depth.

2.2.3. Constant Volume

This method of operation is based upon maintaining a relatively constant water volume in each canal pool at all times. The water surface will pivot about a point near midpool as the flow changes from one steady-state to another. The constant volume method of operation is sometimes called simultaneous operation, because the simultaneous gate opening technique often is used to keep the pool volume constant. Storage wedges will exist on either side of the midpool pivot point as shown on Figure 2.5. For any given flow change, volume change in each of these wedges is equal and opposite. When flow

decreases, volume of water in the upstream wege decreases and volume increases in the downstream wedge. When flow increases, the opposite occurs.

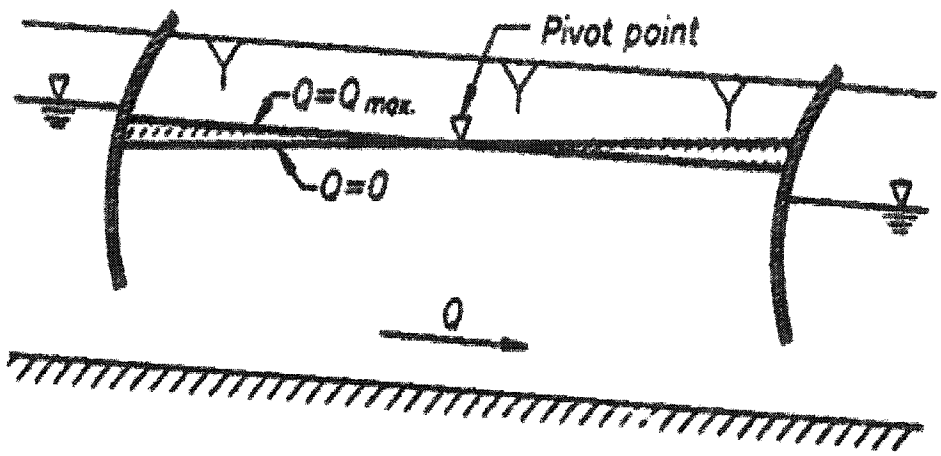

Figure 2.5. Constant Volume.

2.2.4. Controlled Volume

A canal system can be operated by managing the water volume contained in one or more canal pools. Volume can be changed to satisfy operational criteria by allowing the pivot point to move within each pool. Because operation is based upon volume, either flow or depth may be used as the measured parameter. The controlled volume method of operation offers the most flexibility of any method of operation. Canal operation can adapt more easily to normal, abnormal, and emergency conditions. Sudden large flow changes that otherwise might require the use of off-channel storage or waste ways often can be controlled successfully within the canal using the controlled volume method. The controlled volume method of operation is particularly suitable to operate canal systems that include off peak pumping considerations. An example of controlled volume method of operation is illustrated on Figure 2.6.

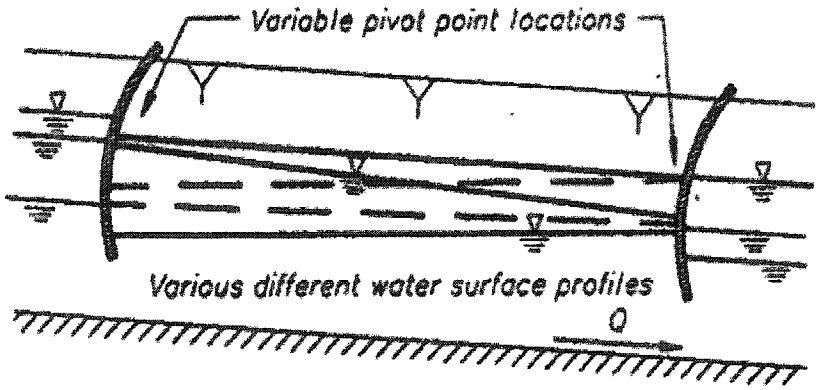

Figure 2.6. Controlled Volume.

2.3. Modelling of Open Channel Flow

To be classified as open-channel flow, water flowing in an aqueduct must have a free surface (Chow 1959). A free surface is a surface exposed to the atmosphere and therefore subject to atmospheric pressure. Open-channel flow itself can be classified according to varying criteria. Depending upon how canal flow depth changes with respect to distance and time, the flow can be classified into several different types: a) Changes with respect to distance are referred to as varied flow: 1) Gradually varied flow, if the depth changes gradually over a long distance. 2) Rapidly varied flow, if depth changes are abrupt over a short distance. b) Changes in with respect to time are referred to as unsteady flow. c) If depth does not change with time flow is steady (steady-state)

During normal operating conditions, an open-channel water distribution system can be classified as gradually varied unsteady flow. Only during certain emergency conditions, such as large uncontrolled inflows or outflows, would it be necessary to classify the flow as rapidly varied unsteady flow. As long as changes and adjustments are being made in the system it would be inappropriate to classify the flow in an open-channel distribution system as steady. With respect to operating automated canals,

unsteady gradually varied flow is an important flow condition. For example a gate movement produces changes in flow and adjacent depth as shown in Figure 2.7. A flow change that is initiated by changing the check gate opening takes the form of traveling translatory waves. A translatory wave is a gravity wave that propagates in an open channel and results in displacement of water particles in a direction parallel to the flow (Chow 1959). For example, if a check gate is opened a small increment (ΔGO), as shown on Figure 2.7, flow in the downstream canal pool will increase-generating a positive translatory wave which will travel downstream Simultaneously, a negative translatory wave is generated upstream of the check gate, this wave travels upstream. Translatory waves also are generated when the check gate closes. However, in this case, a negative translatory wave progress in the downstream direction and a positive wave progresses upstream.

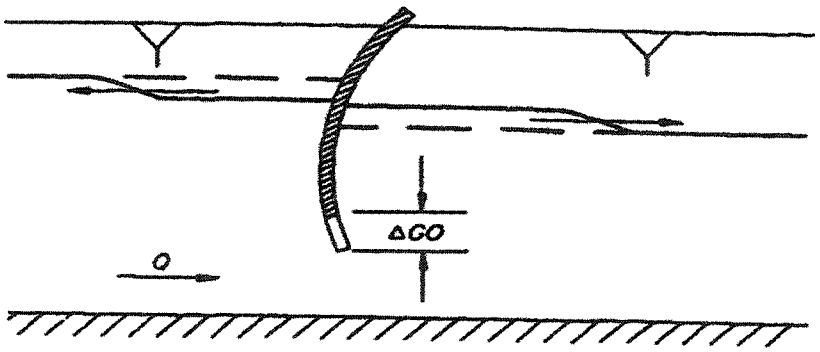

Figure 2.7. Flow change due to Gate Movement.

Figure 2.8 is a schematic of a translatory wave profile. The height of the translatory waves is a function of the magnitude of flow change and canal prism geometry. Friction forces will attenuate of decrease the height of the wave front as the wave transverses the

entire canal pool. The two equations that mathematically describe a translatory wave are the continuity and dynamic equations for gradually varied unsteady flow.

2.3.1. Derivation of the Saint-Venant Equations

A from of two partial differential equations was first published by Barre de Saint-Venant in 1871 and for this reason are known as the de Saint-Venant equations (Yevjevich 1975). The fundamental assumptions underlying the development of the de Saint-Venant equations are:

1) The wave surface gradually varies, which is equivalent to stating that the pressure distribution along a vertical is hydrostatic, or that the vertical acceleration is small;
2) Friction losses in unsteady flow are not significantly different from those in the steady flow;
3) Velocity distribution across the wetting are does not substantially affect the wave propagation;
4) The wave movement can be considered as two dimensional, with the effects of eventual difference of levels in cross sections negligible; and
5) The average slope of the channel bottom is so small that sin α by unity, were α is the angle made by the channel bottom with the horizontal.

Chow (1959) established the continuity equation for unsteady flow by considering the conservation of mass in an infinitesimal space between two channel sections shown in Figure 2.9. By considering water to be an incompressible fluid, the principle of

conservation of matter requires that during a short interval of time, Δt, the net inflow into the elemental section plus the changes in channel storage should be zero; that is;

$$\partial Q / \partial x + T \partial y / \partial t = 0 \qquad \text{(Eq. 2.1)}$$

where Q is the discharge in the channel, T is the top width of the channel, x is the length of the channel, and y is the depth of water in the channel. The continuity equation for steady open-channel flow is given by:

$$Q = VA \qquad \text{(Eq. 2.2)}$$

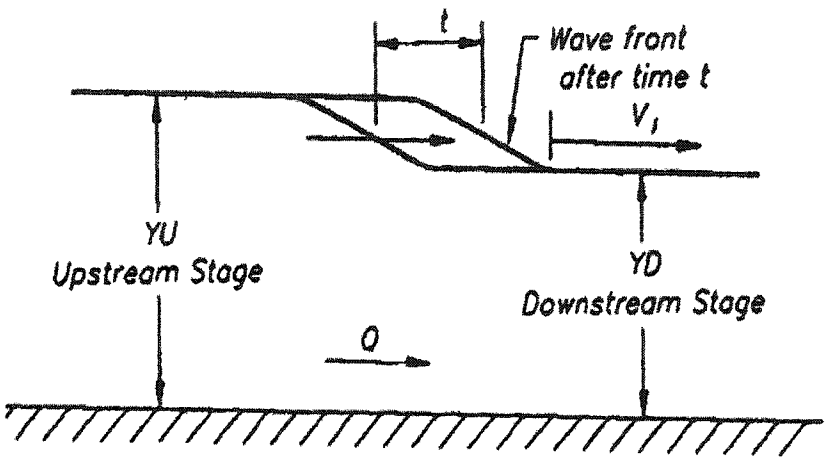

Figure 2.8. Translatory Wave Profile.

where V is the mean velocity and A is the flow cross-sectional are normal to the direction of flow. Hydraulic depth, D, is defined as the ratio of the area divided by the top width, T:

$$D = A / T \qquad \text{(Eq. 2.3)}$$

The change in the area ∂A, can be expressed as the top width times the change in depth:

$$\partial A = T \partial y \qquad \text{(Eq. 2.4)}$$

Using this definition and Equations 2.3 and 2.4, Equation 2.1 can also expressed as

$$\partial Q / \partial x + \partial A / \partial t = 0 \qquad \text{(Eq. 2.5)}$$

or,

$$\partial (VA) / \partial x + \partial A / \partial t = 0, \qquad \text{(Eq. 2.6)}$$

or,

$$A\partial V / \partial x + V\partial A / \partial x + T\partial y / \partial t = 0, \qquad \text{(Eq. 2.7)}$$

or,

$$D\partial V / \partial x + V\partial y / \partial x + \partial y / \partial t = 0 \qquad \text{(Eq. 2.8)}$$

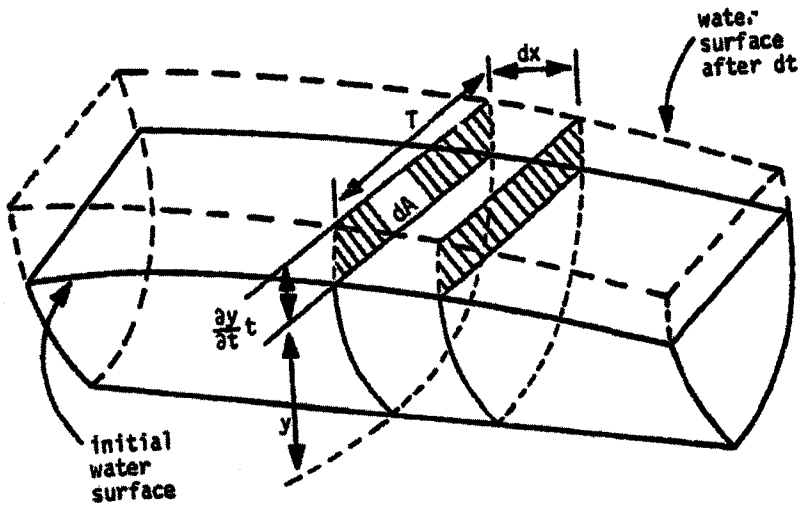

Figure 2.9. Continuity of Unsteady Flow.

Equation 2.1 and Equations 2.5 through 2.8 are all considered to be forms of the continuity equation for unsteady flow in open channels. For a rectangular channel:

$$Q = qT \qquad \text{(Eq. 2.9)}$$

where q is the discharge per unit width. Using Equation 2.9, Equation 2.1 becomes:

$$\partial q / \partial x + \partial y / \partial t = 0, \qquad \text{(Eq. 2.10)}$$

which is the form in which the de Saint-Venant equations were originally published.

The dynamic equation for unsteady flow was developed by referring to Figure 2.10. which shows an elementary control volume that is one unit in width normal to the direction of flow, and has a depth y and an average velocity V at the midpoint of the section. The conservation of momentum states that the net rate of momentum entering the elementary volume plus the sum of the forces acting on the volume must equal the rate of accumulation of momentum. The momentum of the flow passing a channel section per unit time is expressed by;

$$\gamma QV/g \qquad \text{(Eq. 2.11)}$$

where γ is the unit weight of water in lb/ft^3, and g is the acceleration due to gravity. The net rate of momentum entering the element was expressed as

$$-\gamma\partial(yV^2)\Delta x/g\partial x \qquad \text{(Eq. 2.12)}$$

The three types of forces acting on the control volume where considered to be gravity, pressure, and frictional resistance. All of these forces were resolved in the x direction. Since the control volume has a unit width, the weight of water contained is $wy\Delta x$. Consistent with the assumption that the channel slope is small, the sine of angle α is taken equal to the tangent of the angle. Therefore, sin α is replaced by the channel slope S_o. The weight component, of gravitational force, along the channel can now be written as;

$$F_g = \gamma\, y\Delta x Sin\alpha = \gamma\, y\Delta x S_o \qquad \text{(Eq. 2.13)}$$

The pressure force was resolved by computing the total hydrostatic force on each end of the control volume. The total hydrostatic force upon a plane surface is equal to the mean pressure times the surface area, namely the unit weight of water, the pressure head at the

centroid of the surface area. For the control volume the centroid of the surface is the total depth divided by two, and the surface area is the total depth times one. From this, the two pressure forces were resolved into a single force, and written as:

$$F_p=(-\gamma\partial y 2\Delta x)/(2\partial x) \qquad \text{(Eq. 2.14)}$$

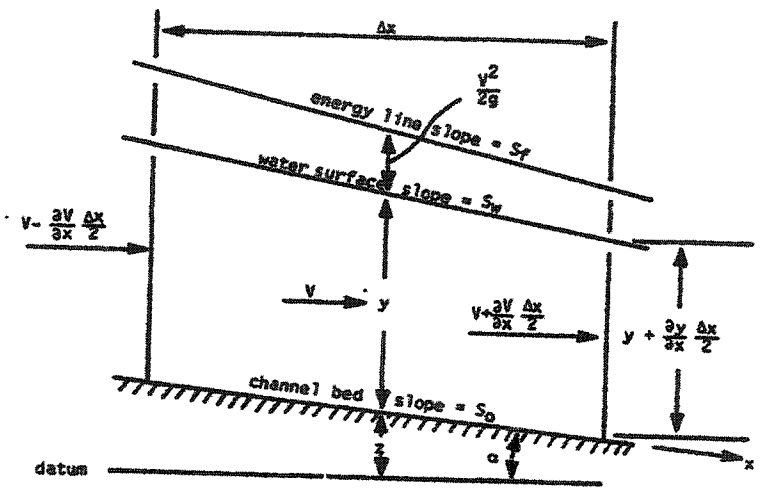

Figure 2.10. Dynamics of Unsteady Flow.

Water flowing in an open channel is retarded by the friction between the water, and the sides and bottom of the channel. The total friction, or shear force acting on the control volume, is equal to the product of the unit weight of water, the wetting area, the length of channel and the energy line slope, i.e. γALS_f, where S_f is the slope of the energy line. From this, the shear resistance, F_s, for the elemental section was expressed as:

$$-\gamma\, y\Delta x S_f \qquad \text{(Eq. 2.15)}$$

Combining these elements into a single equation for conservation of momentum resulted in:

$$(-\gamma\partial(yV^2)\Delta x)/(g\partial x) + F_g + F_p + F_s = \partial/\partial t[\gamma Vy/g]\,\Delta x \qquad \text{(Eq. 2.16)}$$

Dividing through by w and Δx, multiplying through by g, and rearranging terms Equation 2.16 becomes;

$$\partial(Vy)/\partial t + \partial(V^2y)/\partial x + (g\partial y^2)/(2\partial x) = gy(S_o - S_f) \qquad \text{(Eq. 2.17)}$$

which is the so-called conservation form. Expanding the derivatives resulted in;

$$y\partial V/\partial t + V\partial y/\partial t + V\partial(Vy)/\partial x + Vy\partial V/\partial x + gy\partial y/\partial x = gy(S_o - S_f) \qquad \text{(Eq. 2.18)}$$

For the control volume the are is equal to the depth and the discharge is equal to the depth times velocity, or

$$A = (y)(1) = y \qquad \text{(Eq. 2.19)}$$

and

$$Q = AV = yv \qquad \text{(Eq. 2.20)}$$

Substituting the above into Equation 2.5, a form of the continuity equation, results in

$$\partial(Vy)/\partial x + \partial y/\partial t = 0 \qquad \text{(Eq. 2.21)}$$

Adding the second and third terms of Equation 2.16 yields

$$V\partial y/\partial t + V\partial(Vy)/\partial x = V[\partial y/\partial t + \partial(Vy)/\partial x] \qquad \text{(Eq. 2.22)}$$

The right hand side of the above equation within the brackets is the same as the left hand side of Equation 2.22; thus, eliminating the second and third terms from Equation 2.18 resulted in;

$$y\partial V/\partial t + Vy\partial V/\partial x + gy\partial y/\partial x = gy(S_o - S_f) \qquad \text{(Eq. 2.23)}$$

After dividing by gy, the above equation was rewritten as

$$(1/g)\ \partial V/\partial t + (V/g)\ \partial V/\partial x + \partial y/\partial x = (S_o - S_f), \text{ or,}$$

$$\partial y/\partial x + (V/g)\ \partial V/\partial x + (1/g)\ \partial V/\partial t + S_f + \partial z/\partial x = 0 \qquad \text{(Eq. 2.24)}$$

where $S_o = -\partial z/\partial x$.

Equation 2.24 is a form of the general dynamic equation for gradually varied unsteady flow. Chow points out that the validity of the continuity and dynamic equations for gradually varied unsteady flow has been verified by many observations and experiments. Chow continues by saying, "However, owing to their mathematical complexity, exact integration of the equations is practically impossible. For practical applications, a solution of the equations may be obtained by using numerical methods. There are two fundamental divisions of methods for the solution of hyperbolic partial differential equations. The method of characteristics is based upon the characteristic form of the equations whereas finite difference methods are based upon the partial differential equations as originally derived.

2.3.2. Preissmann Implicit Scheme

In this research a finite-difference method was used for the solution of the Equations 2.23 and 2.24. The objective is to solve the equations of motion at finite number of grid points in the (x,t)-plane as indicated Figure 2.11. There are two basic types of fixed grid finite difference schemes. In the explicit scheme the unknown quantities from the initial condition of from the previous calculation are used for forward calculations. In the implicit scheme the value at the advance time, which is still unknown for the time being, is entered into the formula for solution. Then the solution at the advance time is obtained either by iteration of by linearizing the nonlinear terms and solving the resulting simplified system of linear equations simultaneously wit the boundary conditions. The implicit methods of finite difference were developed because of the limitations imposed on time step Δt when using the explicit scheme. The main advantage of the implicit

scheme is that the stability of the solution is not limited by the condition that the grid ratio, $\Delta t/\Delta x$, must be equal to or les than $1/|Q/A \ \forall(gA/B)^{0.5}|$. In this research Preissmann implicit scheme was used for the solution of de Saint-Venant equations. The basic equations of unsteady flow were derived above as follows:

1) The continuity equation: Conservation of mass for a control volume states: The net rate of flow into the volume = rate of storage change in the volume.

$$\partial z/\partial t + (1/B)(\partial Q/\partial x) - q_i = 0 \qquad \text{(Eq. 2.25)}$$

where z = water level as referred to a horizontal datum, t = time, B = with of the water surface, Q = discharge across a section, x = current abscissa (positive in the direction of flow), q_i = lateral in or outflow (positive for inflow, negative for outflow). In our solution we will assume no lateral inflow or outflow ($q_i = 0$).

2) The momentum equation: Conservation of momentum states: the net rate of momentum entering the element + the sum of the forces acting on the element = the rate of accumulation of momentum.

$$(\partial U/\partial t) + \partial/\partial x(\alpha U^2/2) + g(\partial z/\partial x) - g(Q/Q/K^2) = 0 \qquad \text{(Eq. 2.26)}$$

where U = velocity, Q/A; K = a coefficient , $K^2 = AR^{4/3}/n^2$; $\partial U/\partial t = 1/A(\partial Q/\partial t) - (QB)/A^2 (\partial z/\partial t)$; $\partial/\partial x(\alpha U^2/2) = \alpha U(\partial U/\partial x) + U^2/2(\partial\alpha/\partial x)$; $\partial U/\partial x = 1/A\partial(Q/\partial x) - Q/A^2(\partial A/\partial x)$.

If we substitute these equations into Eq. 2.26, we will get a final equation:

$$\partial Q/\partial t - (QB/A)(\partial z/\partial t) + (\alpha Q/A)(\partial Q/\partial x) - (\alpha Q^2/A^2)(\partial A/\partial x) + (Q^2/2A)(\partial\alpha/\partial x) - Ag(Q/Q/K^2) = 0 \qquad \text{(Eq. 2.27)}$$

in this equation $(Q/Q/)$ takes care of the direction of flow such that the friction resistance will always be against the motion.

The following equations and Figure 2.11. shows the actual discretization of dependent variables and its derivatives according to Preissmann. As we see, the Equations 25 and 27 are non-linear equations, so also are the difference equations obtained from by using the approximation of the following equations:

$$f(x,t) = (\theta/2)(f_{j+1}^{n+1} + f_j^{n+1}) + ((1-\theta)/2)(f_{j+1}^{n} + f_j^{n}) \quad \text{(Eq. 2.28)}$$

$$\partial f/\partial x = \theta((f_{j+1}^{n+1} - f_j^{n+1})/\Delta x) + (1-\theta)((f_{j+1}^{n} - f_j^{n})/\Delta x) \quad \text{(Eq. 2.29)}$$

$$\partial f/\partial t = (f_{j+1}^{n+1} - f_{j+1}^{n} + f_j^{n+1} - f_j^{n})/2\Delta t \quad \text{(Eq. 2.30)}$$

where θ is a weighting coefficient, $0 \leq \theta \leq 1$ which controls the stability of the numerical results, f is any dependent variable on Q or z. In Equations 2.25 and 2.27 replacing the derivatives by finite differences according to Equation 2.29 by writing $f^{n+1} = f^n + \Delta f$ and by dropping the superscript so that $f^n = f$, one gets for Equation 2.25:

$$((\Delta z_{j+1} + \Delta z_j)/2\Delta t) + 2/(\theta(\Delta B_j + \Delta B_{j+1}) + (B_j + B_{j+1}))[\ \theta((\Delta Q_{j+1} - \Delta Q_j)/\Delta x) +$$

$$(Q_{j+1} - Q_j)/\Delta x] = 0 \quad \text{(Eq. 2.31)}$$

Lets linearize the second term in Equation 2.31:

$$2/(\theta(\Delta B_j + \Delta B_{j+1}) + (B_j + B_{j+1})) = (2/(B_{j+1} + B_j))(1 + \theta[(\Delta B_{j+1} + \Delta B_j)/(B_j + B_{j+1})]^{-1}$$

$$= (2/(B_{j+1} + B_j))(1 - \theta(\Delta B_{j+1} + \Delta B_j)/(B_j + B_{j+1})) \quad \text{(Eq. 2.32)}$$

The substitution of the Equation 2.32 in to Equation 2.31 and further linearization according to the principle that $(\Delta f)^2 \cong \Delta f \Delta g \cong 0$ and we can get following equation:

$$((\Delta z_{j+1} + \Delta z_j)/2\Delta t) + (2/(B_{j+1} + B_j))[\ \theta((\Delta Q_{j+1} - \Delta Q_j)/\Delta x) + (Q_{j+1} - Q_j)/\Delta x] -$$

$$(2\theta/(B_{j+1} + B_j)^2)(\Delta B_{j+1} + \Delta B_j)((\Delta Q_{j+1} - \Delta Q_j)/\Delta x) = 0 \quad \text{(Eq. 2.33)}$$

where $\Delta B_j = (dB_j/dz)\,\Delta z_j \qquad \Delta B_{j+1} = (dB_{j+1}/dz)\,\Delta z_{j+1}$. Hence Equation 2.31 becomes:

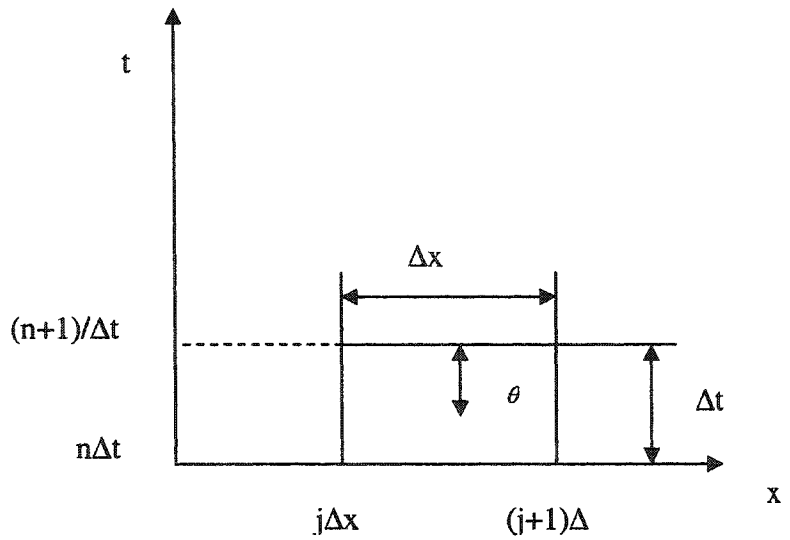

Figure 2.11. Preissmann's Scheme

$$\Delta z_{j+1}\{1-(4\theta\Delta t(Q_{j+1}-Q_j)\,dB_{j+1})/((B_{j+1}+B_j)^2\Delta x\,dz)\}+\Delta Q_{j+1}\{4\theta\Delta t/(\Delta x(B_j+B_{j+1}))\}+$$

$$\Delta z_j\{1-(4\theta\Delta t(Q_{j+1}-Q_j)\,dB_j)/((B_{j+1}+B_j)^2\Delta x\,dz)\}+\Delta Q_j\{-4\theta\Delta t/(\Delta x(B_j+B_{j+1}))\}+$$

$$(4\Delta t/(\Delta x(B_j+B_{j+1})))(Q_{j+1}-Q_j)=0 \qquad \text{(Eq. 2.34)}$$

This equation can be written symbolically as

$$H_j\Delta z_{j+1}+b_j\Delta Q_{j+1}=C_j\Delta z_j+D_j\Delta Q_j+G_j \qquad \text{(Eq. 2.35)}$$

where $H_j = 1-(4\theta\Delta t(Q_{j+1}-Q_j)\,dB_{j+1})/((B_{j+1}+B_j)^2\Delta x\,dz)$; $b_j = 4\theta\Delta t/(\Delta x(B_j+B_{j+1}))$; $C_j = 1-(4\theta\Delta t(Q_{j+1}-Q_j)\,dB_j)/((B_{j+1}+B_j)^2\Delta x\,dz)$; $D_j = -4\theta\Delta t/(\Delta x(B_j+B_{j+1}))$; $G_j = (4\Delta t/(\Delta x(B_j+B_{j+1})))(Q_{j+1}-Q_j)$. Descritize the momentum equation Eq. 2.27:

$$((\Delta Q_{j+1}-\Delta Q_j)/2\Delta t)-\{\theta/2[((Q_{j+1}-\Delta Q_{j+1})(B_{j+1}+\Delta B_{j+1})/(A_{j+1}+\Delta A_{j+1}))+((Q_j-\Delta Q_j)(B_j+\Delta B_j)/(A_j+\Delta A_j))]+(1-\theta)/2[(Q_{j+1}B_{j+1}/A_{j+1})+Q_jB_j/A_j]\}(\Delta z_{j+1}+\Delta z_j)/2\Delta t+$$

$$\{\theta/2[((\alpha_{j+1}-\Delta\alpha_{j+1})(Q_{j+1}+\Delta Q_{j+1})/(A_{j+1}+\Delta A_{j+1}))+((\alpha_j-\Delta\alpha_j)(Q_j+\Delta Q_j)/(A_j+\Delta A_j))]+$$

$$(1-\theta)/2[(\alpha_{j+1}Q_{j+1}/A_{j+1})+\alpha_jQ_j/A_j]\}\{\theta((\Delta Q_{j+1}-\Delta Q_j)/\Delta x)+(Q_{j+1}-Q_j)/\Delta x\}-$$

$$\{\theta/2[((\alpha_{j+1} - \Delta\alpha_{j+1})(Q_{j+1} + \Delta Q_{j+1})^2/(A_{j+1} + \Delta A_{j+1})^2) + ((\alpha_j - \Delta\alpha_j)(Q_j + \Delta Q_j)^2/(A_j + \Delta A_j)^2)]$$

$$+ (1-\theta)/2[(\alpha_{j+1}Q_{j+1}^2/A_{j+1}^2) + \alpha_j Q_j^2/A_j^2]\}\{\theta((\Delta A_{j+1} - \Delta A_j) + (A_{j+1} - A_j))/\Delta x\} +$$

$$\{(g\theta/2)(\Delta A_{j+1} + \Delta A_j) + (g/2)(A_{j+1} + A_j)\}\{\theta(\Delta z_{j+1} - \Delta z_j)/\Delta x + (z_{j+1} - z_j)/\Delta x\} +$$

$$\{\theta/2[((Q_{j+1} - \Delta Q_{j+1})^2/2(A_{j+1} + \Delta A_{j+1})) + ((Q_j + \Delta Q_j)^2/2(A_{j+1} + \Delta A_{j+1}))] +$$

$$(1-\theta)/2[(Q_{j+1}^2/2A_{j+1}) + Q_j^2/2A_j]\}\{\theta((\Delta\alpha_{j+1} - \Delta\alpha_j)/\Delta x) + (\alpha_{j+1} - \alpha_j)/\Delta x\} -$$

$$(g\theta/2)[(A_{j+1} + \Delta A_{j+1})(Q_{j+1} + \Delta Q_{j+1})/Q_{j+1} + \Delta Q_{j+1}/ + (A_j + \Delta A_j)(Q_j + \Delta Q_j))/Q_j + \Delta Q_j/] -$$

$$(g(1-\theta)/2)[(A_{j+1}Q_{j+1}/Q_{j+1}/)/K^2_{j+1} + A_j Q_j/Q_j/K_j^2] = 0 \qquad \text{(Eq. 2.36)}$$

Equation 2.36 can be linearized as was Eq. 2.31, first developing all terms in power series and neglecting the terms of second and higher orders, then by retaining only the terms in which the increments Δz and ΔQ are raised to the first power. It should be noted that:

$$1/(A_j + \Delta A_j) = 1/A_j(1+(\Delta A_j/A_j)) = 1/A_j(1 - \Delta A_j/A_j) \qquad \text{(Eq. 2.37)}$$

$$1/(A_j + \Delta A_j)^2 = 1/A_j^2(1+(\Delta A_j/A_j)^2) = 1/A_j^2(1 - 2\Delta A_j/A_j) \qquad \text{(Eq. 2.38)}$$

$$(Q_j + \Delta Q_j)^2 = Q_j^2 + 2Q_j\Delta Q_j \qquad \text{(Eq. 2.39)}$$

$$(Q_j + \Delta Q_j))/Q_j + \Delta Q_j/ = Q_j/Q_j/ + 2/Q_j/\Delta Q_j \qquad \text{(Eq. 2.40)}$$

$$\Delta A_j = (dA_j/dz_j)\,\Delta z_j = B_j\Delta z_j \qquad \text{(Eq. 2.41)}$$

$$\Delta K_j = (dK_j/dz_j)\,\Delta z_j \qquad \text{(Eq. 2.42)}$$

$$\Delta B = (dB_j/dz_j)\,\Delta z_j \qquad \text{(Eq. 2.43)}$$

$$\Delta\alpha = (d\alpha_j/dz_j)\,\Delta z_j \qquad \text{(Eq. 2.44)}$$

After this linearization, we can simplify Equation 2.36 as follows:

$$H'_j\Delta z_{j+1} + B'_j\Delta Q_{j+1} = C'_j\Delta z_j + D'_j\Delta Q_j + G'_j \qquad \text{(Eq. 2.45)}$$

where

$$H'_j = -1/2((Q_{j+1}B_{j+1}/A_{j+1}) + Q_jB_j/A_j) + \theta\Delta t/\Delta x\,\{(Q_{j+1} - Q_j)(Q_{j+1}d\alpha_{j+1})/(A_{j+1}dz_{j+1}) -$$

$$(Q_{j+1}B_{j+1}\alpha_{j+1})/A^2_{j+1}) - B_{j+1}(((Q^2_{j+1}\alpha_{j+1})/A^2_{j+1}) + \alpha_jQ_j^2/A^2_j) - (Q^2_{j+1}/A^2_{j+1})$$

$$(A_{j+1}-A_j)((d\alpha_{j+1}/dz_{j+1}) - 2\alpha_{j+1}B_{j+1}/A_{j+1}) + gB_{j+1}(z_{j+1}-z_j) - (Q^2_{j+1}B_{j+1}/2A^2_{j+1})$$

$$(\alpha_{j+1} - \alpha_j) + g(A_{j+1} + A_j) + 1/2((Q^2_{j+1}/A_{j+1}) + Q^2_j/A_j)(d\alpha_{j+1}/dz_{j+1})\} -$$

$$g\theta\Delta t((Q_{j+1}/Q_{j+1}/)/K^2_{j+1})\,(B_{j+1} - (2A_{j+1}dK_{j+1})/(K_{j+1}dz_{j+1}))$$

$$B'_j = 1 + (\theta\Delta t/\Delta x)\,\{(_{j+1}Q_{j+1}/A_{j+1}) + \alpha_jQ_j/A_j + (Q_{j+1} - Q_j)\,(\alpha_{j+1}/A_{j+1}) -$$

$$(A_{j+1}-A_j)(2\alpha_{j+1}Q_{j+1})/A^2_{j+1}) + (\alpha_{j+1}-\alpha_j)(Q_{j+1}/A_{j+1})\} - 2g\theta\Delta t(A_{j+1}/Q_{j+1}//K^2_{j+1})$$

$$C'_j = 1/2((Q_{j+1}B_{j+1}/A_{j+1}) + Q_jB_j/A_j) - \theta\,\Delta t/\Delta x\,\{(Q_{j+1} - Q_j)((Q_jd\alpha_j/A_jdz_j) - (Q_j\alpha_jB_j/A^2_j)) -$$

$$B_j((Q^2_{j+1}\alpha_{j+1})/A^2_{j+1}) + \alpha_jQ_j^2/A^2_j) - (Q^2_j/A^2_j)\,(A_{j+1}-A_j)((d\alpha_j/dz_j) - (2\alpha_jB_j/A_j) +$$

$$gB_j(z_{j+1} + z_j) - (Q^2_jB_j/21/2(A^2_j)(\alpha_{j+1}-\alpha_j) - g(A_{j+1}-A_j) -$$

$$1/2((Q^2_{j+1}/A_{j+1}) + Q^2_j/A_j)\,(d\alpha_j/dz_j)\} + g\theta\Delta t((Q_j/Q_j/)/K^2_j)$$

$$(B_j - (2A_{j+1}dK_{j+1})/(K_{j+1}dz_j))$$

$$D'_j = -1 - (\theta\Delta t/\Delta x)\,\{-(\alpha_{j+1}Q_{j+1}/A_{j+1}) - \alpha_jQ_j/A_j + (Q_{j+1} - Q_j)\,(\alpha_j/A_j) -$$

$$(A_{j+1}-A_j)(2\alpha_jQ_j)/A^2_j) + (\alpha_{j+1}-\alpha_j)(Q_j/A_j)\} + 2g\theta\Delta t(A_j/Q_j//K^2_j)$$

$$G'_j = -\Delta t/\Delta x\{(Q_{j+1} - Q_j)(Q_{j+1}\alpha_{j+1}/A_{j+1}) + \alpha_jQ_j/A_j) - (A_{j+1}-A_j)$$

$$(\alpha_{j+1}Q^2_{j+1})/A^2_{j+1}) - (\alpha_jQ^2_j)/A^2_j) + g(z_{j+1} + z_j)\,(A_{j+1}-A_j) + ((Q^2_{j+1}/2A_{j+1}) + (Q^2_j/2A_j)$$

$$(\alpha_{j+1} - \alpha_j)\} + g\Delta t(((Q_{j+1}/Q_{j+1}/A_{j+1})/K^2_{j+1}) + (Q_j/Q_j/A_j)/K^2_j))$$

Equations 2.35 and 2.45 may be written for any pair of computational points *(j, j+1)*. They are not sufficient to find the values of Δz_j, ΔQ_j, Δz_{j+1}, and ΔQ_{j+1} because for these four unknowns only two equations are available. But if there are *N* computational points in the model *(j=1, 2, ...N-1, N)*, we can write *2(N-1)* of such equations for *2N* unknowns. As two boundary conditions must be available there is actually a system of

$2(N-1) + 2 = 2N$ algebraic equations for $2N$ unknowns (ΔQ_j, Δz_j). Thus this system may be solved for any time step at Δt.

2.3.3. Lateral Discharge Rates (Disturbances)

The canals that take-off from the supply (or main) canal are defined as lateral canals. Lateral canals are usually scattered throughout the length of the supply canal. Depending upon the design, two types of structures are used at the head of a lateral canal: a manually controlled discharge regulator and an automated constant-discharge regulator. The mathematical representation of flow through these structures is given as follows:

$$q_i = C_d b_l w_l (2g(Z-Z_l)^{1/2} \text{ for submerged flow} \qquad \text{(Eq. 2.46)}$$

$$q_i = C_d b_l w_l (2g(Z-E_s)^{1/2} \text{ for free flow} \qquad \text{(Eq. 2.47)}$$

in which, q_i = lateral discharge rate, m^3/s; C_d = outlet discharge coefficient; b_l = width of outlet structure, m; w_l = height of gate opening of outlet structure, m; Z= water surface elevation in supply canal, m; and Z_l = water surface elevation in lateral canal, m; and E_s = sill elevation of head regulator, m. Obviously, the flow rate through a head regulator depends upon the water surface elevation in the supply canal. The water surface elevation in the lateral canal is a function of the discharge rate through the head regulator. Therefore, this equation is an implicit equation. In the case of free flow, the discharge rate through the head regulator is independent of the water surface elevation in the lateral canal. Therefore, once the required discharge into a lateral is specified, then the gate opening is adjusted to get the required flow rate through the head regulator, assuming that the water surface elevation in the supply canal is maintained constant at the target level. When a manually controlled head regulator is used, for simulation purposes the gate

opening or the variation in gate opening is specified as a function of time. Conversely when an automated discharge rate regulator is used, for simulation purposes the lateral discharge rate as a function of time is specified as a known input, i.e., $q_i = f_q(t)$.

2.3.4. Water Regulation Structures

In the regulation of irrigation canals, decisions regarding the opening of gates in response to random changes in water withdrawal rates into lateral canals are required to maintain the flow rate into laterals close to the desired value. This is accomplished by either maintaining the depth of flow in the immediate vicinity of the turnout structures in the supply canal constant or by maintaining the volume of water in the canal pools at the target value. When the latter option is used, the outlets are often fitted with discharge rate regulators. The water levels or the volumes of water stored in the canal pools are regulated using a series of spatially distributed gates (control elements). Hence, irrigation canals are modeled as distributed control systems. Therefore, in the solution of Equation 2.25 and 2.26, additional boundary conditions are specified at the control structures in terms of the flow continuity and the gate discharge equations, which are given by:

$$Q_{i-1,N} = Q_{gi} = Q_{i,1} \quad \textit{(continuity)} \qquad \text{(Eq. 2.48)}$$

$$Q_{gi} = C_{di} b_i u_i (2g(Z_{i-1,N} - Z_{i,1})^{1/2} \quad \textit{(gate discharge)} \qquad \text{(Eq. 2.49)}$$

in which, $Q_{i-1,N}$ = flow rate through downstream gate (or node N) of pool i-1, m^3/sec; Q_{gi} = flow rate through upstream gate of pool i, m^3/sec; $Q_{i,1}$ = flow rate through upstream gate (or node 1) of pool i, m^3/sec; C_{di} = discharge coefficient of gate i; b_i = width of gate i, m; u_i = opening of gate i, m; $Z_{i-1,N}$ = water surface elevation at node N of pool i-1, m;

$Z_{i,1}$ = water surface elevation at node 1 of pool i, m; and i = pool index ($i=0$ refers to the upstream constant level reservoir).

2.3.5. Double-Sweep Method

Depending upon the type of head regulator structure used, the variation in lateral withdrawal rate (δq) to the canal dynamics is specified. In the case of an open-loop simulation, the variations in gate opening as a function of time are pre-specified, and the evoluations of the system variables (Q and z) as a function of time is computed using the Equations 2.35 and 2.45. Each node, in general, has two unknowns, δQ and δZ. For j number of nodes, there will $2j$ number of variables. Since the number of independent equations available is only $(2j-2)$, Equations 2.35 and 2.45 must be supplemented with one boundary condition at each end of the canal. Then any standard method of solving a set of linear algebraic equations can be used. We can use double sweep method to solve these equations. Consider the system of Equations 2.35, $H_j\Delta z_{j+1} + b_j\Delta Q_{j+1} = C_j\Delta z_j + D_j\Delta Q_j + G_j$, and Equation 2.45, $H'_j\Delta z_{j+1} + B'_j\Delta Q_{j+1} = C'_j\Delta z_j + D'_j\Delta Q_j + G'_j$. Assume that there is a linear relationship of the type:

$$\Delta Q_j = E_j \Delta z_j + F_j \qquad \text{(Eq. 2.50)}$$

for a point j. If this is true, we can prove that an analogous linear relationship also exists for the next point, $j+1$:

$$\Delta Q_{j+1} = E_{j+1} \Delta z_{j+1} + F_{j+1} \qquad \text{(Eq. 2.51)}$$

If we substitute Equation 2.47 into Equations 2.35 and 2.45:

$$H_j\Delta z_{j+1} + b_j\Delta Q_{j+1} = (C_j+D_jE_j)\,\Delta z_j + G_j + D_jF_j \qquad \text{(Eq. 2.52)}$$

$$H'_j\Delta z_{j+1} + B'_j\Delta Q_{j+1} = (C'_j+D'_jE_j)\,\Delta z_j + G'_j + D'_jF_j \qquad \text{(Eq. 2.53)}$$

From first of Equations 2.52 and 2.53 we can find the relation between Δz_j and the increments of dependent variables Δz, ΔQ at point $j+1$:

$$\Delta z_j = (H_j \Delta z_{j+1} / (C_j + D_j E_j)) + (b_j \Delta Q_{j+1} / (C_j + D_j E_j)) - ((G_j + D_j F_j) / (C_j + D_j E_j)) \quad \text{(Eq. 2.54)}$$

We can write this equation as follows:

$$\Delta z_j = L_j \Delta z_{j+1} + M_j \Delta Q_{j+1} + N_j \quad \text{(Eq. 2.55)}$$

where

$$L_j = H_j / (C_j + D_j E_j) \qquad M_j = b_j / (C_j + D_j E_j) \qquad N_j = -(G_j + D_j F_j) / (C_j + D_j E_j) \quad \text{(Eq. 2.56)}$$

If we eliminate Δz_j between the two Equations 2.52 and 2.53 and than expressing ΔQ_{j+1} as a function of Δz_{j+1}:

$$\Delta Q_{j+1} = \{(H_j (C'_j + D'_j E_j) - H'_j (C_j + D_j E_j)) / (B'_j (C_j + D_j E_j) - b_j (C'_j + D'_j E_j))\} \Delta z_{j+1} +$$

$$\{(G'_j + D'_j F_j)(C_j + D_j E_j) - (G_j + D_j F_j)(C'_j + D'_j E_j)\} / (B'_j (C_j + D_j F_j) - b_j (C'_j + D'_j E_j)$$

(Eq. 2.57)

As we see here, this equation is the linear relationship of the form indicated by Equation 2.50. Thus we can say that if the relationship Equation 2.50 exists for any point of the model, it will also be true for all the following points. From Equation 2.57, we can see the following relationships:

$$E_{j+1} = f(E_j, H_j, \ldots.) \quad \text{(Eq. 2.58)}$$

$$F_{j+1} = f(E_j, F_j, H_j, \ldots.) \quad \text{(Eq. 2.59)}$$

Both coefficients E_{j+1}, F_{j+1} may be computed for any point $j+1$ if the analogous coefficients E_j, F_j for the preceding point j are known. In Equation 2.55, the coefficients are determined by Equation 2.56, permits the computation of Δz_j when the increments Δz and ΔQ are known for point $j+1$. These equations relationships suggest the method of

computing z^{n+1} and Q^{n+1} for all point j =1, 2, ..., N-1, N of a given reach. The boundary conditions must be locally linearized:

a) On one boundary, j-1, we need to know the relationship:

$$\Delta Q_1 = E_1 \Delta z_1 + F_1 \qquad \text{(Eq. 2.60)}$$

where coefficients E_1 and F_1 must be known.

b) On the other boundary, $j = N$, we need the value of Δz_N.

As we saw in the double sweep method of solution of algebraic equations, the exterior boundary conditions, at the limit of the model, should furnish either the values of coefficients E_1, F_1 or the value of the water stage increment Δz_N. The exterior boundary conditions are of three kinds:

1) $z_1 = z_1(t)$ is given. We want to determine the coefficients E_1 and F_1 in the formula.

$$\Delta Q_1 = E_1 \Delta z_1 + F_1 \qquad \text{(Eq. 2.61)}$$

The water stage at time $n\Delta t$, z_1^n is known as well as the water stage at time $(n+1)\,\Delta t$, $z_1^{n+1} = z_1(t_n+\Delta t)$. Consequently Δz_1 is known value. From Equation 2.38:

$$\Delta z_1 = (\Delta Q_1/E_1) - (F_1/E_1) \qquad \text{(Eq. 2.62)}$$

Actually Δz_1 should be independent of ΔQ_1. Indeed, the aim is to have Δz_1 equal to its imposed value whatever the computed value ΔQ_1 is or might be. To achieve this

$$E_1 = \alpha$$

$$F_1 = -\,\alpha z[(n+1)\,\Delta t] - z_1^n \qquad \text{(Eq. 2.63)}$$

where $\alpha >> \Delta Q_1$

The coefficient α should be very large, say of the order of 10^4 to 10^6. Then when the computations are made,

$$\Delta z_1 = 0 + z((n+1)\,\Delta t) - z_1^n \qquad \text{(Eq. 2.64)}$$

2) $Q_1 = Q(t)$ is given. E_1 and F_1 should be determined such that $\Delta Q_1 = Q(t_n+\Delta t) - Q_1^n$. According to Equation 2.51, ΔQ_1 depends upon Δz_1, but it should be independent of Δz_1 for use as an arbitrary boundary condition. Put $E_1 = 0$

$$F_1 = Q(t_n + \Delta t) - Q_1^n \qquad \text{(Eq. 2.65)}$$

Then, whatever the computed value of Δz_1 and ΔQ_1 will always be equal to the boundary condition value.

3) $Q = f(z)$ is given, where $f(z)$ is either a polynomial for a tabulated function. The needed coefficients are E_1, F_1 of the relationships

$$\Delta Q_1 = E_1 \Delta z_1 + F_1 \qquad \text{(Eq. 2.66)}$$

On the other hand

$$Q_1^{n+1} = Q_1^n + \Delta Q_1 \qquad \text{(Eq. 2.67)}$$

where Q_1^n is the computed value while, from the given condition:

$$Q_1(t_n + \Delta t) = f(z^n) + df\, \Delta z_1/dz_1 \qquad \text{(Eq. 2.68)}$$

A comparison gives

$$Q_1^n + \Delta Q_1 = f(z^n) + df\, \Delta z_1/dz_1 \qquad \text{(Eq. 2.69)}$$

Upon solving for ΔQ_1

$$\Delta Q_1 = f(z^n) - Q_1^n + df\, \Delta z_1/dz_1 \qquad \text{(Eq. 2.70)}$$

$$E_1 = df/dz_1$$

$$F_1 = f(z^n) - Q_1^n \qquad \text{(Eq. 2.71)}$$

It is obvious that $F_1 = 0$, but it is never exactly zero because of truncation and other errors. Thus F_1 is a corrective factor.

We can give an example to explain the interior boundary conditions. Because there can be too many possibilities for the interior boundary conditions. Consider a canal

and a basin linked to the canal as we see in the Figure 2.12. When the coefficients E, F are computed, they are found automatically for point j as they were for point j-1. To continue the computations the coefficients E_{j+1}, F_{j+1} are needed. The coefficients L_j, M_j, N_j are also needed in order to compute Δz_j and Δz_{j+1} and ΔQ_{j+1} are known. All these coefficients depend upon the characteristics of the transition. Suppose for simplicity's sake that the

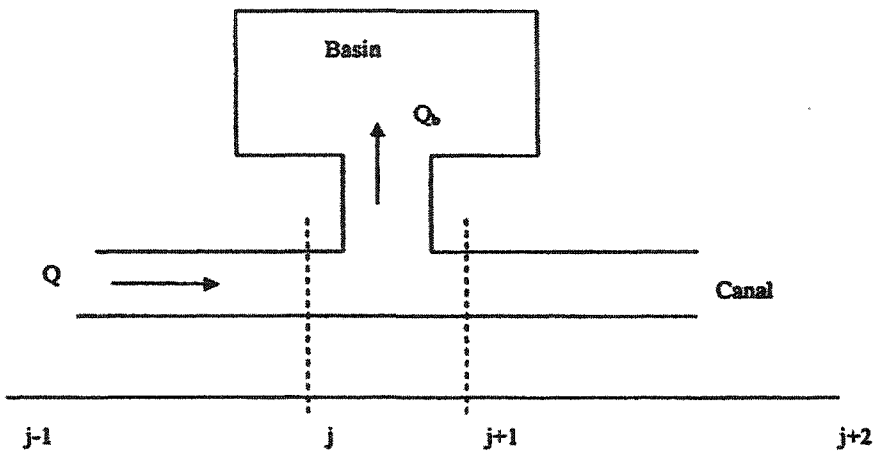

Figure 2.12. Interior Boundary Conditions.

water level within the basin is always same as the water level in the canal, $z_b = z_c$. On the other hand, if the velocities are nearly equal at cross sections j and $j+1$,

$$z_j^{n+1} = z_{j+1}^{n+1} = z_b^{n+1} \qquad \text{(Eq. 2.72)}$$

The continuity equation between j and $j+1$ is

$$Q_{j+1}^{n+1} = Q_j^{n+1} - Q_b^{n+1} \qquad \text{(Eq 2.73)}$$

Where Q_b is the discharge from the canal in to the basin. The continuity of the volume stored in the basin leads to the equation

$$A_b \Delta z_b / \Delta t_j = Q_b^{n+1} \qquad \text{(Eq. 2.74)}$$

Where A_b is the horizontal water surface area of the basin with the $A_b = A_b(z_b)$. The two preceding equations can be written as

$$Q_{j+1}^{n} + \Delta Q_{j+1} = Q_j^{n} + \Delta Q_j - A_b^{n+1}\Delta z_{j+1}/\Delta t \qquad \text{(Eq. 2.75)}$$

Since $\Delta Q_j = E_j \Delta z_j + F_j$ and since $z_j^{n} + \Delta z_j = z_{j+1}^{n} + \Delta z_{j+1}$ we can get the following equations:

$$\Delta z_j = \Delta z_{j+1} + (z_{j+1}^{n} - z_j^{n}) \text{ and } \Delta Q_j = E_j \Delta z_{j+1} + E_j(z_{j+1}^{n} - z_j^{n}) + F_j \qquad \text{(Eq. 2.76)}$$

If we substitute these equations into Equation 2.76.:

$$\Delta Q_{j+1} = (E_j - A_b/\Delta t)\,\Delta z_{j+1} + [Q_j^{n} - Q_j^{n+1} + F_j + E_j(z_{j+1}^{n} - z_j^{n})] \qquad \text{(Eq. 2.77)}$$

$$E_{j+1} = E_j - A_b(z_j^{n})/\Delta t \qquad \text{(Eq. 2.78)}$$

$$F_{j+1} = Q_j^{n} - Q_j^{n+1} + F_j + E_j(z_{j+1}^{n} - z_j^{n}) \qquad \text{(Eq. 2.79)}$$

Coefficinets L_j, M_j, N_j may be found from the following relationship:

$$\Delta z_j = \Delta z_{j+1} + (z_{j+1}^{n} - z_j^{n}) \qquad \text{(Eq. 2.80)}$$

hence,

$$L_j = 1,\ M_j = 0\ N_j = z_{j+1}^{n} - z_j^{n} \qquad \text{(Eq. 2.81)}$$

2.4. Feedback control

A control system is an interconnection of components forming a system configuration that will provide a desired system response. The basis for analysis of a system is the foundation provided by linear system theory, which assumes a cause-effect relationship for the component of a system. An open-loop control system utilizes a controller or control actuator to obtain the desired response. In contrast to an open-loop control system, a closed-loop control system utilizes an additional measure of the actual output to

compare the actual output with the desired output response. The measure of the output is called the feedback signal.

Feedback control is another term to describe closed-loop control. In canals, feedback type control systems are used to minimize the magnitude and duration of the mismatch between the supply and the demand. The elements of a simple feedback control system consist of the sensor, comparator, control element and actuator, as shown in Figure 2.13.

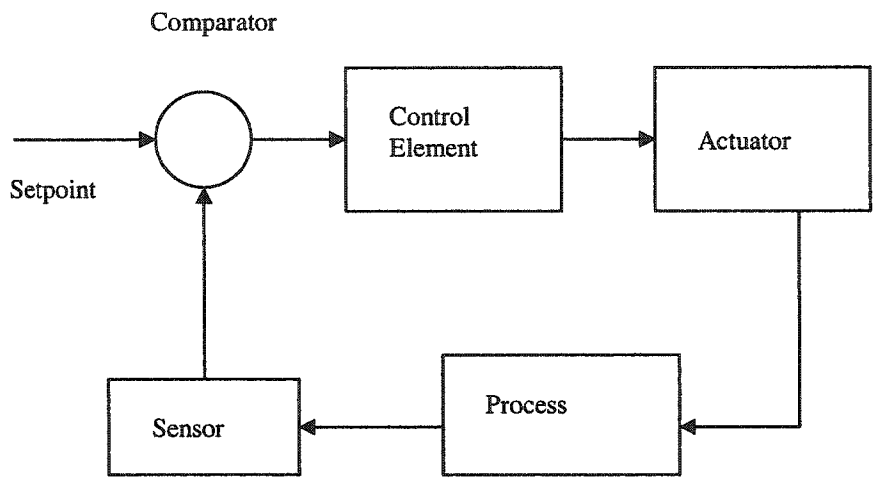

Figure 2.13. Simple Feedback Control System.

The sensor provides input to the control system. The sensor also converts an observable parameter such as water level, flow or gate position to a quantity that can be used by the control system. A setpoint is a reference input to the comparator element. A sensor input quantity that is different from the setpoint value causes the control element to initiate an output to the actuator. The setpoint reference value is sometimes referred to as the target value for canal control systems. The deviation from setpoint is called the error. A comparator is a device that compares two inputs and provides an error as an output. In a

canal application, a comparator would compare the input value from the sensor with the setpoint value and produce the appropriate error signal to the control element. The control element performs the same set of steps that ditchrider does to adjust a canal system based upon observed conditions. The control element often is referred to as the controller. Sometimes, the complete system, from the sensor to the actuator, is called the controller. The actuator converts output of the control element to a mechanical operation that effects the process operation. In a canal system the actuator converts the output of the control element to an electrical, mechanical, or hydraulic action to: open or close check gates, open or close valves, and start or stop pumps.

2.4.1. The z-Transform

The Laplace transform can be used to solve linear ordinary differential equations. For linear difference equations and linear systems with discrete or digital data, the z-transform is more appropriate to use. One way of describing the discrete nature is to consider that the input and the output of the system are sequences of numbers. These numbers appears at uniform intervals of time T. Thus, the input sequence and the output sequence may be represented by $u(kT)$ and $y(kT)$, respectively, where k = sequence numbers or sampling interval. The ideal sampler is regarded as the sampler which produces a series of impulses, $f^*(t)$, weighted by the input value, $f(kT)$. For a continues-time system, we can write a Laplace transform of the ideally sampled signal, $F^*(s)$, as follows:

$$F^*(s) = \sum_{k=0}^{\infty} f(kT)e^{-kTs} \qquad \text{(Eq. 2.82)}$$

If we define a variable z such that $z=e^{Ts}$, we can write the Equation 2.78 as follows:

$$F(z) = \sum_{k=0}^{\infty} f(kT)e^{-k} \qquad \text{(Eq. 2.83)}$$

$F(z)$ is called the z-transform of $f(kT)$, and is denoted by $z\{f(kT)\}$. The z-transform is more useful in studying discrete systems then the Laplace transform. Because the former incorporates the sampling interval T, which is a characteristic of discrete systems. the expression for digital transfer functions in terms of the z-transform are easier to manipulate, as they are free from the time-shift factor, e^{-Ts}, of the Laplace transform.

2.4.2. Feedback controllers and estimators

In feedback control systems, the exact relationship between the error and the controller $(\delta u(k) = f(e(k))$ is defined as follows:

$$e(k) = Z_t - Z(k) \quad \text{for constant – level control} \qquad \text{(Eq. 2.84)}$$

$$e(k) = V_t - V(k) \quad \text{for controlled – volume control} \qquad \text{(Eq. 2.85)}$$

in which $e(k)$ = error between the target water surface elevation (Z_t) and the actual water surface elevation $(Z(k))$ or the target pool volume (V_t) and the actual pool volume $(V(k))$. The relationship between the error and the control action depends upon the type of control algorithm selected. The most commonly used feedback control algorithms are: the proportional (P), the proportional-plus-integral (PI), and the proportional-plus-integral-plus-derivative (PID). In the case of an open-loop simulation, the values of $\delta u(k)$ are pre-specified for the entire duration of simulation, whereas in the case of a feedback control simulation the values of $\delta u(k)$ are computed in a subroutine for each sampling period. Depending upon the type of control algorithm used, the appropriate variables are transferred to the subroutine to compute the value of $\delta u(k)$.

The control structures (gates) in an irrigation canals are frequently adjusted in order to maintain the target water levels at specified points or target pool volumes in the presence of disturbances acting on the system. The required change in the opening of the gates can be computed by applying a proportional control, in which the change in gate opening is proportional to the changes in flow depths and flow rates in the system, of the following form:

$$\delta u(k) = -K(k)\, \delta x(k) \qquad \text{(Eq. 2.86)}$$

where $K(k)$ = controller gain matrix. The selection of values for the elements of the gain matrix is the design problem that is posed here. Large components in control gains could saturate the actuator device, and might cause overtopping of the canals due to the surge waves. Conversely, if the control is not sufficient magnitude, the system would return to the equilibrium condition very slowly, causing large deviations in depths of flow in the pools. There is a trade-off between the overtopping of canal banks and the rate of return to the equilibrium condition.

2.4.2.1. Input-Output Based Controllers

1) Proportional (P) Control: Proportional control responds to the deviation from the set point using a fixed linear relationship between the value of the controlled variable and the position of the final controlled element. The proportional controller moves the final controlled element to a definite position for each value of the controlled variable. The amount of deviation from the set point represents the error and this error represents the magnitude of the output. A definite relationship can be established to couple the input to the output of the process. In canal control, proportional mode of control operates the

check structure gate based upon the amount of deviation (error) between the measured water level and the set point (target value) and a proportionality constant. The final control action from the actuator is to move the controlled element in direct proportion to the error amount. A residual error, characteristic of proportional control, remains and is referred to as water level offset in canal control applications. The proportionality factor is sometimes referred to as the gain of the control systems. Most proportional controllers have an adjustable gain. The gain determines the amount of gate movement for any change in the canal water level. Therefore, a rule of thumb: the larger the gain, the greater the change in gate position for any given change in the water level. The major disadvantage of the proportional control is that a system demand change results in an offset. An offset is a sustained deviation of the water level from the set point as a result of the demand change. The magnitude of this offset may present difficulties for canal systems having gravity type turnouts.

The objective of control theory is to find a control law that will bring an initially disturbed system to the desired target value in the presence of external disturbances acting on the system. This can be accomplished by applying a large proportional control. Proportional control is a common feedback control mechanism that is used to bring an initially disturbed system back to its original state. The equation is of the following form:

$$\delta u(k) = -Ke(k) \qquad \text{(Eq. 2.87)}$$

in which K is proportionality.

2) Proportional-Integral Control: One of the most simple and widely applied feedback controllers is the PI controller. Integral control responds to a deviation from the set point collecting a time history of the error or integrating the error. The magnitude of the

integral control action depends on the accumulation of the reset control action depends on the accumulation of corrective action and is based upon the magnitude and duration of the error. In the proportional-integral control, the integral control action provides a restoration of the proportional offset. As soon as an error develops (deviation above or below the set point) a gradual and automatic shift originates to bring the input variable to the set point value to eliminate the offset error. The integral control is added to proportional control to eliminate offset that is experienced with the proportional control. The PI controller could be described as:

$$\delta u(k) = -K\,[\, e(k) + T/t_I(\sum_{i=1}^{k-1} e(i) + e(k))] \qquad \text{(Eq. 2.88)}$$

in which K, t_I, and t_D are proportionality, integral time and derivative time constants, respectively.

3) Proportional-Integral-Derivative (PID) Control: PID control responds to time rate of change in the magnitude and direction of the error deviation. Derivative control provides an initially large response when the deviation from set point occurs, so that the final controlled device is operated longer at first than it normally would without rate control. Then, having made this large initial change, the other modes of control take action to remove this effect and position the final control element as a proportional integral control action. Derivative control provides a temporary overcorrection to the system that is proportional to amount of the rate of deviation per unit time. Most often, derivative control is used in process control systems that have a usually large delay or lag time. Canal systems have these characteristics. The proportional gain must be set exceptionally small, and the integral is unusually slow. The addition of rate control to canal control

algorithms should prove beneficial to canal control. Combining all the above yields the PID controller:

$$\delta u(k) = -K \left[e(k) + T/t_I \left(\sum_{i=1}^{k-1} e(i) + e(k) + t_d/T \left(e(k) - e(k-1) \right) \right) \right] \qquad \text{(Eq. 2.89)}$$

in which, K, t_I, t_d are proportionality, integral time and derivative time constants, respectively.

2.4.2.2. Optimal Controller

During the last two decades, the concepts of the optimal control theory have been applied for deriving feedback control algorithms for real-time control of irrigation canals (Reddy 1999). Most of the optimal control concepts to multi-pool systems is more involved because of the interactions between pools. Balogun et al (1988), Reddy (1992, 1995), and Malaterre (1995) demonstrated the application of optimal control theory concepts for derivation of global control algorithms for multi-pool canals. Application of optimal control theory for the derivation of canal control algorithms eliminates the trial end error procedure that has been traditionally used.

A system is considered an optimal control system when the system parameters are adjusted so that the index reaches an extremum value, commonly a minimum value. A performance index, to be useful must be a number that is always positive or zero. During the last two decades, the concepts of optimal control theory have been applied for deriving feedback control algorithms for real-time control of irrigation canals (Reddy et al 1992). Application of optimal control theory for the derivation of canal control algorithms eliminates the trial and error procedure that has been traditionally used.

In order to apply the concepts of linear optimal control theory, the system dynamic equation must be transformed into a set of first-order, ordinary, differential equations with an appropriate forcing function. In a compact form, the discrete-time version of the system state equations are given as follows:

$$\delta x(k+1) = \Phi\, \delta x(k) + \Gamma\, \delta u(k) + \Psi\, \delta q(k) \qquad \text{(Eq. 2.90)}$$

in which $\Phi = l \times l$ system transition matrix; $\delta x(k) = l \times 1$ state vector; $\delta u(k) = m \times 1$ variation in the control vector value; $\Gamma = l \times m$ control distribution matrix; $\Psi = l \times p$ disturbance distribution matrix; $\delta q(k) = p \times 1$ matrix representing the changes in the disturbances (changes in water withdrawal rates) acting on the system; l = number of dependent (state) variables in the system; m = number of controls (gates); k = index of sampling intervals; and p = total number of outlets on canal. The elements of the matrices Φ, Γ and Ψ depend upon the canal parameters and the assumed average operating condition of the canal. For the situation where the upstream and downstream boundary conditions are specified in terms of water surface elevations, the vector of state variables in Equation 2.90 is defined as follows:

$$\delta x = (\delta Q_{i,1}, \delta Z_{i,2}, \delta Q_{i,2}, \ldots\ldots \delta Z_{i,N-1}, \delta Q_{i,n-1}, \delta Q_{i,N}) \qquad \text{(Eq. 2.91)}$$

The Saint-Venant equations are used to obtain the above set of equations. Give the initial conditions, the variations in lateral withdrawal rates, and the gate opening as a function of time, Equation 2.91 can be used to simulate the system dynamics.

2.4.2.2.1. Linear Quadratic Gaussian (LQG) Controller

Optimal control, building on the optimal filtering work of Wiener in the 1940's, reached maturity in the 1960's with what we now call linear quadratic Gaussian or LQG control.

In traditional LQG control, it is assumed that the system dynamics are linear and known and that the measurement noise and process noise are stochastic with known statistical properties. That is, we have a system:

$$\delta x(k+1) = \Phi\, \delta x(k) + \Gamma \delta u(k) + \Psi\, \delta q(k) \qquad \text{(Eq. 2.92)}$$

$$y(k) = H\delta x(k) + \eta(k) \qquad \text{(Eq. 2.93)}$$

where Φ, Γ, Ψ are the real matrices and $\delta x(k+1)$, $\delta u(k)$ are state and controlled variables at each time k, $\delta q(k)$ and $\eta(k)$ are the disturbance and measurement noise inputs respectively, which are mutually independent zero-mean Gaussian white-noise processes with covariance matrices given by Q and $R=\rho I$ respectively where ρ is spectral density.

The solution of LQG problem, known as the Separation Theorem or Certainty Equivalence Principle (Figure 2.14), is surprisingly simple and elegant. It consists of first determining the optimal control to a deterministic linear quadratic regulator (LQR).

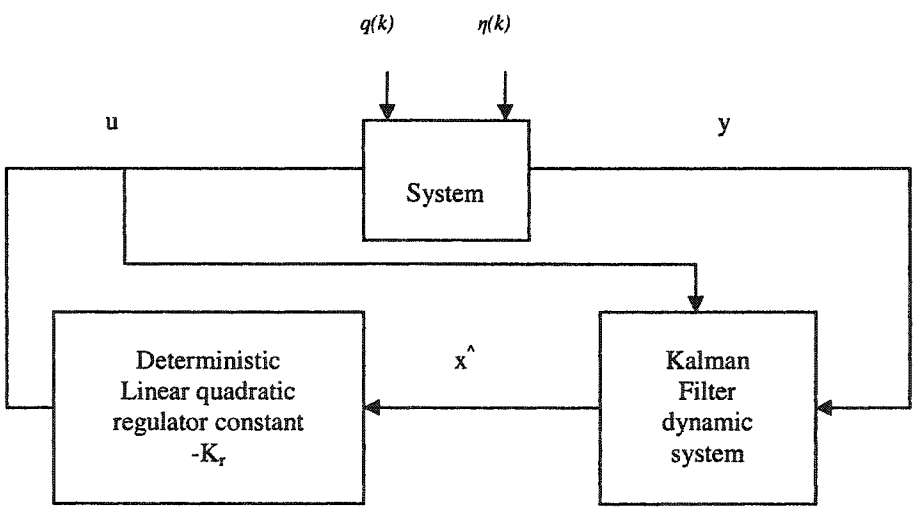

Figure 2.14 The Separation Theorem.

In LQR design, the system equations are like LQG system equations but without $\delta q(k)$ and $\eta(k)$.

$$\delta x(k+1) = \Phi\, \delta x(k) + \Gamma \delta u(k) \qquad \text{(Eq. 2.94)}$$

$$y(k) = H\delta x(k) \qquad \text{(Eq. 2.95)}$$

In LQR control theory, the control problem as an optimization problem in which the cost function to be minimized is given as follows:

$$J = \sum_{i=1}^{K_\infty} [\delta x(k)^T Q_{lxl}\, \delta x(k) + \delta u(k)^T R_{mxm}\, \delta u(k)] \qquad \text{(Eq. 2.96)}$$

subject to the constraint that:

$$-\delta x(k+1) + \Phi\, \delta x(k) + \Gamma\, \delta u(k) = 0 \quad k = 0,\ldots\ldots,K\infty \qquad \text{(Eq. 2.97)}$$

where K_∞ = number of sampling intervals considered to derive the steady state controller; Q_{lxl} = state cost weighting matrix; and R_{mxm} = control cost weighting matrix. The matrices Q and R are symmetric, and to satisfy the non-negative definite condition, they are usually selected to be diagonal with all diagonal elements positive or zero. The first term in Equation 2.94 represents the cost of control. This term is included in an attempt to limit the magnitude of the control signal $\delta u(k)$. Unless a cost is imposed for use of control, the design that emerges is liable to generate control signals that cannot be achieved by the actuator. In this case the saturation of the control signal will occur resulting in a system behavior that is different from the closed loop system behavior that was predicted assuming that saturation will not occur. Therefore, the control signal weighting matrix elements are selected to be large enough to avoid saturation of the control signal under normal operating conditions.

Equations 2.96 and 2.97 constitute a constrained-minimization problem that can be solved using the method of Lagrange multipliers. This produces a set of coupled difference equations which must be solved recursively backwards in time. In the optimal steady-state case, the solution for change in gate opening, $\delta u(k)$, is of the same form as:

$$\delta u(k) = -K\, \delta x(k) \qquad \text{(Eq. 2.98)}$$

where K is given by:

$$K = [R + \Gamma^T S_\infty \Gamma]^{-1} \Gamma^T S_\infty \Phi \qquad \text{(Eq. 2.99)}$$

S_∞ is a solution of the discrete algebraic Riccati equation (DARE):

$$\Phi^T S_\infty \Phi - \Phi^T S_\infty \Gamma [R + \Gamma^T S_\infty \Gamma]^{-1} \Gamma^T S_\infty \Phi + Q = S_\infty \qquad \text{(Eq. 2.100)}$$

where $R = R^T > 0$ and $Q = Q^T = H^T H \geq 0$

The control law defined by Equation 2.98 brings an initially disturbed system to an equilibrium condition in the absence of any external disturbances acting on the system. Known or unknown disturbances (changes in lateral withdrawal rates) always act on the system. In the presence of these external disturbances, the system cannot be returned to the equilibrium condition using the above control law. An integral control in which the cumulative (or integrated) deviation of a selected output variable is used in the feedback control loop, is required to return the system to the equilibrium condition in the presence of external disturbances (Kwakernaak and Sivan 1972). Integral control is achieved by appending additional state variables of the following form to the system state equation (Equation 2.90):

$$\delta x_I(k+1) = H\, \delta x(k) + I\, \delta x_I(k) \qquad \text{(Eq. 2.101)}$$

in which δx_I = integral state variables; I = identity matrix of appropriate dimension; and H = integral feedback matrix. This produces a new control law of the form:

$$\delta u(k) = -K\, \delta x(k) - K_I\, \delta x_I(k) \qquad \text{(Eq. 2.102)}$$

The first term in Equation 2.102 accounts for deviations at the beginning of each time increment (proportional control), whereas the second term accounts for external disturbances that act continuously on the system during the computational time increment (integral control). Equation 2.102 calculates the desired gate opening as a function of the measured deviations in the values of the state variables in the canal.

When lumped parameter models are used to derive feedback control algorithms for irrigation canals (Balogun et al 1988; Reddy et al 1992; Garcia et al 1992; Malaterre 1995), the number of state variables (which depends upon the number of finite-difference nodes used per pool) that must be measured and used in the feedback loop becomes large. For the linearization scheme used by Malaterre (1995), the number of measurements required for state feedback is given as:

$$N_m = N_p\,(3 + 2(N-2)) \qquad \text{(Eq. 2.103)}$$

where N_m = number of measurements required for full state feedback; and N_p = number of pools in the system. Since it is expensive to measure all the state variables (flow rates and flow depths) in a canal system, the number of measurements per pool must be kept to an absolute minimum. Usually the flow depths at the upstream and downstream ends of each pool are measured. The relationship between the state variables and the measure (or output) variables is:

$$\delta y(k) = H\,\delta x(k) + \eta(k) \qquad \text{(Eq. 2.104)}$$

in which $\delta y(k) = N_{mo}\,x\,1$ vector of output variables; $H = N_{mo}\,x\,l$ output matrix; $\eta(k) = N_{mo}\,x\,1$ vector of random measurement noises; and N_{mo} = number of measured outputs. Since only one or two flow depths per pool are measured in practice, it is necessary to estimate values for the state variables that are not measured. This can be done by using an estimator or observer. An estimator is a mathematical model of the system that estimates values for the state variables that are not measured based upon measured values for one or more state variables in a pool. Reddy et al (1992) applied the pole-placement technique, a trial-and-error approach, to design and observer. Though this technique is convenient for single-input-single-output (SISO) systems, it becomes very tedious for multi-input-multi-output (MIMO) systems, particularly in the presence of random disturbances.

Irrigation canals with multiple pools and gates are MIMO systems. Therefore, for a robust performance of the system, the estimation of the state variables must be done

based upon the statistical parameters of the random disturbances. Reddy (1995) compared the performance of the estimators designed based upon the pole placement technique, the steady state Kalman Filter, and the time-varying Kalman Filter for a single canal pool. Considering the accuracy and computational complexity of the techniques, the steady state Kalman Filter was found to be the best choice for irrigation canals. In the derivation of the Kalman filter, it is assumed that the disturbances can be described by a white (no time correlation among the disturbances), zero-mean Gaussian random sequence. For irrigation canals that run for a long time, the steady-state Kalman filter is very appropriate and the observer gain matrix in this case is calculated as follows:

$$L = P_\infty H^T [H P_\infty H^T + R_1]^{-1} \qquad \text{(Eq. 2.105)}$$

where P_∞ is a solution of the discrete algebraic Riccati equation (DARE):

$$\Phi^T P_\infty \Phi - \Phi P_\infty H^T [R_1 + H^T P_\infty H]^{-1} H P_\infty \Phi^T + Q_1 = P_\infty \qquad \text{(Eq. 2.106)}$$

where $R_1 = R_1^T > 0$ and $Q_1 = Q_1^T = \Gamma^T \Gamma \geq 0$

If the initial conditions and the inputs (control inputs and the disturbances) are known without error, the system dynamic equation (Equation 2.26) can be used to estimate the state variables that are not measured. Since part of the disturbances are random and usually are not measured, the canal parameters are not known very accurately, the estimated values of the state variables would diverge from the actual values. This divergence can be minimized by utilizing the difference between measured output and the estimated output (error signal), and by constantly correcting the system model with the error signal. Therefore, the modified state equations are given as:

$$\delta\hat{x}(k+1) = \phi\delta\hat{x}(k) + \Gamma\delta u(k) + L[\delta y(k) - H\delta\hat{x}(k)] \qquad \text{(Eq. 2.107)}$$

in which $\delta\hat{x}(k)$ = estimated values of the state variables; and L = observer gain matrix. Equation 2.107 is called and observer and estimator which is basically a mathematical model that is used in an on-line computer. The observer is driven by the error between the measured and the predicted values of the selected state variables in the system. The determination of the observer poles is a compromise between sensitivity to measurement

error and rapid recovery of initial errors. Hence, there is a need for an optimum selection of the observer poles, and the Kalman filtering is and efficient way of designing and observer for MIMO systems in the presence of random disturbances (Stengel 1986).

2.5. Robust Control

The design of highly accurate control systems in the presence of significant uncertainty requires the designer to seek a robust system. The goal of robust systems design is to retain assurance of system performance in spite of model inaccuracies and changes. A system is robust when the system has acceptable changes in performance due to model changes or inaccuracies. A robust control system exhibits the desired performance despite the presence of significant process uncertainty. Designing highly accurate systems in the presence of significant process uncertainty is a classical feedback design problem. The purpose of a designer is to obtain a system that performs adequately over a large range of uncertain parameters. A system is said to be robust when it is durable, hardy, and resilient. A control system is robust when it has low sensitivities, it is stable over the range of unknown disturbances. Robustness is the sensitivity of effects that are not considered in the analysis and design phase, for example, disturbances, measurement errors, and unmodeled dynamics. The systems should be able to withstand these neglected effects when performing the tasks for which it was designed.

Robustness of a control system is related to its sensitivity to unmodeled dynamics, i.e. part of the behavior of an actual control system which is not included in the mathematical model of the control system (governing differential equations, transfer function, etc.). When we deal with an actual control system, it is impossible (or difficult)

to mathematically model all physical processes. Disturbances such as wind velocity, unexpected outflow, canal roughness etc. cannot be mathematically modeled for an open channel canal. If a control system meets its performance and stability objectives in the presence of all kinds of expected disturbances then the control system is said to be robust. Hence, robustness is a desirable property that dictates whether a control system is immune to uncertainties in its mathematical model. More specifically, robustness can be subdivided into stability robustness and performance robustness, depending upon whether we are looking at the robustness of the stability of a system or that of its performance objectives.

The design of robust control systems is based on two tasks: determining the structure of the controller and adjusting the controller's parameters to give an optimal system performance. This design process is normally done with assumed complete knowledge of performance. This design process is normally done with assumed complete knowledge of the system. The structure of the controller is chosen such that the system's response can meet certain performance criteria. One possible objective in the design of a control system is that the controlled system's output should exactly and instantaneously reproduce its input. That is, the transfer function of the closed-loop system should be unity:

$$F(z) = Y(z)/U(z) = 1 \qquad \text{(Eq. 2.108)}$$

where $Y(z)$ is output and $U(z)$ is input. In practice, this is not possible, since every system will contain inductive and capacitive type components that store energy in some form. Another important goal of a control system design is that the effect on the output of the system due to disturbances is minimized. This we wish to minimize $F(z)/D(z)$ over a

range of frequency. Consider a control system shown in Figure 2.15., where system transfer function $G(z) = Gc(z)G1(z)G_2(z)$ and $D(z)$ is the disturbance. We then have:

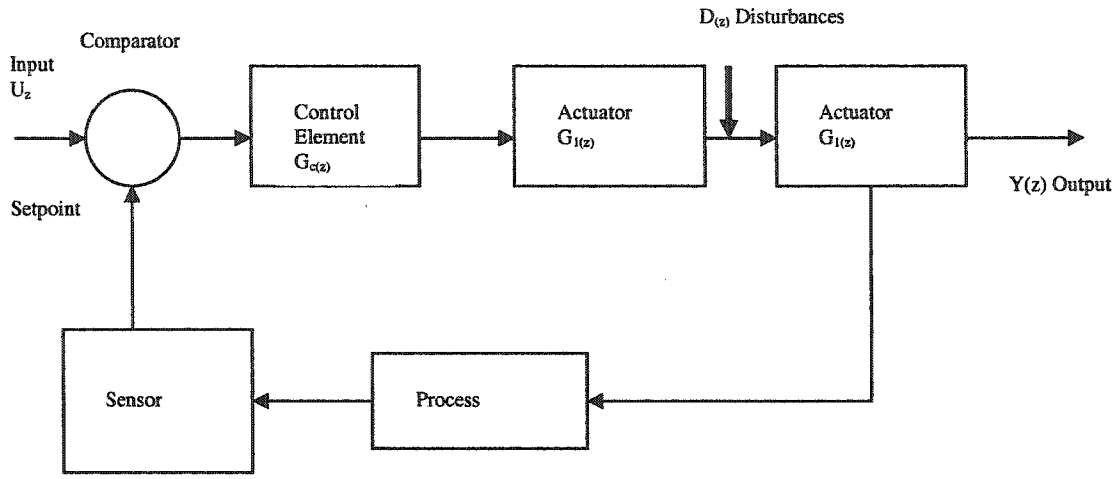

Figure 2.15. A Closed-loop Control System with a Disturbance

$$F(z) = Y(z)/U(z) = (KG(z))/(1+ KG(z)) \qquad \text{(Eq. 2.109)}$$

where K is controller transfer function. Note that both the reference and disturbance transfer functions have the same denominator, or, in other words, they have the same characteristics equation-that is:

$$1 + G_c(z)G_1(z)G_2(z) = 1+ L(z) = 0 \qquad \text{(Eq. 2.110)}$$

Furthermore, we recall that the sensitivity of $T(z)$ with respect to $G(z)$ is:

$$S^T_G = 1/(1+ G_cG_1G_2(z)) \qquad \text{(Eq. 2.111)}$$

and the characteristic equation is the influencing factor on the sensitivity. Equation 2.111 shows that for low sensitivity S we require a high value of loop gain $L(jw)$, but it is known that high gain could cause instability or poor responsiveness of $T(z)$. Thus the designer seeks the following: a) $F(z)$ with wide bandwidth and faithful reproduction of

$U(z)$; b) large loop gain $L(z)$ in order to minimize sensitivity S; c) large loop gain $L(z)$ attained primarily by $G_c(z)G_1(z)$, since $Y(z)/Dz \approx 1/(G_cG_1(z)$.

2.5.1. Robust Control with Loop Transfer Recovery (LTR)

The Controllers utilizing complete state feedback designed via linear quadratic optimal control theory have several impressive properties. There is at least 60^0 phase margin in each input channel. This implies that pure phase changes up to 60^0 can be tolerated in each input channel while guaranteeing the closed-loop stability. There is an infinite gain margin implying that the gain in each channel can be increased indefinitely without loosing stability. Additionally there is a margin of at least 6 dB against gain reductions. However, these impressive properties are generally lacking when a full-state feedback controller (LQR) is implemented via an observer (Kalman) based measurement feedback controller.

For a LQG controlled system with a combined Kalman filter and LQR control law there are no guaranteed stability margins. This was brought starkly to the attention of the control community by Doyle (1979). He showed, by example, that there exist LQG combinations with arbitrarily small gain margins. However, for an LQR controlled system (i.e. assuming all states are available and no stochastic inputs) it is well known (Safonov and Athans, 1977) that, if the weight R is chosen to be diagonal, the sensitivity function $S = (I + K_r(zI - A)^{-1}B)^{-1}$ satisfies:

$$\hat{\sigma}(S(j\omega)) \leq 1, \forall \omega \qquad \text{(Eq. 2.112)}$$

From this it can be shown that the system will have a gain margin equal to infinity, a gain reduction margin equal to 0,5, and a (minimum) phase margin of 60^0 in

each system input control channel. This means that in the LQR controlled system $u = -Kx$, a complex perturbation diag $\{k_i e^{j\theta_i}\}$ can be introduced at the system inputs without causing instability providing: 1) $\theta_i = 0$ *and* $0.5 \leq k_i \leq \infty$, $I = 1, 2, \ldots, m$; 2) $k_i = 1$ *and* $|\theta_i| \leq 60^0$, $i = 1, 2, \ldots, m$; where m is the number of system inputs. A LQR controlled system has good stability margins at the plant inputs, and a Kalman filter has good stability margins at the plant inputs, and no guarantees for LQG control? To answer this, consider the LQG controller shown in Figure 2.16. At points 3 and 4 we have the guaranteed robustness properties of the LQR system and the Kalman filter respectively. But at the actual input and output of the system (points 1 and 2) where we are most interested in achieving good stability margins, we have complex transfer functions which, in general, give no guarantees of satisfactory robustness properties. Notice also that points 3 and 4 are effectively inside the LQG controller which has to be implemented, most likely as software, and so we have good stability margins where they are not really needed and no guarantees where they are. The LQG loop transfer function can be made to approach to target transfer function, with it is guaranteed stability margins, if K in the LQR problem is designed to be large using the sensitivity recovery procedure of Kwakernaak *et al.*, (1969).

The usual guideline in designing an observer is to make its dynamics much faster then the desired state feedback dynamics so that the state reconstruction can be expedited. Thus one might expect that if the eigenvalues of the observer dynamic matrix were to be pushed sufficiently far into the left half complex plane, one would obtain the optimum state feedback properties. Such a speeding up of observer dynamics, however, as shown by Doyle and Stein (1981) does not in general attain the desired results. For left invertible

and minimum phase continuous-time systems, Doyle and Stein (1981) in their historical paper give a method of designing the observer which recovers the optimum state full state feedback properties in an asymptotic sense. Their method, Loop Transfer Recovery (LTR), places some of the observer poles at or near the zeros of the given plant while the

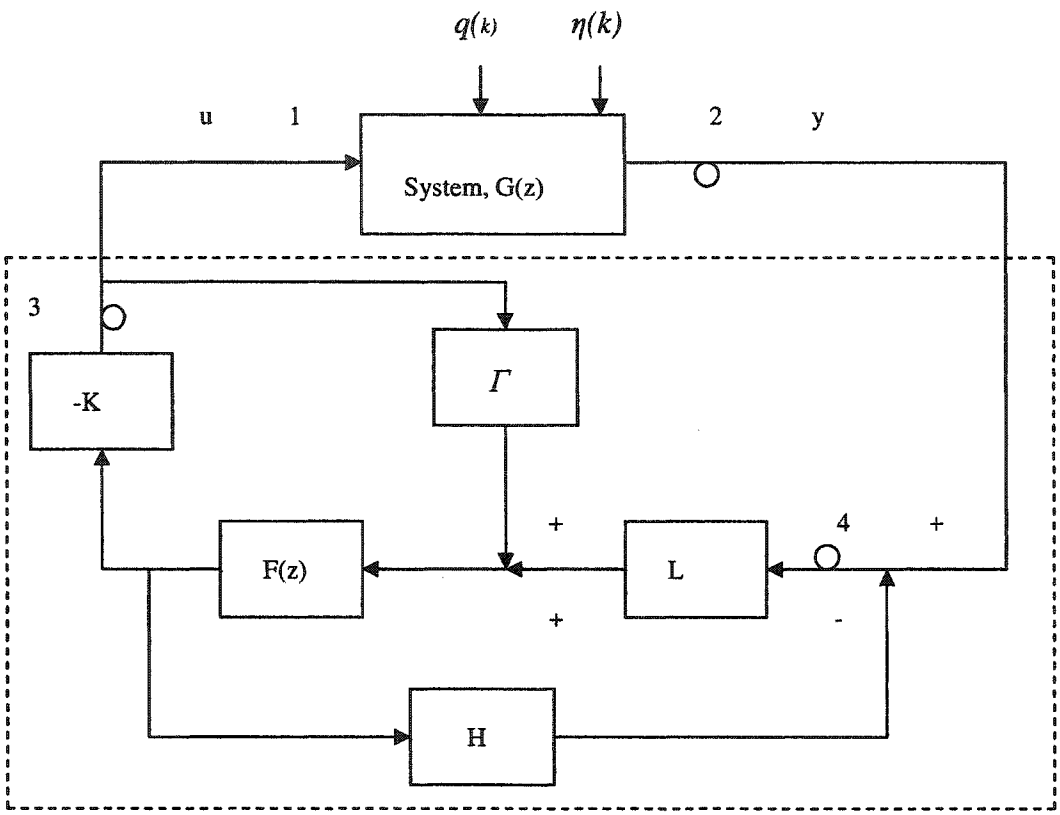

Figure 2.16 LQG Controlled System.

remainder of observer poles are allowed to tend to infinity in order to speed up the observer dynamics. The LTR method of Doyle and Stein (1981) turns out to be a dual of a sensitivity recovery procedure. LTR in general can be considered as a design methodology which falls under the broad category of loop shaping. In loop shaping, many desired performance objectives such as command following, disturbance rejection,

closed-loop bandwidth, stability robustness with respect to unstructured dynamic uncertainties etc, are reflected in frequency domain in terms of the requirements on the singular values of some closed-loop sensitivity and complementary sensitivity functions. Such sensitivity and complementary sensitivity functions are related to some open-loop transfer functions evaluated by breaking the control loop at some critical points, commonly either the input or the output point of the given plant. Thus typically, one is interested in designing a closed-loop control system to arrive at a specified open-loop transfer function. The point where the loop is broken to specify an open-loop transfer function depends on where the expected uncertainties are modeled in a nominal plant model. As explained above, one of the prominent time domain design tools that emerged out of modern control theory is LQG design. By first postulating the use of a state feedback controller, one can resort to utilize the well developed LQR theory to arrive at the necessary state feedback gain that attains the required loop transfer function and thus the required sensitivity and complementary sensitivity functions. Of course, the way of arriving at such a state feedback gain is indeed an engineering art and it often involves the use of cost matrices in the quadratic performance index as free design parameters to be tuned appropriately. The loop transfer function that is attained by a state feedback controller can be termed as a target loop transfer function. The next goal of design will then be to arrive at the target loop transfer function by utilizing only a measurement feedback controller rather then a full state feedback controller. This part of design has come to be known as loop transfer recovery (LTR). Obviously, the above design philosophy, termed as LQG/LTR, has two main steps. In the first step of the method, loop shaping is done utilizing a state feedback controller, and a target loop transfer functions is

prescribed in terms of the state feedback gain. One could utilize LQG theory or any other theory to do this. The next step of design called, LTR, is to recover the target loop transfer function attainable by a state feedback controller by utilizing only a measurement feedback controller. To recover robustness of the Linear Quadratic Gaussian (LQG) controller a loop-shaping technique LTR (Loop Transfer Recovery) procedure is often employed as mentioned above (Doyle 1979).

Loop-shaping technique is an adjustment of the singular values of return ratio matrices to achieve desired closed-loop robustness and performance. This term derived from single-loop systems where scalar return ratios of a loop are to be adjusted. For compensated systems (LQG) based on an observer (i.e. the Kalman filter), generally there is a loss of robustness, when compared to full-state feedback control systems. To recover the robustness properties associated with full-state feedback, the Kalman filter must be designed such that the sensitivity of the plant's input to process and measurement noise is minimized. As seen above, this requires that the smallest singular value of the return ratio at plant's input, $\sigma_{min}[H(z)G(z)]$, should be maximized, where $H(z)$ and $G(z)$ are controller transfer matrix and system transfer matrix, respectively. Theoretically, this maximum value of $\sigma_{min}[H(z)G(z)]$, should be equal to that of the return ratio at the plant's input with full-state feedback. LTR technique is a process of designing a Kalman filter based on compensator to recover the robustness of full-state feedback. Optimal compensators designed with loop transfer recovery are called LQG/LTR compensators. The loop transfer recovery can either be conducted at the plant's the input or at the plant's output. The design of optimal LQG compensators for loop transfer recovery at plant's input can be stated as follows: 1) Design a full-state feedback optimal regulator by selection Q and

R weighting matrices such that the desired performance objectives are met, and the singular values of the return ratio at the plant's input are maximized. With full-state feedback, the return ratio at the plant's input is $H(z)G(z) = -K(zI- \Phi)^{-1}\Gamma$, where Φ and Γ are the plant's state coefficient matrices and K is the full-state feedback regulator gain matrix. 2) Design a Kalman filter by selecting the measurement (R_1) and process noise spectral densities (Q_1) matrices, such that the singular values of the return ratio at the plant's input, $H(z)G(z)$, approach the corresponding singular values with full-state feedback. Hence, R_1, Q_1, are treated as design parameters of the Kalman filter to achieve full-state feedback return ratio at the plant's input, rather than actual parameters of process and measurement noises.

There is no unique set of Kalman filter design parameters R_1, Q_1, to achieve loop transfer recovery. Specifically, if the plant is square (i.e. it has equal number of output and inputs) and minimum phase (i.e. the system's transfer matrix has no zeros in the right-half plane), then by selecting the measurement noise spectral density as $R_1=I$ and $Q_1 = Q_o + \rho I$, where ρ is a scaling parameter, it can be shown from the Kalman filter equations that in the limit $\rho \rightarrow \infty$, the compensated system's return ratio converges to $-K(zI- \Phi)^{-1}\Gamma$ the return ratio of the full-state feedback system at the plant input. In most cases, at the plant output, better loop transfer recovery can be obtained by choosing $Q_1=\rho H^T H$, and making ρ large. However making ρ extremely large reduces the roll-off (i.e. slope of decreasing magnitude with frequency) of the closed-loop transfer function at high frequencies, which is undesirable. Hence, instead of making ρ very large to achieve perfect loop transfer recovery at all frequencies, we should choose a value of ρ which is

sufficiently large to approximately recover the return ratio over a given range of frequencies.

There are three different design techniques for an appropriate design of a LQG control system for the purpose of loop transfer recovery. First one is a non-optimization method of direct eigenstructure assignment scheme, and the other two are optimization based designs. The eigenstructure assignment method yields a controller design which attains any chosen recovery error matrix among a set of admissible recovery error matrices (Saberi *et al.*, 1993). On the other hand, one of the optimization based design method minimizes the H_2 norm and the other the H_∞ norm of the recovery matrix over the set of all possible estimator gains. In discrete-time systems, one does not have the option of assigning the asymptotically infinite eigenvalues, no two or multiple time-scale structure assignment is warranted. Regarding the optimization based design methods, partial results based on the H_2 norm minimization were developed earlier. In discrete-time systems, when one talks about recovery, one need not distinguish between the notations of 'exact' and 'asymptotic' recovery as they both imply one and the same (Saberi *et al.*, 1993).

2.5.2. Robustness Analysis of Control Systems

When an engineer designs a control system, the design is usually based on some mathematical model for the system to be controlled. However, the system model is only an approximation. In reality the system may behave differently than the model indicates, or the disturbances may vary with time. In practice, though, the control systems that are designed on the basis of some system model often work quite well. To test the stability of

the control systems there are several robustness analysis methods which show how robust a control system is to system uncertainties. That is, given a stable control system, how much can the system gain change before the system becomes unstable (i.e., what are the gain margins of the system)? How much can the phase shift change before the system becomes unstable (i.e., what is the phase margin of the system). Bode diagrams, Nyquist polar plot and diagrams, Singular Values, and Structured Singular Value (μ analysis) are the methods to test the robustness of a control system.

Typical Bode diagram contains two plots in rectangular coordinates, in which the magnitude is expressed in decibels (dB), and the phase angle in degrees, both plotted as functions of the logarithm of frequency in rad/unit time (normally, rad s^{-1}). Bode diagrams are normally plotted on semi-logarithmic graph paper, so that the dB values plotted on the linear vertical axis have the effect of producing a logarithmic scale, while the frequency values can be plotted directly on the horizontal axis, allowing the logarithmic axis to do the work of conversion. The frequency response magnitude ratio is expressed in decibels using:

$$M(\omega)_{dB} = 20 \log_{10} M(\omega) \qquad \text{(Eq. 2.113)}$$

where $M(\omega)_{dB}$ is the log modulus in decibels and $M(\omega)$is the magnitude ratio. Typical Bode plots are show in Figure 2.17. For convenience, the two types of diagram are shown together. As usual, the magnitude ratio falls off and the phase angle becomes increasingly lagging with increasing frequency. One of the main reasons for using a logarithmic scale for the magnitude ratio is the ease with which the dynamic elements in a control loop can be manipulated. At a given frequency, the magnitude ratio is obtained by multiplying together the individual magnitude ratios of the elements (which becomes adding in dB),

and the phase angle is obtained by summing individual phase angle elements. For a control system having input $U(t)$ and output $Y(t)$, the transfer function model is defined as the z transformed output $Y(z)$ divided by input $U(z)$, such that:

$$Y(z)/U(z) = F(z) \qquad \text{(Eq. 2.114)}$$

Consider the Bode form of a transfer function $F(z)$ for which the frequency response is:

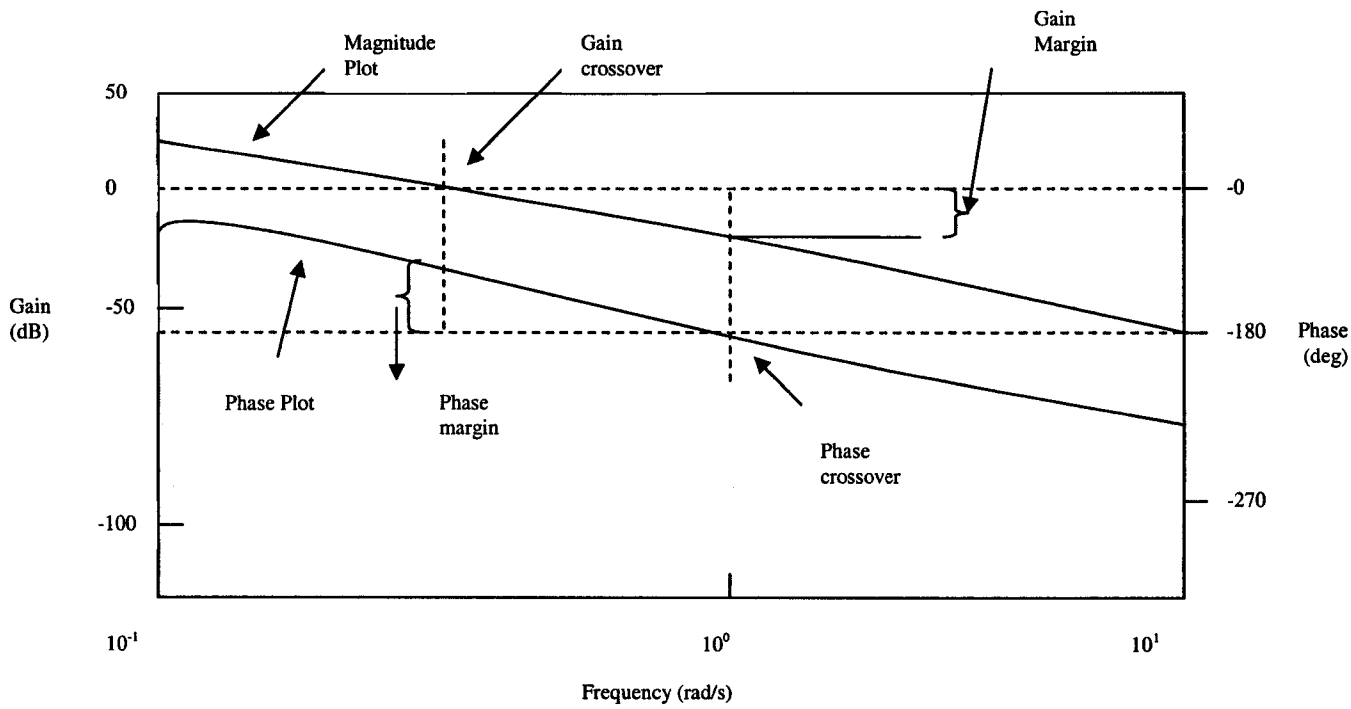

Figure 2.17 Stability Margins on Bode Diagram.

$$F(j\omega) = K_B \frac{\prod_{i=1}^{m} [1+j(\omega/z_i)]}{(j\omega)^r \prod_{i=1}^{n-r} [1+j(\omega/p_i)]} \qquad \text{(Eq. 2.115)}$$

where K_B is Bode gain, m and n are the numbers of terms in the numerator and denominator, respectively, z_i and p_i are the non-zero finite zeros and poles respectively of $F(z)$, r is system type. A constant K_B provides a magnitude contribution of $20\ log_{10}\ |K_B|$

and a phase angle of 0^0 if K_B is positive, or -180^0 if K_B is negative. If $K_B = 1$, then $20 \log_{10}$ $|K_B|$ is zero dB; if $K_B = 2$, then the *dB* magnitude is 6 and if $K_B = 0.5$, the *dB* magnitude is -6. In all three cases the phase angle contribution is 0^0. For K_B = -2 or -0.5, the *dB* magnitude would be 6 or -6, respectively, but the phase contribution would be -180^0.

The Nyquist stability diagrams were developed in 1932 as a graphical method of determining the stability of a linear feedback control systems. Nyquist diagrams are particularly useful as they can be sued to determine the closed-loop stability of a system directly from an open-loop plot. The Nyquist criterion determines a closed-loop system's stability usingthe complex-variable theory. It employs a polar plot of the open-loop frequency response, $G(i\omega)H(i\omega)$, as ω increases from $-\infty$ to ∞. Such a polar plot is called a Nyquist plot. In the z-plane, the imaginary axis denotes an increase of ω from $-\infty$ to ∞ is said to be a mapping in the $G(z)H(z)$ plane (i.e. the plane defined by real and imaginary parts of $G(z)H(z)$) of all the points on the imaginary axis in the z-plane. The direction of the Nyquist plot indicates the direction of increasing ω. A polar plot is usually restricted to ω between 0 and ∞. However, note that a polar plot of $G(i\omega)H(i\omega)$ drawn for negative frequencies is the complex conjugate of the polar plot of $G(i\omega)H(i\omega)$ drawn for positive frequencies. In other words, the Nyquist plot is symmetrical about the real axis. Hence, the practical technique of plotting Nyquist plot is to first make the polar plot for ω increasing from 0 and ∞, and then draw a mirror image of the polar plot (about the ral axis) to represent the other half of the Nyquist plot (i.e. the frequency range $-\infty < \omega < 0$). The direction of the mirror image polar plot would be clear from the $\omega = 0$ point location on the original polar plot, where the two plots should necessarily meet. The two mirror images should also meet at $\omega \rightarrow \infty$ and $\omega \rightarrow -\infty$, respectively. Hence, $\omega \rightarrow \pm\infty$ is a single

point on the Nyquist plot and the positive and negative frequency branches of a Nyquist plot from a closed contour. It is quite possible that the two polar plots for positive and negative frequencies of some functions may overlap. Since the Nyquist plot of $G(z)H(z)$ is a closed contour for $z = i\omega$ when $-\infty < \omega < \infty$, whose direction is indicated by increasing ω, the only possibility of the positive and negative frequency branches meeting at $\omega \rightarrow \pm\infty$ is that the Laplace variable, s, must traverse an infinite semi-circle in the right-half z-plane. In other words, the region enclosed by the Nyquist plot in the $G(z)H(z)$ plane is a mapping of the entire right half z-plane. The Nyquist plot of $G(z)H(z)$ can be utilized to convey information about a system's stability robustness (i.e. how robust is the stability of the system with respect to variations in the system's model). From Nyquist stability theorem, the closed-loop system's stability is determined from the encirclements by the locus of $G(z)H(z)$ of the point -1 in the $G(z)H(z)$ plane. Therefore, a measure of stability robustness can be how far away the locus of $G(z)H(z)$ is to the point -1, which indicates how far the system is from being unstable. The farther away the $G(z)H(z)$ locus is form -1, the greater is its stability robustness, which is also called the margin of stability. The closest distance of $G(z)H(z)$ from -1 can defined in the complex $G(z)H(z)$ plane by two quantities, called the gain margin and phase margin which are illustrated in Figure 2.17 depicting a typical Nyquist diagram for a stable closed loop system. A circle of unit radius is overlaid on the Nyquist plot. The closest distance of the Nyquist plot of $G(z)H(z)$ to -1 is indicated by two points A and B. Point A denotes the intersection of $G(z)H(z)$ with the negative real axis nearest to the point -1, while point B denotes the intersection of $G(z)H(z)$ with the unit circle. Point A is situated at a distance α from the origin, while point B is located on the unit circle at an angle of θ from the

positive real axis. It is clear that the gain of $G(z)H(z)$ at point B is unity, while its phase at the same point is θ. The gain margin is defined as the factor by which the gain of $G(z)H(z)$ can be increased before the locus of hits the point -1. From Figure 2.18, it is evident that the gain margin is equal to $1/\alpha$, or in dB it is given by

$$Gain\ Margin\ in\ dB = 20*\log_{10}(1/\alpha) \qquad \text{(Eq. 2.116)}$$

A negative gain margin indicates that the system is unstable. The phase margin is defined as the difference between the phase of $G(z)H(z)$ at the point B, θ, and the phase of the negative real axis, -180^0 (on which the point -1 is located). Thus, phase margin is given by the angle β in Figure 2.17:

$$Phase\ Margin = \beta = \theta - (-180^0) = \theta + 180^0 \qquad \text{(Eq. 2.117)}$$

The Nyquist stability diagrams continue to be useful but most real control systems are multiple-input-multiple-output (MIMO) and hence are not amenable to robustness analysis via the Nyquist criterion.

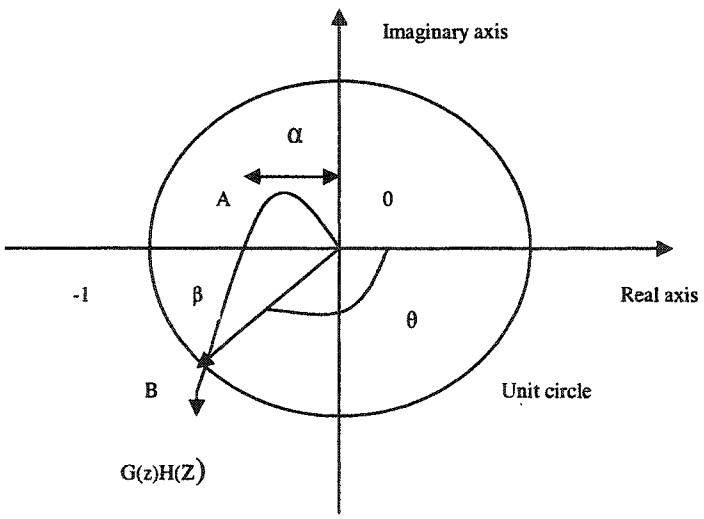

Figure 2.18. The Nyquist Plot of G(z)H(z) Showing the Gain and Phase Margin.

The singular values help us analyze the properties of a multivariable feedback (called a multi-loop) system in a manner quite similar to a single-input, single-output feedback (called in a single-loop) system. For analyzing robustness, we can treat the largest and smallest singular values of a return difference (or return ratio) matrix as providing the upper and lower bounds on the scalar return difference (or return ratio) of an equivalent single-loop system. For example if system transfer matrix is $G(z)$ and feedback controller matrix $H(z)$, then to maximize robustness with respect to the process noise, we should minimize the singular values of the sensitivity matrix, $[I+G(z)H(z)]^{-1}$ which implies minimizing the largest singular value, $\sigma_{max}[\{I + G(z)H(z)\}^{-1}]$, or maximizing the singular values of the return difference matrix at the output, i.e. maximizing $\sigma_{min}[I + G(z)H(z)]$. The latter requirement is equivalent to maximizing the smallest singular value of the return ratio at the output, $\sigma_{min}[G(z)H(z)]$. Similarly, minimizing the sensitivity to the measurement noise requires minimizing the largest singular value of the matrix $[I-\{I+G(z)H(z)\}^{-1}]$, which is equivalent to minimizing the largest singular value of the return ratio at the output, $\sigma_{max}[G(z)H(z)]$, On the other hand, tracking a desired output, $Y_d(z)$, requires that the sensitivity to $Y_d(z)$ be maximized, which requires maximizing $\sigma_{min}[I - \{I + G(z)H(z)\}^{-1}]$, which is equivalent to minimizing $\sigma_{min}[G(z)H(z)]$. Also, optimal control (i.e. minimization of control input magnitudes) requires minimization of $\sigma_{max}[H(z)\{I + G(z)H(z)\}^{-1}]$, or alternatively, a minimization of $\sigma_{max}[H(z)]$. In summary, the following conditions on the singular values of the return ratio at output result from robustness, optimal control and tracking requirements: a) For robustness with respect to the process noise, $\sigma_{min}[G(z)H(z)]$ should be maximized; b) for robustness with respect to the measurement noise, $\sigma_{max}[G(z)H(z)]$, should be minimized;

c) For optimal control, $\sigma_{max}[H(z)]$ should be minimized; d) for tracking a changing desired output, $\sigma_{min}[G(z)H(z)]$ should be maximized. Clearly, the second requirement conflicts with the first and the fourth. Also, since $\sigma_{max}[G(z)H(z)] \leq \sigma_{max}[G(z)]\ \sigma_{max}[H(z)]$ (a property of scalar norms), the third requirement is in conflict with the first and the fourth. However, since measurement noise usually has a predominantly high-frequency content (i.e. more peaks in the power spectrum at high frequencies), we achieve a compromise by minimizing $\sigma_{max}[G(z)H(z)]$ (and $\sigma_{max}[H(z)]$) at high frequencies, and maximizing $\sigma_{min}[G(z)H(z)]$ at low frequencies. In this manner, good robustness properties, optimal control, and tracking system performance can be obtained throughout a given frequency range. The singular values of the return difference matrix at the output in the frequency domain $\sigma[I + G(i\omega)H(i\omega)]$, can be used to estimate the gain and phase margins of a multivariable system. One can make singular value plots against frequency, ω, in a similar manner as the Bode gain plots. The way in which multivariable gain and phase margins are defined with respect to the singular values is as follows: take the smallest singular value, σ_{min}, of all the singular values of the return difference matrix at the output, and find a real constant, a, such that $\sigma_{min}\ [I + G(i\omega)] \geq a$ for all frequencies, ω, in the frequency range of interest. Then the gain and phase margins can be defined as follows:

$$Gain\ Maring = 1/(1 \pm a) \qquad \text{(Eq. 2.118)}$$

$$Phase\ Margin = \pm 2sin^{-1}(a/2) \qquad \text{(Eq. 2.119)}$$

The adjustment of the singular values of return ratio matrices to achieve desired closed-loop robustness and performance is called loop shaping. This term derived from single-loop systems where scalar return ratios of a loop are to be adjusted. For

compensated systems based on an observer (i.e. the Kalman filter), generally there is a loss of robustness, when compared to full-state feedback control systems. To recover the robustness properties associated with full-state feedback, the Kalman filter must be designed such that the sensitivity of the plant's input to process and measurement noise is minimized. This requires that the smallest singular value of the return ratio at plant's input, $\sigma_{min}[H(z)G(z)]$, should be maximized. Theoretically, this maximum value of $\sigma_{min}[H(z)G(z)]$ should be equal to that of the return ratio at the plant's input with full-state feedback. As mentioned above such a process of designing a Kalman filter based compensator to recover the robustness of full-state feedback is called loop transfer recovery (LTR). Optimal compensators designed with loop transfer recovery are called LQG/LTR compensators.

The structured singular value (μ analysis, SSV) can be used to determine the stability of a system that is subject to structured perturbations. SSV is a function which provides a generalization of the singular value, σ, and the spectral radius, ρ. SSV is used to get necessary and sufficient conditions for robust stability and also for robust performance. SSV is defined the smallest structured perturbation, Δ (measured in terms of $\sigma(\Delta)$), which makes $det(I-M\,\Delta) = 0$ *then* $\mu(M) = 1/\sigma(\Delta)$. M represents a system transfer function. Clearly, $\mu(M)$ depends on not only on M but also on the allowed structure for Δ. Also SSV depends on the structure of Δ. If Δ is a diagonal matrix, then we need a larger perturbation to make $det(I-M\,\Delta) = 0$. If Δ is a full matrix, then we need smaller Δ which yields singularity has $\sigma(\Delta) = 1/\sigma(M)$ and we have $\mu(M) = \sigma(M)$. Mathematically $\mu(M)$ can be defined:

$$\mu(M) = \frac{1}{\min\{k_m | \det(I - k_m M \Delta) = 0 \text{ for structured } \Delta,\ \sigma(\Delta) \leq 1\}} \qquad \text{(Eq. 2.120)}$$

k_m is a factor. If no such structured Δ exists then $\mu(M) = 0$. A value of $\mu = 1$ means that there exists a perturbation with $\sigma(\Delta) = 1$ which is just large enough to make $I - M\Delta$ singular. A largest value of μ is bad as means a smaller perturbation makes $I - M\Delta$ singular, whereas a smaller value of μ is good. To fine factor k_m by which the system robustly stable, we scale the uncertainty Δ by k_m, and look for the smallest k_m which yields borderline instability, namely $\det(I - k_m M\Delta) = 0$. From the definition of μ in this value is $k_m = 1/\mu(M)$. If we assume that the nominal system M and the perturbations Δ are stable, then the $M\Delta$ system is stable for all allowed perturbations with $\sigma(\Delta) \leq 1, \Delta\omega$, if and only if

$$\mu(M(j\omega)) < 1, \Delta\omega \qquad \text{(Eq. 2.121)}$$

In other words, if $\mu(M) < 1$, then $k_m > 1$, so if $\mu(M) < 1$ at all frequencies the required perturbation Δ to make $\det(I - M\Delta) = 0$ is larger than 1, and the system is stable. On the other hand, if $\mu(M) = 1$, then $k_m = 1$, so if $\mu(M) = 1$ at some frequency there does exist a perturbation with $\sigma(\Delta) = 1$ such that $\det(I - M\Delta) = 0$ at this frequency, and the system is unstable.

CHAPTER 3

METHODOLOGY

3.1. Introduction

A robust control procedure for open-channel water distribution systems was developed with two primary objectives in mind. The first objective was to provide the means whereby a system would react to changes in the amount of water being delivered out of the system. The second objective was to establish a high level of operational performance in the system, where performance is measured in terms of the stability of the water surface elevations in the system being controlled under external unknown disturbances. The highest level of performance is represented by a system in which water surface elevation does not deviate from its designated target elevation. Accordingly, the level of performance decreases in direct proportion to the magnitude and duration of the deviation between the controlled or actual water surface elevation and the target elevation. The control procedure, which is a robust control as described in Chapter II, was developed in the form of a computer algorithm.

Mathematical analysis and hydraulic engineering are combined to form a basis for the control algorithm. The present and future status of each control structure was modeled using a set of finite-difference equations. Knowledge about the performance of the control structures and the reaction of the system to changes at these control structures was provided through an understanding of the principles of hydraulic engineering. The inputs

to this control algorithm are the change in water surface elevation and flow rate at each computational node of the model, plus the cumulative variation in water surface elevation upstream of each control structure. The output is an adjustment in the position, or opening, of the gates in the canal. The mathematical model also simulates unsteady flow in gated open-channels. In order to control the system, the control structures in the canal must be instrumented and monitored. If there is one turnout upstream of each control structure, the requirements for monitoring are essentially doubled if each delivery point and each control structure is to be monitored. The monitoring requirement increases proportionally if there are additional delivery points. Thus, it is desirable to develop a control procedure that relied only on monitoring at the control structures and did not require monitoring at each of the turnouts.

Monitoring at the control structures is also a viable approach to answering the question of whether or not the system becomes unstable or approaches stability at an elevation other than the target elevation. The monitoring location should be selected at a point that provides the best intelligence to relate downstream demands to upstream inflow and to provide stability of control. This generally means that the monitoring location should be at the downstream end of the reach of canal, namely immediately upstream of the control structures. Downstream control forms the basic framework for the present control algorithm. Downstream control provides for a demand-type operation in which the overall operation is controlled by the amount of water needed to satisfy the delivery requirements. Downstream control minimizes operational waste because the amount of water being supplied to the turnout is determined by the demand. The control algorithm uses the monitored value of water surface elevation upstream of each control structure in

the system during each control cycle and, if necessary, computes an adjustment in gate opening at each structure under external unknown disturbances.

3.2. Algorithm Development

The control algorithm developed consists of four different parts. The first part defines the global variables, calls data from input files, computes initial flow rates and elevations at all nodes and calculates steady backwater profile in the gated open-channel. The second part computes coefficients for the linear state variable description of the system. In this part, the algorithm calculates the coefficients of the continuity and the momentum equations. The third part designs an optimal feedback controller in order to maintain the target water levels (or volumes) in the pools at specified values. In the presence of random disturbances acting on the system, the control structures (gates) in the irrigation canal are frequently adjusted. Robustness analysis of linear quadratic regulator is also done in this part using singular values and Bode diagrams. Fourth part is related to design of an observer, combination of observer and full-state feedback and adjustments for the robustness properties of the control system and robustness analysis of the compensator. To minimize the divergence between estimated and actual values of the state variables, the random nature of the disturbances and measurements must be incorporated into the state estimation equation.

3.2.1. Initial Steady Backwater Profile Computations

The control algorithm starts with defining the global variables and calling the data from input files. Input files have pool, gate and turnout data. Gate data includes gate width,

gate coefficient, sill height, drop at the gates, and target depth upstream of gates in the pools. Pool input file specifies length increment, pool bottom width, pool side slope, pool bottom slope, pool roughness, and turnout initial flow rate. In the algorithm, there are three node types: gate (nodetype2), turnout (nodetype3) and computational (nodetype1). Turnout data defines turnout flow rate, structure geometry, initial flow rate, and discharge coefficient. As shown in Figure 3.1, the lateral canals were assumed to be located immediately upstream of the gate node in each pool.

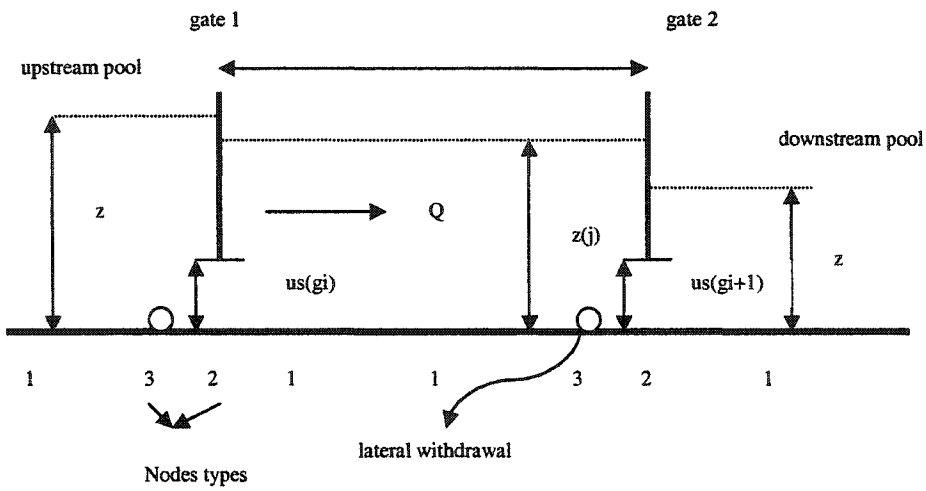

Figure 3.1. Schematic of an Irrigation Canal Pool

At the beginning, the control algorithm calculates initial flow rates and elevations at all nodes with the following equation:

$$Q(j)=Q(j+1)+q(j);\ EL(j)=EL(j+1)+So(j)Dx(j) \qquad \text{(Eq. 3.1)}$$

in which j = number of nodes, $Q(j)$=flow rate through the channel at node j, m^3/s; $q(j)$=turnout demand at node j, m^3/s; $EL(j)$=elevation at node j, m; $So(j)$=channel bottom slope downstream of node j, $Dx(j)$=length increment of section j, m. After calculating

the initial values at all nodes the algorithm computes the initial steady state backwater profile.

If the node type is 2 (a gate node), the initial values are calculated as follows:

$$us(gi)=Q(j)/(Cd(gi)b(gi)\ sqrt(2g(Y(j)-Y(j+1)))); \quad Z(j)=EL(j)+Y(j) \qquad \text{(Eq. 3.2)}$$

in which $us(gi)$ = height of the gate opening of the structure at gate gi, m; $Q(j)$ = discharge rate at node j, m^3/s; $Cd(gi)$ = gate discharge coefficient at gate gi; $b(gi)$ = bottom width of gate at gate gi, m; g = acceleration of gravity, m^2/s; $Y(j)$ = water depth at node j, m; $Y(j+1)$ = water depth at node $j+1$, m; $Z(j)$ = water surface elevation at node j, m; $EL(j)$ = channel bottom elevation at node j, m.

If the node type is 3 (a turnout node), then the algorithm calculates initial values with the following equations:

$$Y(j)=Y(j+1); \quad Z(j)=EL(j)+Y(j) \qquad \text{(Eq. 3.3)}$$

Finally for the computational node (nodetype1), the algorithm computes the initial values using some subroutines and functions Figure 3.2 as follows:

$$[T,A,R]=geom(Y(j+1),Z(j+1),B(j+1)) \qquad \text{(Eq. 3.4)}$$

$$V=Q(j+1)/A; \qquad SFJ1=Q(j+1)^2*n(j+1)^2/(A^2*R^{4/3}) \qquad \text{(Eq. 3.5)}$$

$$CONST=EL(j)-EL(j+1)-Y(j+1)-V^2/(2*G)-SFJ1/2*Dx(j);\ YI=Y(j+1) \qquad \text{(Eq. 3.6)}$$

$$c1=B(j);\ c2=z(j);\ c3=n(j);\ c4=Dx(j);\ c5=Q(j);\ Y(j)=fzero('nrap',YI,0.001) \qquad \text{(Eq. 3.7)}$$

```
function [T,A,R]=geom(Y,z,B)
A=(B+z*Y)*Y; P=B+2*Y*sqrt(1+z^2);
R=A/P; T=B+2*z*Y;
```

Figure 3.2. Geom subroutine

Equation 3.4 calculates canal properties according to variables; water depth, Y, water surface elevation, Z, and bottom width of canal, B, at node $j+1$ using *geom* subroutine

(Figure 3.2). In this equation, *T, A, R* represent top width, flow area and hydraulic radius at node *j+1* respectively. Equation 3.5 computes friction slope, *SFJ1*, and velocity, *V*, at node *j* in the canal. Equation 3.6 calculates a constant value for *nrap* subroutine (Figure 3.3). *c1*, *c2*, *c3*, *c4* and *c5* are constant values and are used in the subroutine *nrap*. *Nrap* subroutine calculates the free surface profile in gradually varied flow. The subroutine is based on the Manning equation for friction slope and the solution employs the Newton-Raphson approximation (Rhodes 1995). Newton-Raphson approach uses standard step method for computations and this method has two advantages over the direct step method: 1) water depth is calculated at prescribed stations as required, without the need for interpolation; 2) the application is not limited to prismatic channels. In Equation 3.7, the function *fzero* of MATLAB is used to compute depth of water depending on *nrap* subroutine at node *j*. The function uses 0.001 as an error tolerance. The algorithm proceeds from the most downstream node in the system, and computes the flow depth and flow rate at the next upstream node using an initial guess and an iterative procedure presented in *nrap*. This procedure repeated until the computations reaches the first node in the canal.

```
function f=nrap(x);
global CONST c1 c2 c3 c4 c5; G=9.81; f(1)=x(1)+c5^2/(2*G)/((c1+c2*x(1))*x(1))^2-
c5^2*c3^2/2/(((c1+c2*x(1))*x(1))^(10/3)/(c1+2*x(1)*sqrt(1+c2^2))^(4/3))*c4+CONST;
```

Figure 3.3. Nrap Subroutine

3.2.2. Computation of Coefficients for Linear State Variable Description of the System

In the operation of irrigation canals, decisions regarding the gate openings in response to arbitrary (random) changes in water withdrawal rates into lateral or branch canals are

required to maintain the depth of flow or the volume of water in a given pool at a target value. This problem is similar to the process-control problem in which the state of the system is maintained close to the desired value by using real-time feedback control. Linear control theory is well developed and is easier to apply than nonlinear control theory. In this study, as explained in Chapter 2, to apply the linear control theory, the Saint-Venant nonlinear, hyperbolic partial differential equations of open-channel flow were linearized about an average operating point. In Chapter 2, the continuity equation for an open-channel flow was defined as follows:

$$\partial A/\partial t + \partial Q/\partial x = q_i \qquad \text{(Eq. 3.8)}$$

After applying the Preissmann implicit finite-difference scheme to the continuity equation, the following equation was obtained (Malaterre 1995d):

$$((A^+_{j+1} + A^+_j)/2\Delta t) - ((A_{j+1} + A_j)/2\Delta t) + (\theta/\Delta x)(Q^+_{j+1} - Q^+_j) +$$

$$((1-\theta)/\Delta x)(Q_{j+1} - Q_j) = (\theta/2)(q^+_{j+1} + q^+_j) + ((1-\theta)/2)(q_{j+1} + q_j) \qquad \text{(Eq. 3.9)}$$

in which A = flow cross-section at node $j+1$, m^2; θ = weighting factor, and q = the lateral flow per unit channel length, m^2/s. In Equation 3.9, A^+, A, Q^+, Q, q^+, q represent A^{n+1}, A^n, Q^{n+1}, Q^n, q^{n+1} and q^n, respectively (Figure 2.11). If we assume $q^+_{j+1} = q_{j+1} = q_{je}$ and $q^+_j = q_j = q_{ie}$, then Equation 3.9 can be rewritten as follows:

$$1/(2\Delta t)(A^+_{j+1} + A^+_j) - 1/(2\Delta t)((A_{j+1} + A_j)) + \theta/\Delta x(Q^+_{j+1} - Q^+_j) +$$

$$(1-\theta)/\Delta x(Q_{j+1} - Q_j) = (q_{je} + q_{ie})/2 \qquad \text{(Eq. 3.10)}$$

Using the Taylor series around the average operating point, and truncating terms higher a first-order, the deviation variables were obtained as follows:

$$Q^+ = Q^{e+} + \delta Q^+ \qquad \text{(Eq. 3.11)}$$

$$z^+ = z^{e+} + \delta z^+ \qquad \text{(Eq. 3.12)}$$

in which Q^{e+} and z^{e+} are the flow rate and water surface elevation respectively, at the equilibrium condition; and δQ^{+} and δz^{+} are the deviations in flow rate and water surface elevation respectively, from the equilibrium condition. If we assume that the flow area, A, at j, is equal to $B\ \delta z$, then we can rewrite Equation 3.10 as follows:

$$1/(2\Delta t)(B_j)(\delta z^{+}_j - \delta z^{+}_j) + 1/(2\Delta t)(B_{j+1})((\delta z_{j+1} - \delta z_j)) + \theta/\Delta x(\delta Q^{+}_{j+1}) -$$

$$(\delta Q^{+}_j) + (1-\theta)/\Delta x(\delta Q_{j+1} - \delta Q_j) = -(Q_{j+1} - Q_j)/\Delta x + (q_{je} + q_{ie})/2 \qquad \text{(Eq. 3.13)}$$

Equation 3.13 can be rewritten as follows:

$$-\theta/\Delta x(\delta Q^{+}_j) + 1/(2\Delta t)(B_j)(\delta z^{+}_j) + \theta/\Delta x(\delta Q_{j+1}) + 1/(2\Delta t)(B_{j+1})(\delta z^{+}_{j+1}) =$$

$$(1-\theta)/\Delta x(\delta Q_j) + 1/(2\Delta t)(B_j)(\delta z_j) - (1-\theta)/\Delta x(\delta Q_{j+1}) + 1/(2\Delta t)(B_{j+1})(\delta z_{j+1}) +$$

$$(q_{je} + q_{ie})/2 - (Q_{j+1} - Q_j)/\Delta x \qquad \text{(Eq. 3.14)}$$

Equation 3.14 is used in the control algorithm to calculate right and left hand side of the coefficients appearing in the continuity equation at a computational node. It is possible to combine the terms in Equation 3.14 according to:

$$\alpha_1 = 1/\Delta x; \quad \alpha_{2j} = B_j/2\Delta t \qquad \text{(Eq. 3.15)}$$

$$A_{11} = -\theta/\Delta x = -\theta\alpha_1 \qquad \text{(Eq. 3.16)}$$

$$A_{12} = B_j/2\Delta t = \alpha_{2j} \qquad \text{(Eq. 3.17)}$$

$$A_{13} = \theta/\Delta x = \theta\alpha_1 \qquad \text{(Eq. 3.18)}$$

$$A_{14} = B_{j+1}/2\Delta t = \alpha_{2j+1} \qquad \text{(Eq. 3.19)}$$

$$A'_{11} = (1-\theta)/\Delta x = (1-\theta)\alpha_1 \qquad \text{(Eq. 3.20)}$$

$$A'_{12} = B_j/2\Delta t = \alpha_{2j} \qquad \text{(Eq. 3.21)}$$

$$A'_{13} = -(1-\theta)/\Delta x = -(1-\theta)\alpha_1 \qquad \text{(Eq. 3.22)}$$

$$A'_{14} = B_{j+1}/2\Delta t = \alpha_{2j+1} \qquad \text{(Eq. 3.23)}$$

$$C_1 = (q_{je} + q_{ie})/2 - (Q_{j+1} - Q_j)/\Delta x \qquad \text{(Eq. 3.24)}$$

in which A_{11}, A_{12}, A_{13} and A_{14} are the coefficients for left-hand side of the continuity equation. A'_{11}, A'_{12}, A'_{13} and A'_{14} are the coefficients for the right-hand side of the continuity equation. Using the above equations, the continuity equation can be rewritten for a computational node as follows:

$$A_{11}\delta Q^{+}_{j} + A_{12}\delta z^{+}_{j} + A_{13}\delta Q^{+}_{j+1} + A_{14}\delta z^{+}_{j+1} =$$

$$A'_{11}\delta Q_{j} + A'_{12}\delta z_{j} + A'_{13}\delta Q_{j+1} + A'_{14}\delta z_{j+1} + C_{1} \qquad \text{(Eq. 3.25)}$$

The control algorithm assumes the weighting coefficient $\theta = 0.65$, time step $\Delta t = 30$ seconds, and $m = j+1$. Row indices of continuity and dynamic equations are calculated as follows:

$$ic=j*2-1-gi-2*li \qquad \text{(Eq. 3.26)}$$

$$mc=j*2-gi-2*li \qquad \text{(Eq. 3.27)}$$

$$jc=(j-1)*2+1-gi-2*li \qquad \text{(Eq. 3.28)}$$

in which *ic* and *mc* are row indices of continuity and momentum equations, respectively, *gi* = index of gates, *li* = index of turnouts and *jc* = column index of continuity and dynamic equations. In the control algorithm, Equations 3.15 through 3.24 were used to calculate the left and right-hand side coefficients of the continuity equation for row *ic* as follows:

$$\alpha_1=1/Dx(j);\ \alpha_{2j}=T(j)/(2dt);\ \alpha_{2m}=T(m)/(2dt) \qquad \text{(Eq. 3.29)}$$

$$AL(ic,jc1)=-theta\ \alpha_1 \qquad \text{(Eq. 3.30)}$$

$$AL(ic,jc2)=\alpha_{2j} \qquad \text{(Eq. 3.31)}$$

$$AL(ic,jc3)=theta\ \alpha_1 \qquad \text{(Eq. 3.32)}$$

$$AL(ic,jc4)=\alpha_{2m} \qquad \text{(Eq. 3.33)}$$

$$AR(ic,jc1)=(1-theta)\ \alpha_1 \qquad \text{(Eq. 3.34)}$$

$$AR(ic,jc2) = \alpha_{2j} \quad \text{(Eq. 3.35)}$$

$$AR(ic,jc3) = -(1\text{-}theta)\,\alpha_1 \quad \text{(Eq. 3.36)}$$

$$AR(ic,jc4) = \alpha_{2m} \quad \text{(Eq. 3.37)}$$

in which AL = left hand side of coefficients; AR = right hand side of coefficients; $Dx(j)$ = length between two nodes, m; $T(j)$ = top width of the canal at node j, m; $T(m)$ = top width of the canal at node m, m; dt = time period, sec; and θ = weighting factor. Using above equations, the continuity equation at node j can be rewritten as follows:

$$AL(ic,jc1)\delta Q^{+}j + AL(ic,jc2)\delta z^{+}_{j} + AL(ic,jc3)\delta Q^{+}_{j+1} + AL(ic,jc4)\delta z^{+}_{j+1} =$$

$$AR(ic,jc1)\delta Q_j + AR(ic,jc2)\delta z_j + AR(ic,jc3)\delta Q_{j+1} + AR(ic,jc4)\delta z_{j+1} + C_1 \quad \text{(Eq. 3.38)}$$

After calculating the coefficients for the continuity equation, the model starts to calculate coefficients for the dynamic equation for a computational node. As explained in Chapter 2, the dynamic equation for an open-channel flow is as follows:

$$\partial Q/\partial t + (\partial Q^2/A)/\partial x + gA\partial z/\partial x + gAS_f = 0 \quad \text{(Eq. 3.39)}$$

in which $S_f = Q^2n^2/A^2R^{4/3}$ = friction slope. After discertization of the first term of Equation 3.39 with Preissmann scheme, the following equations are obtained:

$$\partial Q/\partial t = (Q^{+}_{j+1} + Q^{+}_{j})/\Delta t - (Q_{j+1} + Q_j)/\Delta t = (1/2\Delta t)\,\delta Q^{+}_{j} + (1/2\Delta t)\,\delta Q^{+}_{j+1} -$$

$$(1/2\Delta t)\,\delta Q_j - (1/2\Delta t)\,\delta Q_{j+1} \quad \text{(Eq. 3.40)}$$

If we assume $\alpha_3 = 1/(2\Delta t)$, then Equation 3.40 can be written:

$$\partial Q/\partial t = \alpha_3(\delta Q^{+}_{j+1} + \delta Q^{+}_{j} - \delta Q_{j+1} + \delta Q_j) \quad \text{(Eq. 3.41)}$$

The second part of Equation 3.39 can be rewritten with discertization as follows:

$$(\partial Q^2/A)/\partial x = (1-\theta)/\Delta x[\,Q^2_{j+1}/A_{j+1} - Q^2_j/A_j\,] +$$

$$\theta/\Delta x\,[\,Q^{2+}_{j+1}/A^{+}_{j+1} - Q^{2+}_{j}/A^{+}_{j}\,] \quad \text{(Eq. 3.42)}$$

Since A is a function of z, than Equation 3.42 is a function of Q and z, then we can write the following function:

$$(\partial Q^2/A)/\partial x = f_1(Q_{j+1},\ Q_j,\ z_{j+1},\ z_j,\ Q^+_{j+1},\ Q^+_j,\ z^+_{j+1},\ z^+_j) \qquad \text{(Eq. 3.43)}$$

If we have first order of Equation 3.42 for Q^+_j and z^+_j and we assume $Q^+_j = Q_j$ and $z^+_j = z_j$ then we have the following equations:

$$(\partial f_1/\partial Q_j)_e = 2\theta Q_j/(A_j \Delta x) \qquad \text{(Eq. 3.44)}$$

If it is assumed that $\alpha_4(j) = 2\ Q_j/(A^+_j \Delta x)$, then,

$$(\partial f_1/\partial z_j)_e = \theta Q^2_j T_{j+1}/(A^2_j \Delta x) = \theta\ \alpha_4(j)\ V^2_j T_j/2 \qquad \text{(Eq. 3.45)}$$

If $\alpha_5(j)$ is equal to $V^2_j T_j/2$, then,

$$(\partial f_1/\partial z_j)_e = \theta\ \alpha_4(j)\ \alpha_5(j1) \qquad \text{(Eq. 3.46)}$$

The third part of Equation 3.39 can be discertized as follows:

$$gA\partial z/\partial x = g\ [((1-\theta)/2)(A_j + A_{j+1}) + (\theta/2)(A^+_j + A^+_{j+1})\ ]\ 1/\Delta x\ [(1-\theta)(z_j + z_{j+1}) + \theta(z^+_j + z^+_{j+1})\ ] \qquad \text{(Eq. 3.47)}$$

Equation 3.47 is a function of z, then we can write the following function:

$$gA\partial z/\partial x = f_2(z^+_j,\ z^+_{j+1},\ z_j,\ z_{j+1}) \qquad \text{(Eq. 3.48)}$$

If we have first order of Equation 3.47 for z^+_j and we assume $z^+_j = z_j$ then we can have the following equations:

$$(\partial f_2/\partial z_j)_e = g\theta/2\Delta x\ [T_j\ (z_{j+1} - z_j) - (A_j + A_{j+1})] \qquad \text{(Eq. 3.49)}$$

$$(\partial f_2/\partial z_{j+1})_e = g\theta/2\Delta x\ [T_{j+1}\ (z_{j+1} - z_j) + (A_j + A_{j+1})] \qquad \text{(Eq. 3.50)}$$

If we assume $\alpha_6 = g/2\Delta x\ [T_j\ (z_{j+1} - z_j) - (A_j + A_{j+1})]$ and $\alpha_7 = g\theta/2\Delta x\ [T_{j+1}\ (z_{j+1} - z_j) + (A_j + A_{j+1})]$, then Equation 3.49 and 3.50 can be written as:

$$(\partial f_2/\partial z_j)_e = \alpha_6\theta \qquad \text{(Eq. 3.51)}$$

$$(\partial f_2/\partial z_{j+1})_e = \alpha_7\theta \qquad \text{(Eq. 3.52)}$$

Fourth part of Equation 3.39 can be discertized as follows:

$$gAS_f = g\,[((1-\theta)/2)(A_j S_{fj} + A_{j+1} S_{fj+1}) + (\theta/2)(A^+_j S^+_{fj} + A^+_{j+1} S^+_{fj+1})] \quad \text{(Eq. 3.53)}$$

$$AS_f = n^2 Q^2 / AR^{4/3} \quad \text{(Eq. 3.54)}$$

This equation can be written as a function of Q and z:

$$gAS_f = f_3(Q_{j+1},\ Q_j,\ z_{j+1},\ z_j,\ Q^+_{j+1},\ Q^+_j,\ z^+_{j+1},\ z^+_j) \quad \text{(Eq. 3.55)}$$

If we have first order of Equation 3.53 and 3.54 for Q and z, we assume $Q^+_j = Q_j$ and $z^+_j = z_j$ then we can have the following equations:

$$(\partial AS_f)/\partial Q = 2\, n^2 Q / A^2\, R^{4/3} \quad \text{(Eq. 3.56)}$$

$$(\partial AS_f)/\partial z = -\, n^2 Q^2 / A^2 R^{4/3}\,[\,T + 4/3(T - R\,\partial P/\partial z)\,] \quad \text{(Eq. 3.57)}$$

$$(\partial f_3/\partial Q_j)_e = (g\theta/2)(2n^2 Q_j / A^2_j R_j^{4/3}) \quad \text{(Eq. 3.58)}$$

$$(\partial f_3/\partial z_j)_e = (-g\theta/2)(2n^2 Q_j / A^2_j\, R_j^{4/3})[\,T_j + 4/3(T_j - R_j(\partial P_j/\partial z_j)_e\,] \quad \text{(Eq. 3.59)}$$

If we assume $\alpha_8(j) = (gn^2 Q_j / A_j R_j^{4/3})$, $\alpha_9(j) = V_j/2$ and $\alpha_{10}(j) = [7/3\ T_j - 4/3(R_j(\partial P_j/\partial z_j)_e]$, then we can rewrite the Equations 3.58 and 3.59 as follows:

$$(\partial f_3/\partial Q_j)_e = \theta\, \alpha_8(j) \quad \text{(Eq. 3.60)}$$

$$(\partial f_3/\partial z_j)_e = -\theta\, \alpha_8(j)\, \alpha_9(j)\, \alpha_{10}(j) \quad \text{(Eq. 3.61)}$$

The last part of the Equation 3.39 can be discertized as follows:

$$kqV = k/2[(1-\theta)(q_j Q_j / A_j + q_{j+1} Q_{j+1} / A_{j+1}) + \theta\,(qjQ^+j / A^+_j + q_{j+1} Q^+_{j+1} / A^+_{j+1})] \quad \text{(Eq. 3.62)}$$

Equation 3.62 can be written as function of Q and z:

$$kqV = f_4(Q_{j+1},\ Q_j,\ z_{j+1},\ z_j,\ Q^+_{j+1},\ Q^+_j,\ z^+_{j+1},\ z^+_j) \quad \text{(Eq. 3.63)}$$

Using Taylor series and having first order derivative of Equation 3.62 for Q and z, we can have the following equations:

$$(\partial f_4/\partial Q_j)_e = k\theta\, q_j / 2A_j \quad \text{(Eq. 3.64)}$$

$$(\partial f_4/\partial z_j)_e = -\, k\theta\, q_j Q_j L_j / 2A^2 j \quad \text{(Eq. 3.65)}$$

If we assume $\alpha_{11}(j) = k\, q_j/2S_j$, then Equations 3.64 and 3.65 can be written as follows:

$$(\partial f_4/\partial Q_j)_e = \theta\, \alpha_{11}(j) \qquad \text{(Eq. 3.66)}$$

$$(\partial f_4/\partial z_j)_e = -2\theta\, \alpha_{11}(j)\, \alpha_5(j) \qquad \text{(Eq. 3.67)}$$

Equation 3.39 used in the control algorithm to calculate right and left hand side of the coefficients for the dynamic equation and the following assumptions were made:

$$A_{21} = \alpha_3 - \theta[\, \alpha_4(j) - \alpha_8(j) + \alpha_{11}(j)] \qquad \text{(Eq. 3.68)}$$

$$A_{22} = \theta[\, \alpha_4(j)\, \alpha_5(j) + \alpha_6 - \alpha_8(j)\, \alpha_9(j)\alpha_{10}(j) + 2\, \alpha_{11}(j)\, \alpha_5(j)\,] \qquad \text{(Eq. 3.69)}$$

$$A_{23} = \alpha_3 + \theta[\, \alpha_4(j+1) + \alpha_8(j+1) - \alpha_{11}(j+1)] \qquad \text{(Eq. 3.70)}$$

$$A_{24} = -\theta[\, \alpha_4(j+1)\, \alpha_5(j+1) - \alpha_7 + \alpha_8(j+1)\, \alpha_9(j+1)\alpha_{10}(j+1) - 2\, \alpha_{11}(j+1)\, \alpha_5(j+1)\,] \qquad \text{(Eq. 3.71)}$$

$$A'_{21} = \alpha_3 + (1-\theta)[\, \alpha_4(j) - \alpha_8(j) + \alpha_{11}(j)] \qquad \text{(Eq. 3.72)}$$

$$A'_{22} = -(1-\theta)[\, \alpha_4(j)\, \alpha_5(j) + \alpha_6 - \alpha_8(j)\, \alpha_9(j)\alpha_{10}(j) + 2\, \alpha_{11}(j)\, \alpha_5(j)\,] \qquad \text{(Eq. 3.73)}$$

$$A'_{23} = \alpha_3 - (1-\theta)[\, \alpha_4(j+1) + \alpha_8(j+1) - \alpha_{11}(j+1)] \qquad \text{(Eq. 3.74)}$$

$$A'_{24} = (1-\theta)[\, \alpha_4(j+1)\, \alpha_5(j+1) - \alpha_7 + \alpha_8(j+1)\, \alpha_9(j+1)\alpha_{10}(j+1) - 2\, \alpha_{11}(j+1)\, \alpha_5(j+1)\,] \qquad \text{(Eq. 3.75)}$$

$$C_2 = k/2\,(\, q_{ie}Q_j/A_j + q_{je}Q_{j+1}/A_{j+1}) - 1/\Delta x\, [Q^2{}_{j+1}/A_{j+1} - Q^2{}_j/A_j] - g/2\Delta x(A_j + A_{j+1})(z_{j+1} - z_j) - g/2(A_jS_{0j} + A_{j+1}S_{0j+1}) \qquad \text{(Eq. 3.76)}$$

in which A_{21}, A_{22}, A_{23} and A_{24} are the left-hand side coefficients of the dynamic equation and A'_{21}, A'_{22}, A'_{23} and A'_{24} are the right-hand side coefficients of the dynamic equation. Using the above equations, the dynamic equation for a computational node can be rewritten as follows:

$$A_{21}\delta Q^+j + A_{22}\delta z^+{}_j + A_{23}\delta Q^+{}_{j+1} + A_{24}\delta z^+{}_{j+1} = A'_{21}\delta Q_j + A'_{22}\delta z_j + A'_{23}\delta Q_{j+1} + A'_{24}\delta z_{j+1} + C_2 \qquad \text{(Eq. 3.77)}$$

In the control algorithm α_3, $\alpha_4(j)$, $\alpha_5(j)$ α_6, α_7, $\alpha_8(j)$, $\alpha_9(j)$, $\alpha_{10}(j)$ and $\alpha_{11}(j)$ were defined as follows:

$$\alpha_3=1/(2*dt) \quad \text{(Eq. 3.78)}$$

$$\alpha_4(j)=2/A(j)*Q(j)/Dx(j) \quad \text{(Eq. 3.79)}$$

$$\alpha_4(m) =2/A(m)*Q(m)/Dx(j) \quad \text{(Eq. 3.80)}$$

$$\alpha_5(j)=Q(j)/A(j)*T(j)/2 \quad \text{(Eq. 3.81)}$$

$$\alpha_5(m)=Q(m)/A(m)*T(m)/2 \quad \text{(Eq. 3.82)}$$

$$\alpha_6=g/2/Dx(j)*(T(j)*(Z(m)-Z(j))-(A(m)+A(j))) \quad \text{(Eq. 3.83)}$$

$$\alpha_7=g/2/Dx(j)*(T(m)*(Z(m)-Z(j))+(A(m)+A(j))) \quad \text{(Eq. 3.84)}$$

$$\alpha_8(j)=g/A(j)*n(j)^2*Q(j)/R(j)^{4/3} \quad \text{(Eq. 3.85)}$$

$$\alpha_8(m)=g/A(m)*n(m)^2*Q(m)/R(m)^{4/3} \quad \text{(Eq. 3.86)}$$

$$\alpha_9(j)=Q(j)/A(j)/2;\ \alpha_9(m)=Q(m)/A(m)/2 \quad \text{(Eq. 3.87)}$$

$$(\partial P_j/\partial z_j) =2*(1+z(j)^2)^{1/2} \quad \text{(Eq. 3.88)}$$

$$(\partial P_m/\partial z_m) =2*(1+z(m)^2)^{1/2} \quad \text{(Eq. 3.89)}$$

$$\alpha_{10}(j)=(7/3*T(j)-4/3*R(j)*(\partial P_j/\partial z_j)) \quad \text{(Eq. 3.90)}$$

$$\alpha_{10}(m)=(7/3*T(m)-4/3*R(m)*(\partial P_m/\partial z_m)) \quad \text{(Eq. 3.91)}$$

$$\alpha_{11}(j)=0;\ \alpha_{11}(m)=0 \quad \text{(Eq. 3.92)}$$

After defining above equations in the algorithm, the coefficients for the left-hand side of Equation 3.77 are calculated as follows:

$$AL(mc,jc1)= \alpha_3-\theta*(\alpha_4(j)-\alpha_8(j)+\alpha_{11}(j)) \quad \text{(Eq. 3.93)}$$

$$AL(mc,jc2)= \theta*(\alpha_4(j)*\alpha_5(j)+\alpha_6-$$

$$\alpha_8(j)*\alpha_9(j)*\alpha_{10}(j)+2*\alpha_{11}(j)*\alpha_5(j) \quad \text{(Eq. 3.94)}$$

$$AL(mc,jc3)= \alpha_3+\theta*(\alpha_4(m)+\alpha_8(m)-\alpha_{11}(m)) \quad \text{(Eq. 3.95)}$$

$$AL(mc,jc4)=-\theta*(\alpha_4(m)*\alpha_5(m)-\alpha_7+$$

$$\alpha_8(m)*\alpha_9(m)*\alpha_{10}(m)-2*\alpha_{11}(m)*\alpha_5(m)) \quad \text{(Eq. 3.96)}$$

The coefficients for the right-hand side of the Equation 3.77 are computed as follows:

$$AR(mc,jc1)=\alpha_3+(1-\theta)*(\alpha_4(j)-\alpha_8(j)+\alpha_{11}(j)) \quad \text{(Eq. 3.97)}$$

$$AR(mc,jc2)=-(1-\theta)*(\alpha_4(j)*\alpha_5(j)+\alpha_6-$$

$$\alpha_8(j)*\alpha_9(j)*\alpha_{10}(j)+2*\alpha_{11}(j)*\alpha_5(j)) \quad \text{(Eq. 3.98)}$$

$$AR(mc,jc3)=\alpha_3-(1-\theta)*(\alpha_4(m)+\alpha_8(m)-\alpha_{11}(m)) \quad \text{(Eq. 3.99)}$$

$$AR(mc,jc4)=(1-\theta)*(\alpha_4(m)*\alpha_5(m)-\alpha_7+$$

$$\alpha_8(m)*\alpha_9(m)*\alpha_{10}(m)-2*\alpha_{11}(m)*\alpha_5(m)) \quad \text{(Eq. 3.100)}$$

If the system is at steady state, then $C_1 = C_2 = 0$. The matrix form of the Equations 3.25 and 3.77 can be written as follows:

$$\underbrace{\begin{bmatrix} A_{11} & A_{12} & A_{13} & A_{14} \\ A_{21} & A_{22} & A_{23} & A_{24} \end{bmatrix}}_{A_L} \begin{bmatrix} \delta Q^+_j \\ \delta z^+_j \\ \delta Q^+_{j+1} \\ \delta z^+_{j+1} \end{bmatrix} = \underbrace{\begin{bmatrix} A'_{11} & A'_{12} & A'_{13} & A'_{14} \\ A'_{21} & A'_{22} & A'_{23} & A'_{24} \end{bmatrix}}_{A_R} \begin{bmatrix} \delta Q_j \\ \delta z_j \\ \delta Q_{j+1} \\ \delta z_{j+1} \end{bmatrix}$$

The above matrix form represents the equation for a computational node (nodetype1). But if node type changes to a gate structure (nodetype2), the algorithm uses the gate equation to calculate the elements of the matrices.

$$Q_g = C_d (2g)^{1/2} b\, u\, (\Delta h)^{1/2} \quad \text{(Eq. 3.101)}$$

where Q_g = gate discharge, m^3/sec, Cd = gate coefficient, b = gate width, m, u = the change in gate opening. Because of changes in flow rate, the following equation is written:

$$\delta Q_{j+2}^{+} - \delta Q_{j+2} = Q_{j+2}^{+} - Q_{j+2} = f(z_{j+1}^{+}, z_{j+2}^{+}, u^{+}) - f(z_{j+1}, z_{j+2}, u) \quad \text{(Eq. 3.102)}$$

then the derivative of Equation 3.102 is:

$$(\partial f/\partial z_{j+1})_e (\delta z_{j+1}^{+} - \delta z_{j+1}) + (\partial f/\partial z_{j+2})_e (\delta z_{j+2}^{+} - \delta z_{j+2}) + (\partial f/\partial u)_e (\delta u^{+} - \delta u) \quad \text{(Eq. 3.103)}$$

where $\delta u^{+} - \delta u = \Delta\, \delta u$ is variation in the gate opening.

$$\underbrace{\begin{bmatrix} A_{11} & A_{12} & A_{13} & A_{14} \\ A_{21} & A_{22} & A_{23} & A_{24} \\ -(\partial f/\partial z_j)_e & 1 & -(\partial f/\partial z_{j+2})_e & \end{bmatrix}}_{A_L} \begin{bmatrix} \delta Q^{+}_{j} \\ \delta z^{+}_{j} \\ \delta Q^{+}_{j+1} \\ \delta z^{+}_{j+1} \\ \delta Q^{+}_{j+2} \\ \delta z^{+}_{j+2} \end{bmatrix} = \underbrace{\begin{bmatrix} A'_{11} & A'_{12} & A'_{13} & A'_{14} \\ A'_{21} & A'_{22} & A'_{23} & A'_{24} \\ -(\partial f/\partial z_j)_e & 1 & -(\partial f/\partial z_{j+2})_e & \end{bmatrix}}_{A_R} \begin{bmatrix} \delta Q_j \\ \delta z_j \\ \delta Q_{j+1} \\ \delta z_{j+1} \\ \delta Q_{j+2} \\ \delta z_{j+2} \end{bmatrix} + \underbrace{\begin{bmatrix} 0 \\ 0 \\ (\partial f/\partial z_j)_e \end{bmatrix}}_{B} \Delta\delta u + \underbrace{\begin{bmatrix} A_{11} - A'_{11} \\ A_{21} - A'_{21} \end{bmatrix}}_{C} \underbrace{\begin{bmatrix} \delta Q_p \\ \delta Q^{+}_{p} \end{bmatrix}}_{\delta\Delta q}$$

The above matrix form is used in the calculations when the node type is a gate. The control algorithm uses the following equations to compute the coefficient for right hand side of the equation:

$$AR(ic,jc1)=1 \quad \text{(Eq. 3.104)}$$

$$AR(ic,jc2)=-0.5*sqrt(2*g)*Cd(gi)*b(gi)*us(gi)/(Z(j)-Z(m)^{1/2}) \quad \text{(Eq. 3.105)}$$

$$AR(ic,jc4)=0 \quad \text{(Eq. 3.106)}$$

$$AR(ic,jc3)=0.5*(2*g)^{1/2}*Cd(gi)*b(gi)*us(gi)/(Z(j)-Z(m)^{1/2}) \quad \text{(Eq. 3.107)}$$

$$B(ic,gi)=sqrt(2*g)^{1/2}*Cd(gi)*b(gi)*sqrt(Z(j)-Z(m)^{1/2}) \quad \text{(Eq. 3.108)}$$

For the gate node type the left hand side of the coefficients are as follows:

$$AL(ic,jc1)=1 \quad \text{(Eq. 3.109)}$$

$$AL(ic,jc2)=-0.5*(2*g)^{1/2}*Cd(gi)*b(gi)*us(gi)/(Z(j)-Z(m)^{1/2}) \quad \text{(Eq. 3.110)}$$

$$AL(ic,jc4)=0 \quad \text{(Eq. 3.111)}$$

$$AL(ic,jc3)=0.5*(2*g)^{1/2}*Cd(gi)*b(gi)*us(gi)/(Z(j)-Z(m)^{1/2}) \quad \text{(Eq. 3.112)}$$

If the node type is a turnout node type, the algorithm will use the following equations to calculate the coefficients for the continuity equation:

$$\alpha_1=1/Dx(j-1);\ \alpha_2(j)=T(j-1)/(2*dt);\ \alpha_2(m)=T(m-1)/(2*dt) \quad \text{(Eq. 3.113)}$$

The coefficients of the dynamic equation for a turnout node type are defined in the algorithm as follows:

$$\alpha_3=1/(2*dt) \quad \text{(Eq. 3.114)}$$

$$\alpha_4(j)=2/A(j-1)*Q(j-1)/Dx(j-1) \quad \text{(Eq. 3.115)}$$

$$\alpha_4(m)=2/A(m-1)*Q(m-1)/Dx(j-1) \quad \text{(Eq. 3.116)}$$

$$\alpha_5(j)=Q(j-1)/A(j-1)*T(j-1)/2 \quad \text{(Eq. 3.117)}$$

$$\alpha_5(m)=Q(m-1)/A(m-1)*T(m-1)/2 \quad \text{(Eq. 3.118)}$$

$$\alpha_8(j)=g/A(j-1)*n(j)^2*Q(j-1)/R(j-1)^{4/3} \quad \text{(Eq. 3.119)}$$

$$\alpha_8(m)=g/A(m-1)*n(m)^2*Q(m-1)/R(m-1)^{4/3} \quad \text{(Eq. 3.120)}$$

$$\alpha_9(j)=Q(j-1)/A(j-1)/2;\ \alpha_9(m)=Q(m-1)/A(m-1)/2 \quad \text{(Eq. 3.121)}$$

$$\partial P_j/\partial z_j=2*(1+z(j)^2)^{1/2} \quad \text{(Eq. 3.122)}$$

$$\partial P_m/\partial z_m=2*(1+z(m)^2)^{1/2} \quad \text{(Eq. 3.123)}$$

$$\alpha_{10}(j)=(7/3*T(j-1)-4/3*R(j-1)*(\partial P_j/\partial z_j)) \quad \text{(Eq. 3.124)}$$

$$\alpha_{10}(m)=(7/3*T(m-1)-4/3*R(m-1)*(\partial P_m/\partial z_m)) \quad \text{(Eq. 3.125)}$$

$$\alpha_{11}(j)=0;\ \alpha_{11}(m)=0 \quad \text{(Eq. 3.126)}$$

After defining the above equations for a turnout node type, the algorithm will compute the coefficients for a turnout node as follows:

$$c1i1=2*li-1;\ \ c1i2=2*li \quad \text{(Eq. 3.127)}$$

$$C(ic-2,c1i1)=-(1-\theta)*\alpha_1 \quad \text{(Eq. 3.128)}$$

$$C(ic-2,c1i2)=-\theta*\alpha_1 \quad \text{(Eq. 3.129)}$$

$$C(mc-2,c1i1)= \alpha_3-(1-\theta)*(\alpha_4(m)+ \alpha_8(m)- \alpha_{11}(m)) \quad \text{(Eq. 3.130)}$$

$$C(mc-2,c1i2)=-(\alpha_3+\theta*(\alpha_4(m)+ \alpha_8(m)- \alpha_{11}(m))) \quad \text{(Eq. 3.131)}$$

The calculation of the left and right-hand side of coefficients for the dynamic and the continuity equations is completed, The dimensions of the control distribution matrix, *B*, depend on the number of state variables and the number of gates in the canal. The dimensions of the disturbance matrix, *C*, depend on the number of disturbances acting on the canal system and the number of dependent state variables. From matrix form of the equations above, the system state equation at any given time *k* can be written, in a compact form, as follows:

$$A_L\delta x(k+1) = A_R \delta x(k) + B\delta u(k) + C\Delta\delta q(k) \quad \text{(Eq.3.132)}$$

where k = time index; $\Delta\delta q$ = variation in demands(or disturbances) at the turnouts, m^2/s. Equation 3.132 can be written in a state-variable form along with the output equations as follows:

$$\delta x(k+1) = \Phi\delta x(k) + \Gamma\delta u(k) + \Psi\delta q(k) \quad \text{(Eq.3.133)}$$

$$\delta y(k) = H\delta x(k) \quad \text{(Eq.3.134)}$$

where $\Phi = (A_L)^{-1} * A_R$ is the system feedback matrix of dimensions *lxl*; $\Gamma = (A_L)^{-1} * B$ is the control distribution matrix of dimensions *lxm*; and $\Psi = (A_L)^{-1} * C$ is the disturbance matrix; $\delta x(k) = l \times 1$ state vector, $\delta u(k) = m \times 1$ control vector, $\delta q(k) = p \times l$ matrix representing external disturbances (changes in water withdrawal rates) acting on the system, $\delta y(k) = r \times 1$ vector of outputs (measured variables), $H = r \times l$ output matrix, l = number of dependent variables in the system, m = number of controls, p = number of disturbed disturbances acting on the system, and r = number of outputs. The elements of the matrices Φ, Γ, and Ψ depend upon the initial conditions.

3.2.3. Design of Linear Quadratic Gaussian (LQG) Controller

This research presents a design strategy based on linear quadratic Gaussian controllers. The LQG theory provides an integrated knowledge base for the development of a flexible controller. The LQG controller integrates the states estimation and the controller design into a single body of knowledge. This research extends this body of knowledge by accounting for robustness considerations and tradeoffs which are made when assigning the relative bandwidth of the controller and estimator. As explained in Chapter 2, a LQG controller consists of an optimal state feedback (LQR) and an optimal state estimator (Kalman filter). An optimal LQG controller based upon a linear system, a quadratic objective function and an assumption of white noise that has a normal, or Gaussian, probability distribution. In short, the optimal LQG design process is the following: a) Design an optimal regulator for a linear system assuming full-state feedback (i.e. assuming all the state variables are available for measurement) and a quadratic objective function. The regulator is designed to generate a control input, $\delta u(k)$, based upon the measured state vector $\delta x(k)$. b) Design a Kalman filter for the system assuming a known control input, $\delta u(k)$, a measured output, $\delta y(k)$, and white noises, $\eta(k)$ and $\delta q(k)$, with known power spectral densities, ρ. The Kalman filter is designed to provide and optimal estimate of the state vector, $\delta\hat{x}(k)$. c) Combine the separately designed optimal regulator and Kalman filter into an optimal compensator, which generates the input vector, $\delta u(k)$, based upon the estimated state-vector, $\delta\hat{x}(k)$, rather then the actual state-vector, $\delta x(k)$, and the measured output vector, $\delta y(k)$.

Since the optimal regulator and Kalman filter are designed separately, they can be selected to have desirable properties that are independent of one another. The closed-loop

eigenvalues consist of the regulator eigenvalues and the Kalman filter eigenvalues. The closed-loop system's performance can be obtained as desired by suitably selecting the optimal regulator's weighting matrices, Q and R, and the Kalman filter's spectral noise densities, Q_{esti} and RC. Hence the matrices Q, R, Q_{esti} and RC are the design parameters for the closed-loop system with an optimal LQG controller.

3.2.3.1. Design of Linear Quadratic Regulator

An important characteristic of transient performance of an open canal is its stability. Once a canal is disturbed from its original equilibrium condition, the responses to the disturbance will result in either a stable, neutral, or unstable response. The stability requirement of the considered system is defined in terms of the eigenvalues, which are the roots of the characteristic equation of matrix Φ and must have values less than unity. The oscillatory behavior of a canal water surface is associated with the presence of complex roots in the solution of the characteristic equation of the system. The response amplitude grows continuously if the absolute value of the complex roots is greater than unity, decays to zero if the absolute value is less than unity, and oscillates at a constant amplitude if the real part of the roots is zero. Also, because of the inertia, it is almost impossible to drive the deviation in water surface elevation (error) instantaneously to zero. Thus the output of the system lags the desired input and results in overshoot or oscillation of the water level about its equilibrium position. The objective here is to find a control law that will bring an initially disturbed water surface to the desired target water surface (or water level) as quickly and smoothly as possible in the presence of external disturbances acting on the canal. This can be accomplished by applying a large

proportional control in which change in gate opening is proportional to the changes in flow depths and flow rates, of the following form:

$$\delta u(k) = -K(k)\, \delta x(k) \qquad \text{(Eq.3.135)}$$

where $K(k)$ = controller gain matrix at time instant k. Controllability ensures the stability of the system and maintains the water level at any desired value by suppressing the influence of external disturbances. A canal is said to be controllable if it is possible to derive it from any initial water level to any specified water level (state) within a finite number of steps. Equation 3.135, which was used throughout the study, is called the discrete-time feedback control law. This equation describes the condition or evolution of the basic internal variables of the system. The variables in the equation (i.e., $\delta x(k)$) are called the state variables. Since the system is also linear, the closed-loop control system would be linear. The control energy can be expressed as $\delta u(k)^T R_{mxm} \delta u(k)$, where R is a square, symmetric matrix called the control cost matrix. Such an expression for control energy is called a quadratic form, because the scalar function, $\delta u(k)^T R_{mxm} \delta u(k)$ is a dot product of elements of the vector by itself, $\delta u(k)$. Similarly, the transient energy can also be expressed in a quadratic form as $\delta x(k)^T Q_{lxl} \delta x(k)$, where Q is a square, symmetric matrix called the state weighting matrix. The objective function can then be written as Equation 2.97. The LQR problem consists of solving for the feedback gain matrix, $K(k)$, such that the scalar objective function, J, given by Equation 2.96 is minimized. However, the minimization must be carried out in such a manner that the state-vector $\delta x(k)$ is the solution of the system's state equation (Equation 2.97). Equation 2.97 is called a constraint (because in its absence, $\delta x(k)$ would be free to assume any value), and the resulting minimization is said to be a constrained minimization. Hence, we are looking

for a regulator gain matrix, $K(k)$, which minimizes J subject to the constraint give by Equation 2.97. Note that the transient term, $\delta x(k)^T Q_{lxl} \delta x(k)$, in the objective function implies that a departure of the system's state, $\delta x(k)$, from the final desired state, $\delta x(k_f) = 0$, is to be minimized. In other words, the design objective is to bring $\delta x(k)$ to a constant value of zero at final time. If the final desired state is non-zero, the objective function can be modified appropriately.

In hydraulic engineering problems, the depth of flow, flow rate, and velocity as a function of distance can be considered as the state or internal variables. Sometimes, the volume of water in a given reach of a canal can also be considered as a state variable. In this study, the depth of flow and flow rate were considered the state variables. Given the initial conditions [$\delta x(0)$], δu, and δq, Equation 3.135 can be solved for variations in flow depth and flow rate as a function of time. If the system is really at equilibrium [i.e., $\delta x\ (0) = 0$ at time $t = 0$] and there is no change in the lateral withdrawal rates (disturbances), the system would continue to be at equilibrium forever; then, there is no need for any control action. Conversely, in the presence of disturbances (known or random), the system would deviate from the equilibrium condition. The actual condition of the system may be either above or below the equilibrium condition, depending upon the sign and magnitude of the disturbances. If the system deviates significantly from the equilibrium condition, the discharge rates into the laterals will be different (either more or less) than the desired values. But in canal operations, the main objective is to keep these deviations to a minimum so that a nearly constant rate of discharge is maintained through the turnouts. This could be achieved by selecting an appropriate change in gate opening (input signal δu) to compensate for changes in withdrawal rates (disturbances δq). In general, this is a

trail and error procedure. The control algorithm uses the concepts of optimal control theory for deriving the feedback control algorithm for real-time control of open-channels. Extension of the optimal control concepts to multi-pool systems is more involved because of the interactions between the pools. Application of optimal control theory for the derivation of canal control algorithms eliminates the trial and error procedure that has been traditionally used. The control algorithm designs the optimal controller by adjusting the dimensions of the matrix H which relates the state variables to measurements. When lumped parameter models are used to derive feedback control algorithms for irrigation canals, the number of state variables (which depends upon the number of finite-difference nodes used per pool) that must be measured and used in the feedback loop becomes large. For the linearization scheme used by Malaterre (1995), the number of measurements required for state feedback is given as follows:

$$N_m = N_p\,(3 + 2(N-2)) \qquad \text{(Eq.3.136)}$$

where N_m = number of measurements required for full state feedback; and N_p = number of pools in the system. The relationship between the state variables and the measured (or output) variables is:

$$\delta y(k) = H\,\delta x(k) + \eta(k) \qquad \text{(Eq. 3.137)}$$

in which $\delta y(k)$ = N_{mo} x 1 vector of output variables; H = N_{mo} x l output matrix; $\eta(k)$= N_{mo} x 1 vector of random measurement noises; and N_{mo} = number of measured outputs. The dimension of the H matrix depends on whether level-control or volume-control is used. Equation 3.137 is called the output equation. In this algorithm the level-control theory was used. Since the example used in this study has 5 pools, H matrix will have 5 rows. The column number of H matrix is 266 which represents the number of dependent (state)

variables in the system. The algorithm designs H matrix as follows:

$$H(1,48)=1;\ H(2,91)=1;\ H(3,136)=1;\ H(4,203)=1;\ H(5,266)=1 \qquad \text{(Eq.3.138)}$$

The numbers 48, 91, 136, 203 and 266 in H matrix represent state variables of the system. Since only one or two flow depths per pool are measured in practice, those numbers represent the index of the measured flow depths in the canal.

The control law defined by Eq. 3.135 brings an initially disturbed system to an equilibrium condition in the absence of any external disturbances acting on the system. Known and unknown disturbances (changes in lateral withdrawal rates) always act on the system. In the presence of constant external disturbances, the system cannot be returned to be equilibrium condition using the above control law. An integral control, in which the cumulative (or integrated) deviation of a selected output variable is used in the feedback control loop, is required to return the system to the equilibrium condition in the presence of external disturbances. Integral control is achieved by appending additional state variables of the following form to the system state Equation 3.137:

$$\delta x_i(k+1) = D\,\delta x(k) + \delta x_i(k) \qquad \text{(Eq.3.139)}$$

in which δx_i = integral state variables; and D = integral feedback matrix. This produces a new control law of the form:

$$\delta u(k) = -K\,\delta x(k) - K_i\,\delta i(k) \qquad \text{(Eq.3.140)}$$

The first term in Equation 3.140 accounts for initial disturbances (proportional control), whereas the second term accounts for external disturbances (integral control). Equation 3.140 calculates the desired gate opening as a function of the measured deviations in the flow depths and flow rates in the given pool(s) at time instant k, and the cumulative variation in flow depth up to time instant k. With minor variations in the selection of

elements for the integral feedback matrix, the above procedure is applicable to both constant-level control and constant-volume control. The dimensions of integral feedback matrix, D, depend on the number of pools or the external disturbances in the system.

This study is a case of a multi-input and multi-output (MIMO) system. Since the poles (or eigenvalues) of the system characteristic equation are not uniquely determined, some systematic procedure for selection of the elements of matrix K is required. In the optimal steady-state case, the solution for change in gate opening, $\delta u(k)$, is of the same form as:

$$\delta u(k) = -K\, \delta x(k) \qquad \text{(Eq. 3.141)}$$

where K is given by:

$$K = [R_1 + \Gamma^T S_\infty \Gamma]^{-1} \Gamma^T S_\infty \Phi \qquad \text{(Eq. 3.142)}$$

and S_∞ is a solution of the discrete algebraic Riccati equation (DARE):

$$\Phi^T S_\infty \Phi - \Phi^T S_\infty \Gamma [R + \Gamma^T S_\infty \Gamma]^{-1} \Gamma^T S_\infty \Phi + Q_1 = S_\infty \qquad \text{(Eq. 3.143)}$$

where $R_1 = R_1^T > 0$ and $Q_1 = Q_1^T \geq 0$. The algorithm calculates the K feedback gain matrix using Φ, Γ, Q_1, R_1 matrices as follows:

$$K=dlqr(\Phi, \Gamma, Q_1, R_1) \qquad \text{(Eq.3.144)}$$

in which Q_1 = state cost weighting matrix; R_1 = control cost weighting matrix, and *dlqr* is a MATLAB function that calculates the optimal gain matrix K. The control algorithm designs linear quadratic regulator for discrete time systems and calculates optimal feedback gain matrix K such that the feedback control law Equation 3.140 minimizes the cost function (Eq. 2.96) subject to the constraint given by Eq. 2.97. After computation of the feedback gain matrix, K, the algorithm calculates the deviation of water depth (YO) and simulates the system dynamics as follows:

$$[YO,X]=dlsim(\Phi - \Gamma K, C2, H1, D, U) \qquad \text{(Eq.3.145)}$$

in which X is a state vector, YO is the output for water depth with a dimension of 500 x 5, U is the input sequence with a dimension of 500 x 10, $C2$ is disturbance matrix with a dimension of 271 x 10, H1 is an output matrix with a dimension of 5 x 271, and *dlsim* is a MATLAB function that simulates the discrete-time linear system. Each row of U corresponds to a new time point. $C2$ and $H1$ matrices are derived from C and H matrices by adjusting their matrix sizes to the system.

3.2.3.2. Design of Optimal Estimator or Kalman Filter

When the controller gain matrix, K, is derived using a lumped parameter model of the Saint-Venant equations, the size of the gain matrix depends upon the number of finite-difference nodes used in the discretization and the number of pools in the system. In this research, the number of elements of the controller gain matrix per pool was equal to $3+2(N-1)$ including the integral control variable. Since it is expensive to measure all the state variables (flow depths and flow rates), it is desirable to minimize the number of measurements per pool and estimate the values for all the variables that are not measured (usually one or two flow depth measurements per pool are available). Kalman filter is an optimal observer, which minimizes a statistical measure of the estimation error $e_o(k) = \delta x(k) - \delta\hat{x}(k)$, where $\delta\hat{x}(k)$ is the estimated state-vector. As explained in Chapter 2, Equation 2.107 is called an observer or estimator, which is basically a mathematical model of the canal that is used in an on-line computer. Being an optimal observer, the Kalman filter is a counterpart of the optimal regulator. However, while the optimal regulator minimizes an objective function based on transient and steady-state response

and control effort, the Kalman filter minimizes the covariance of the estimation error, $RC(k,k) = E[e_o(k)e_o^T(k)]$. It is useful to minimize the covariance of the estimation error because the state-vector, $\delta x(k)$, is a random vector. The estimated state, $\delta\hat{x}(k)$, is based on the measurement of the output, $\delta y(k)$, for a finite time. However, a true statistical average (or mean) of $\delta x(k)$ would require measuring the output for an infinite time (i.e. taking infinite number of samples), and then finding the expected value of $\delta x(k)$. Hence, the best estimate that the Kalman filter could obtain, $\delta\hat{x}(k)$, is not the true mean, but a conditional mean, $\delta x_m(k)$, based on only a finite time record of the output, $\delta y(k)$, for $T \leq k$.

The Kalman filter is driven by the error between the measured and predicted values of the selected state variables in the canal. Before designing the observer, the observability of the canal must be verified. The observability is an important aspect in the context of system control because the generation of the system inputs should be based on the observation of the outputs. Thus good control requires both the ability to infer what the status of the canal (observability) and the ability to change the behavior (controllability) of the system. The canal was found to be observable. The values of the elements in matrix L, the observer gain matrix, depend upon the eigenvalues (poles) of the characteristic equation of the estimator-error equation ($\Phi - LH$). A normal procedure for determining the matrix L is to decide on suitable poles for the observer-error equation, and then to find the matrix L that gives the desired poles. The determination of the observer poles is a compromise between sensitivity to measurement error and rapid recovery of initial errors. As fast observer (large negative values for the poles) will converge quickly but it will also be sensitive to measurement error. Though this procedure is simple in the case of SISO systems (irrigation canal with a single pool), it

becomes a tedious trail-and-error procedure for MIMO systems, particularly in the presence of random disturbances. The Kalman filtering is a more efficient way of designing an observer for MIMO systems in the presence of random disturbances. To minimize the divergence between the estimated and actual values of the state variables, the random nature of the disturbances must be incorporated in to the state estimation Equation 2.107. This is done by designing the observer gain matrix (L) based upon the stochastic nature of the disturbances as well as the measurement error (noise). In the derivation of the Kalman filter, it is assumed that the disturbances can be described by a white (no time correlation among the disturbances), zero-mean Gaussian random sequence. This is stated mathematically as follows:

$$E[\delta q(k)] = 0 \qquad \text{(Eq.3.146)}$$

$$E[\delta q(k)\, \delta q(k)^T] = Q_{esti} \qquad \text{(Eq.3.147)}$$

$$E[\delta q(k)\, \delta q(j)^T] = 0,\ j \neq k \qquad \text{(Eq.3.148)}$$

in which $E(*)$ = expected value of the variable in parenthesis, and Q_{esti} = covariance of disturbances. It is also assumed here that no cross-correlation exists between the several disturbance sequences that act simultaneously on the system. In the presence of measurement error, the output equation is given as:

$$\delta y(k) = H\, \delta x(k) + \eta(k) \qquad \text{(Eq.3.149)}$$

in which $\eta(k)$ = random measurement (flow depth) noise, and is assumed to be a white, zero-mean Gaussian random sequence. This is mathematically stated as:

$$E[\eta(k)] = 0 \qquad \text{(Eq.3.150)}$$

$$E[\eta(k)\eta(k)^T] = RC \qquad \text{(Eq.3.151)}$$

$$E[\eta(k)\eta(j)^T] = 0,\ j \neq k \qquad \text{(Eq.3.152)}$$

in which RC = covariance of measurement noise. The above relationships, along with the initial conditions are used to minimize the variance of the estimator error, which is denoted by $P(k)$. The initial conditions are given as follows:

$$E[\delta x(0)] = 0, \quad P(0) = \Psi Q_1 \Psi' \tag{Eq.3.153}$$

The system dynamic equation is used to predict the state and the estimation error covariance, as follows. Time update equations (effect of system dynamics) are:

$$P(k+1)^- = \Phi P(k)\, \Phi^T + \Psi Q_1 \Psi' \tag{Eq.3.154}$$

$$\delta\hat{x}(k+1)^- = \phi\delta\hat{x}(k) + \Gamma\delta u(k) \tag{Eq.3.155}$$

As soon as measured values for the output variables $\delta y(k)$ are available, the time-updated values are corrected using the measurement update equations as follows. Measurement update equations (effect of measurement $\delta y(k)$) are:

$$L(k+1) = P(k+1)^- H^T [HP(k+1)^- H^T + R_1]^{-1} \tag{Eq.3.156}$$

$$P(k+1) = [I - L(k+1)H]P(k+1)^- \tag{Eq.3.157}$$

$$\delta\hat{x}(k+1) = \phi\delta\hat{x}(k) + \Gamma\delta u(k) + L[\delta y(k) - H\delta\hat{x}(k)] \tag{Eq.3.158}$$

The process is repeated as long as needed. As shown in Figure 3.4, Eqs 3.154 and 3.157 constitute the time-varying Kalman filter. As $k \rightarrow \infty$, the value of the state error covariance matrix approaches a constant value, and the estimator gain matrix L approaches its steady-state value. Usually this steady-state value is approached very quickly. Therefore, for irrigation canals that run for a long time, the steady-state Kalman filter is very appropriate, and the observer gain matrix in this case is calculated as follows:

$$L_\infty = P_\infty H^T (H\, P_\infty\, H^T + R_1)^{-1}, \quad P_\infty = \Lambda_1 X_1^{-1} \tag{Eq.3.159}$$

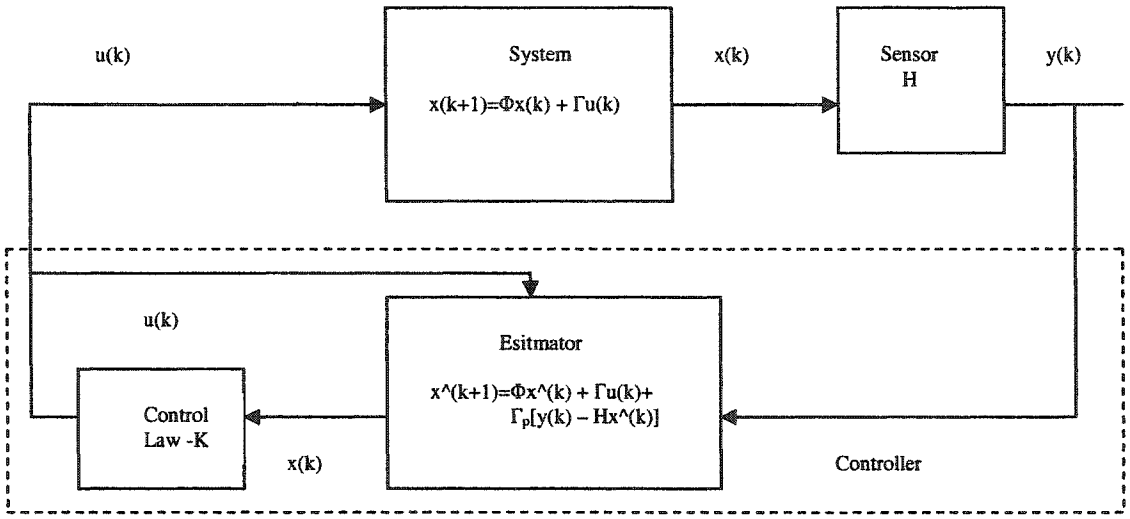

Figure 3.4 Estimator and Controller Mechanization

in which $[\Lambda_1 \; X_1]$ = eigenvectors associated with the stable eigenvalues of the estimation Hamiltonian matrix, H_e, which is defined as follows:

$$H_e = \begin{pmatrix} \Phi^T + H^T R_1^{-1} H \; \Phi^{-1} \Psi Q_1 \Psi^T & -H^T R_1^{-1} H \Phi^{-1} \\ \Phi^{-1} \Psi Q_1 \Psi^T & \Phi^{-1} \end{pmatrix} \qquad \text{(Eq.3.160)}$$

Whether it is time-varying or constant, the Kalman filter is basically an on-line computer model that provides statistically optimal estimated values for the states. When the estimated values of the state variables are used in the feedback loop, Equation 3.135 becomes:

$$\delta u(k) = -K\delta\hat{x}(k) - K_i \delta x_i(k) \qquad \text{(Eq.3.161)}$$

Equation 3.161 computes the desired change in the gate opening as a function of the estimated (instead of measured) deviations in the state variables. The integral feedback term in Eq. 3.161 usually uses the measured deviation in the state variables. The control algorithm uses the above equations to design a Kalman filter for the system.

In the system, the lateral canals were assumed to be located immediately upstream of the last node in each pool. The lateral withdrawal rates are not constant throughout the season. These vary from season to season and continually during a given season. In a demand delivery schedule, these lateral withdrawals are not known in advance. It may be possible, with historical data on withdrawals or climatic data, to describe the lateral withdrawals mathematically as follows:

$$\delta q_{i,N}(k) = q_{i,N}(k) - \hat{q}_{i,N} \qquad \text{(Eq.3.162)}$$

in which $q_{i,N}(k)$ = historical or calculated withdrawal rate from node N of the pool i at time instant k, $\hat{q}_{i,N}(k)$ = historical or calculated average withdrawal rate from node N of pool i, and $\delta q_{i,N}(k)$ = deviation from the average flow rate at node N of pool i at time instant k and is called a disturbance acting on the system. As the disturbance component, $\delta q(k)$, becomes negligible compared with the average withdrawal rate, the irrigation canals can be operated more or less on an arranged delivery basis. However, as the disturbance component becomes significant compared with the average withdrawal rate, then a mechanism to incorporate the random nature of the disturbances into the operation of the irrigation canals is required. As explained above, the random disturbances were considered through the Kalman filter. In the design of the Kalman filter, in lieu of actual field data on withdrawal rates from the turnouts, the random disturbances were assumed to have some prespecified levels of variance. The actual time series of the demands is not used in the design of the filter; only the variance of the time series enters into the design of the filter. In the algorithm the assumed variances, w, for the five pools are as follows:

$$w1=1.0;\ w2=1.2;\ w3=0.8;\ w4=1.4;\ w5=1.2 \qquad \text{(Eq.3.163)}$$

And from w values a diagonal matrix Q_{esti} were created as follows:

$$Q1=w1\text{^}2;\ Q2=w2\text{^}2;\ Q3=w3\text{^}2;\ Q4=w4\text{^}2;\ Q5=w5\text{^}2 \quad \text{(Eq.3.164)}$$

$$Q_{est}=[Q1\ \ Q1\ \ Q2\ \ Q2\ \ Q3\ \ Q3\ \ Q4\ \ Q4\ \ Q5\ \ Q5] \quad \text{(Eq.3.165)}$$

$$RC=0.0005 \quad \text{(Eq.3.166)}$$

where RC is a tolerance value for the RC covariance matrix which is an identity matrix; Q_{esti} is a diagonal matrix which is extracted from Q_{est} matrix and w values are assumed variances for the five pools. Q_{est} has 10 elements because the system has 10 external inputs (disturbance), two for each pool (one at the beginning of the sampling interval and the other at the end of the sampling interval). Q_{esti} and RC are Kalman filter's spectral noise density matrices. Since the closed-loop eigenvalues of the compensated system are the eigenvalues of the regulator and the eigenvalues of the Kalman filter, if we wish to achieve the same performance in the compensated system as the full-state feedback system, ideally we must select a Kalman filter such that the Kalman filter eigenvalues do not dominate the closed loop system, i.e. they should not be closer to the imaginary axis than the regulator eigenvalues. As the Kalman filter does not require a control input, its eigenvalues can be pushed closer to unity without causing concern of large required control effort (as in the case of the regulator). In other words, the Kalman filter can have faster dynamics than the regulator, which is achieved free of cost. However, as we will see in the present example, it is not always possible to push all the Kalman filter poles closer to unity than the regulator poles by varying the noise spectral densities of the Kalman filter. In such cases, a judicious choice of Kalman filter spectral densities would yield the best recovery of the full-state feedback dynamics. To design the Kalman filter to recover the full-state feedback performance of linear quadratic regulator, the process noise spectral density matrix for the system is selected after some trial and error to be

$Q_{esti}=Q_{esti} + \rho*H*H^T$. As explained above, the full-state feedback control system's performance can be recovered by properly designing a Kalman filter to estimate the state-vector in the LQG controlled system. In other words, the Kalman filter part of the optimal LQG controller can be designed to yield approximately the same performance as that of the full-state feedback regulator.

After selecting the covariance matrices, the algorithm calculates the Kalman filter gain matrix, L, as a function of $\Phi, C1, H, Q_{esti}$ *and* RC matrices as follows:

$$[L,M,P]=dlqe(\Phi,C1,H,Q_{esti},RC) \qquad \text{(Eq.3.167)}$$

in which M and P are steady-state error covariance matrices; $C1$ is a disturbance matrix derived by adjusting C matrix to the system dimensions, and *dlqe* is a MATLAB function to design the Kalman filter (state estimator). The algorithm solves the discrete Riccati equation by an iterative method to determine the optimal steady-state gain (and optional covariance matrices) for a discrete Kalman filter or state estimator.

After calculation of optimal regulator and Kalman filter separately, the algorithm combines both optimal regulator and Kalman filter into an optimal LQG regulator, which generates the input vector, $\delta u(k)$, based upon the estimated state-vector, $\delta\hat{x}(k)$, rather than the actual state-vector, $\delta x(k)$ and the measured output vector, $\delta y(k)$. The LQG closed-loop system's performance can be obtained as desired by suitably selecting the optimal regulator's weighting matrices, Q_1 and R_1 and the Kalman filter's spectral density noise densities matrices, Q_{esti} and RC. Hence the matrices Q_1, R_1, Q_{esti} and RC are the design parameters for the closed loop system with LQG controller. The algorithm combines these design parameters to form a dynamic regulator or compensator (LQG) for a given state-space model of the system, a state-feedback gain matrix K, and an estimator gain

matrix *L*. The gains K and L are typically designed using LQG techniques. To combine both regulator and Kalman filter, the control algorithm uses matrix operations and produces new combined matrices as output matrix, GHO, control and feedback matrix, GO1, and disturbance matrix, GCO. Then the algorithm simulates the system dynamics for LQG controller using the newly produced matrices as follows:

$$[Y,XO]=dlsim\ (GO1,GCO,GHO,D,U,X00) \qquad \text{(Eq.3.168)}$$

in which Y = output vector (flow depths at the downstream end of the each pool), *GO1,GCO,GHO,D,U* are the simulation matrices and *X00* initial state vector at time (*k*). The algorithm simulates the (time) response of the discrete-time linear system to arbitrary inputs and shows the response of the system to an initial condition *X00* on the states. The duration of simulation is determined depending upon the number of rows used in the U matrix.

Now we can examine the robustness of the designed LQG controller with respect to process noise in comparison with the full-state feedback system. Such a comparison is valid because both control systems use the same feedback gain matrix, *K*. Next section will explain how robust is the LQG control algorithm in the presence of external disturbances with white noise.

3.2.4. Evaluation of System Robustness

The robust design strategy of the control algorithm is based on linear quadratic gaussian controllers with a loop transfer recovery (LQG/LTR technique). The closed-loop LQG controlled systems are less sensitive (or more robust) to variations in the mathematical model of the system (called process noise and measurement noise), when compared to the

corresponding open-loop systems. Also, the robustness of a single-input, single-output feedback control system is related to the return difference, $1 + G(z)H(z)$, where $G(z)$ and $H(z)$ are the transfer functions of the system and controller, respectively. The larger the return difference of the feedback loop, the greater will be the robustness when compared to the corresponding open-loop system. The control system consists of a feedback controller (LQG) with transfer matrix, $H(z)$, a canal system with transfer matrix, $G(z)$, with desired output, $Y(z)$ and disturbances, $\delta q(k)$ (Figure 3.5). The sensitivity of the output with respect to process and measurement noise depends upon the matrix $[1 + G(z)H(z)]^{-1}$, while the sensitivity of the input to process and measurement noise depends upon the matrix $[1 + H(z)G(z)]^{-1}$. The larger the elements of these two matrices, the larger will be the sensitivity of the output and input to process and measurement noise. Since robustness is inversely proportional to sensitivity, we can extend the analogy to multivariable systems by saying that the robustness of the output is measured by the matrix $[I + G(z)H(z)]$, called the return-difference matrix at the output and robustness of the input is measured by the matrix $[I + H(z)G(z)]$, called the return difference matrix at the system input. Therefore, for multivariable control systems, there are two return difference matrices to be considered: the return difference at the output, $[I + G(z)H(z)]$, and that at the system's input, $[I + H(z)G(z)]$. Alternatively, we can define the return ratio matrices at the system's output and input, as $G(z)H(z)$ and $H(z)G(z)$, respectively, and measure robustness properties in terms of the return ratios rather than the return differences. The robustness of a feedback control system is related to the return ratio matrix $G(z)H(z)$ [*i.e.* $H(zI - \Phi)^{-1}\Gamma$] for full state feedback and return ratio matrix

$G(z)H(z)$ *[i.e.* $H(zI - \Phi)^{-1}\ \Gamma(-K(zI - \Phi + \Gamma K + LH)^{-1}\ K)]$ for LQG. The return ratio matrix of LQG is represented by M, the norm matrix as follows:

$$Norm\ Matrix\ (M) = H(zI - \Phi)^{-1}\ \Gamma(-K(zI - \Phi + \Gamma K + LH)^{-1}K) \quad \text{(Eq. 3.169)}$$

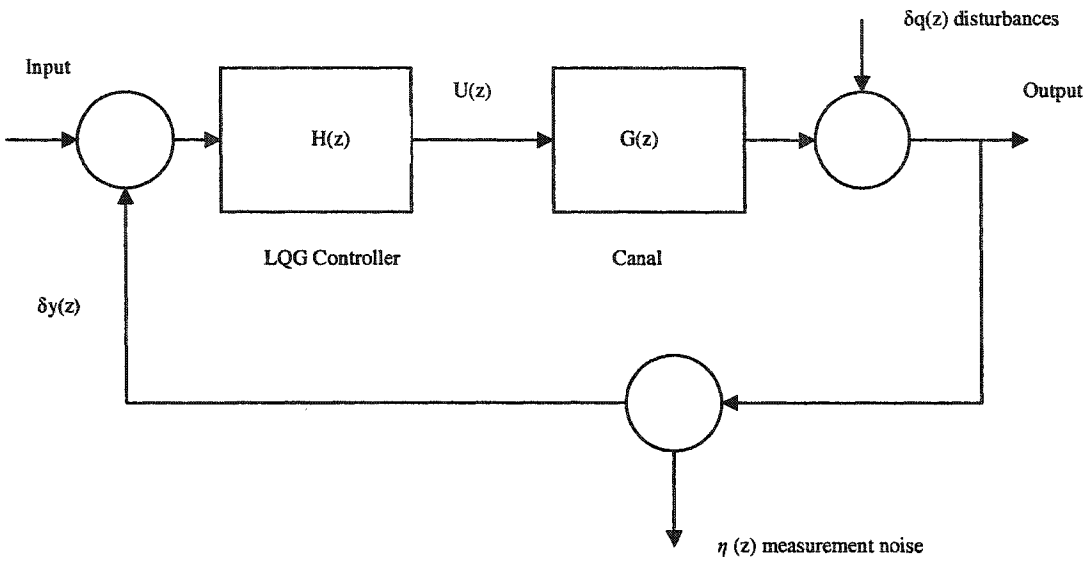

Figure 3.5. A Multivariable Feedback Control System.

To recover the robustness of the LQG controller a loop transfer recovery (LTR) procedure a H_2 norm minimization loop shaping technique, was employed in the algorithm. Goodman (1984) is the first person who formulated the LTR problem for discrete-time systems as a H_2 norm minimization problem of the recovery norm matrix *M*. Equation 3.170 is known as the Linear Quadratic or H_2 Optimal control problem. The "H" comes from the term 'Hardy Space', and is a mathematical description of the domain within which the solution is sought. Simply, the H_2 norm minimizes the average magnitude of the weighted sensitivity function, and the robust H_2 optimal controller performs this minimization for the worst system within the family of systems. What makes robust H_2 optimal control so attractive is the existence of very effective computer-based solutions, and its ability to deal with multi-input-multi-output systems (Dutton *et*

al. 1997). The algorithm minimizes the H_2 norm of recovery matrix, M, over all the possible stabilizing Kalman filter gain matrice, L. If there are disturbances on the system, Kalman filter gain, L, minimizes the norm of the recovery matrix, if and only if L is a solution to the discrete LQR problem:

$$J = \sum_{i=1}^{K_\infty} [\delta\hat{x}(k)^T Q_{lxl} \delta\hat{x}(k) + \delta u(k)^T R_{mxm} \delta u(k)] \qquad \text{(Eq. 3.170)}$$

subject to

$$-\delta\hat{x}(k+1) + \phi\delta\hat{x}(k) + \Gamma\delta u(k) = 0 \qquad \text{(Eq. 3.171)}$$

where

$$\delta u(k) = -L^T \delta\hat{x}(k) \qquad \text{(Eq. 3.172)}$$

where

$$L = PH^T[HPH^T + RC]^{-1} \qquad \text{(Eq. 3.173)}$$

where P is a solution of the discrete algebraic Riccati equation (DARE):

$$\Phi^T P \Phi - \Phi PH^T[RC + H^T P H]^{-1} H P \Phi^T + Q_{esti} = P \qquad \text{(Eq. 3.174)}$$

where $RC = RC^T > 0$ and $Q_{esti} = Q_{esti}{}^T = \Gamma^T\Gamma \geq 0$ then equation 3.174 can be rewritten as:

$$\Phi^T P \Phi - \Phi PH^T[RC + H^T P H]^{-1} H P \Phi^T + \Gamma^T\Gamma = P \qquad \text{(Eq. 3.175)}$$

It is possible to assign a scalar measure to robustness, rather than deal with the two return-difference (or return ratio) matrices. Using H_2 norm minimization loop shaping technique, the control algorithm makes adjustments on the singular values of return ratio matrice to achieve desired closed-loop robustness and performance. To recover the LQR robustness properties, the algorithm redesigns the Kalman filter such that the sensitivity of the system's input to process and measurement noise is minimized. In other words, the maximum values of return ratio at system's input should be equal to that of the return

ratio at the system's input with LQR. Then we can say that Q_{esti} and RC are treated as design parameters of the Kalman filters to achieve LQR return ratio at the system's input, rather than an actual parameter of process and measurement (white) noises. There is no unique set of Kalman filter parameters Q_{esti} and RC to achieve loop shaping. Specifically, if the system is square and minimum-phase, then we can select the measurement noise spectral density as $RC = I$ and $Q_{esti}=Q_{est} + \rho I$, where ρ is a scaling parameter, it can be in the limit $\rho \rightarrow \infty$. In most cases, for better loop shaping, these parameters can be chosen as $RC=HH^T$ and $Q_{esti} = \rho \Gamma^T\Gamma$ and making ρ large. The algorithm uses *25, 75, 260, 2500, 3000* values for the scaling parameter, ρ, to recover the robustness properties of the LQR regulator. High values of ρ reduce the roll of the closed loop transfer function at high frequencies, which is not desirable. Therefore, at high frequencies, the slope of decreasing magnitude with frequency (roll-off) is at least steep as -40 dB/decade. Thus, any higher ρ is used in the solution of Kalman filter is disqualified if roll-off is only -20 dB/decade (Goodman 1984).

3.2.5. Robustness and Stability Analysis of LQG/LTR Controller

The control algorithm uses two different robustness and stability analysis methods for the system: Singular values and Bode Diagram analysis. Singular values help us analyze the properties of the multivariable feedback control system. The Bode Diagram tests the stability and robustness of the system. Bode diagram contains two different plots, in which gain margin is expressed in magnitude (dB) and phase margin is expressed in degrees. The algorithm computes the magnitude and phase of the frequency response of discrete-time models. In the MIMO case, bode produces an array of Bode plots, each plot

showing the Bode response of one particular I/O channel. The frequency range is determined automatically based on the system poles and zeros. The computer algorithm tests the Bode stability and robustness of the system as function of Φ, Γ, K, C, H, and D matrices, as follows:

$$dbode(phi1\text{-}b1*K,C2,H1,D,30);\ dbode(GO1,GCO,GHO,D,30) \qquad \text{(Eq. 3.176)}$$

in which *dbode* is a MATLAB function to plot frequency response diagrams for discrete-time linear systems; and 30 represents the sampling time in seconds.

For dynamic systems the singular values and their associated directions vary with frequency, and for control purposes it is usually the frequency range corresponding to the closed-loop bandwidth (frequency range). The control algorithm calculates singular values (*sv*) of the system matrices as a function of Φ, Γ, K, C, H, and D matrices as follows:

$$sv=dsigma(phi1\text{-}b1*K,C2,h5,D1,30,w);$$

$$sv2=dsigma(GO1,GCO,GHO5,D1,30,w) \qquad \text{(Eq. 3.177)}$$

in which dsigma, a MATLAB function, produces a singular value (sv) plot of the frequency response of the discrete-time linear systems. The frequency range, ω, is between 10^{-6} and 10^{2} and the sample time is 30 sec. Since the range of frequencies required to study a linear system is usually very large, it is often useful to plot the magnitude of singular values (*sv*), with respect to the frequency, ω, on a logarithmic scale of frequency. The magnitude is usually converted to gain in decibels (dB) by taking the logarithm of *sv* to the base 10 and multiplying the result with 20 as follows:

$$sv = 20\ log_{10}(sv) \qquad \text{(Eq.3.178)}$$

The algorithm computes the singular values of the complex system matrix as a function of frequency, ω. The frequency range is chosen automatically and incorporates more points where the plot is changing rapidly. The minimum singular value of the system, evaluated as a function of frequency, is a useful measure for evaluating the feasibility of achieving acceptable control. Maximum singular value is also very useful in terms of frequency domain performance and robustness. It gives us useful information about the effectiveness of feedback control. In this research, the minimum singular values are used for the robustness analysis.

CHAPTER 4

RESULTS AND ANALYSIS

4.1. Introduction

An example canal with five pools and six gates was considered to demonstrate the design of LQG/LTR controller for real-time control of irrigation canals. See Appendix-B for detailed data on the irrigation scheme used in the simulation study. The process to be controlled is a 5-pool open-channel receiving water from a source located at the upstream end of the canal. The control system aims to match the water level at the downstream end of each pool with the target value. The control algorithm adjusts upstream inflow and opening of all the upstream gates. The observed variables are water levels at the upstream and downstream ends of each pool. The canal data was obtained from the Department of Hydraulic Works in Turkey to simulate the performance of robust control algorithm in a gated open-channel. The remainder of this chapter is a simulation study and robustness analysis of the control algorithm.

4.2. Model System and Control Parameter Selection

The robust control algorithm was applied to the Harran main canal having a wide range of design capacities. The system was selected to represent a part of an irrigation system delivering water directly to irrigation water users. The irrigation canal is located in Southeastern Anatolia Project (GAP) development area (Appendix-A). The GAP area

covers the Euphrates and Tigris river basins which represent over 28% of Turkey's surface water. The total economically irrigable land area in the region corresponds to 19% of the whole area of the country. Thirteen major groups of water resources development projects, primarily for irrigation and hydropower generation and for control of floods and droughts, were planned for the mobilization of the water and soil resources of the region. GAP involves the construction of 22 dams and 19 hydropower plants on the Euphrates and Tigres rivers and irrigation canal networks for an area of 1,700,000 ha. The Harran main canal is one of the largest irrigation canals in the GAP region. The first part of the Harran canal is 118 km long and the canal has a discharge rate of 74 m^3/sec at the beginning of the canal. It is designed to serve an irrigation area of 97,000 ha in the Harran Plain. Harran main canal is supplied from the Atatürk Dam reservoir via the Şanlıurfa tunnels.

The control algorithm was applied to the first 38,943 meter of the canal, i.e. 39 kilometers. This part of the canal includes 6 gates to maintain constant water levels immediately upstream of the gates. As shown in Figure 4.1, the irrigation canal has 5 pools and each pool has its canal geometry, gate and turnout properties. For numeric solution purposes, each pool was divided into nodes and all 5 pools together have 141 nodes. Pool geometries, gates and turnouts data is given in Appendix B. The downstream flow requirement at the end of the five pools, i.e, through gate 6, is 44.4 m^3/sec, and the opening of the last gate (gate 6) in the system was fixed at its initial steady state value. The target water levels, the initial flow rates into the lateral canals, and the disturbances are given in Table 4.1. The initial backwaters profile, and the initial gate openings for the canal are presented in Figure 4.2.

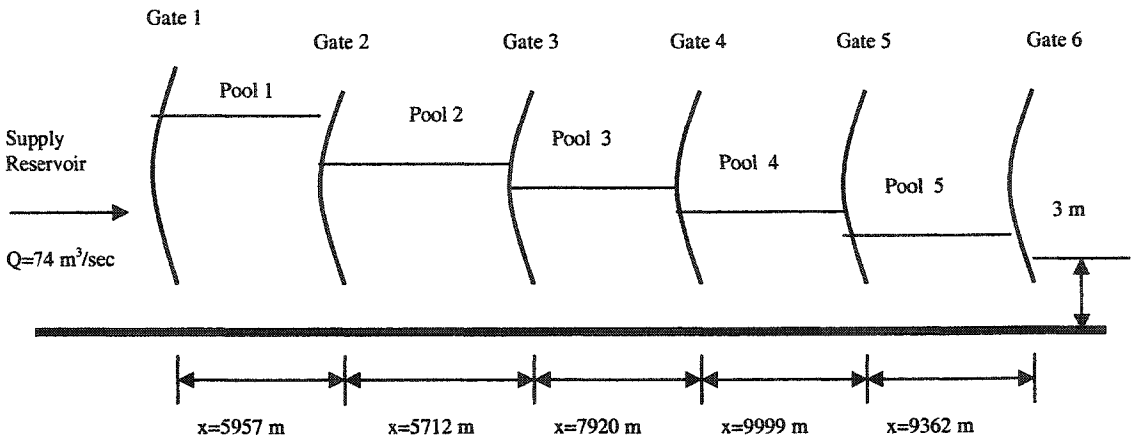

Figure 4.1. Physical Dimensions of the Canal System.

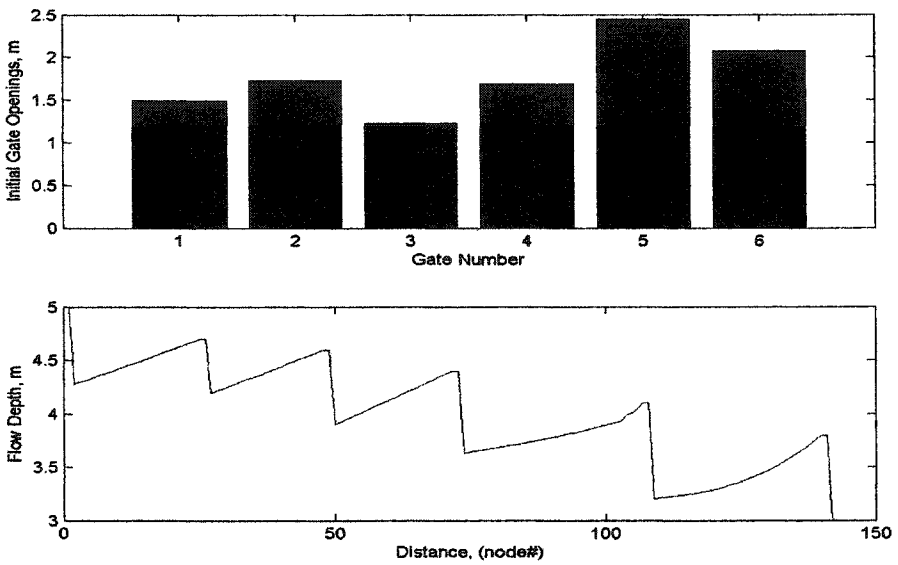

Figure 4.2. Initial Gate Openings and Backwater Profile.

Constant-level reservoirs were assumed to exist at the upstream and downstream end of the canal. Each pool in the canal has different number of nodes and each node has a linear set of equations. Pool1, Pool2, Pool3, Pool4 and Pool5 have 49, 45, 47, 69 and 65 set of state variables (flow depth and flow rate at each node), respectively, including the integral feedback variables in the problem. Based upon this information, the elements of all the matrices required in the analysis were calculated. In the derivation of the linear

equations, the turnouts of the pools were assumed to be located immediately upstream of the gates. In reality, the turnouts in the canal were at different locations. The principles of optimal control theory were applied to derive feedback controllers for constant-level control in all the pools.

Table 4.1 Data Used in Simulation Study.

Pool Number	Turnout initial flow rate (m^3/s)	Target Depth (m)	Disturbances (m^3/sec)
1	2.398	5	2.5
2	11.807	4.7	2.5
3	0.63	4.6	2.5
4	4.314	4.4	2.5
5	11.097	4.1	2.5

First, the canal data were used to calculate the steady state values for the state variables and the initial gate openings, which in turn were used to compute the initial gate openings and the elements of the A, B, and C matrices. The matrices Φ, Γ, and Ψ were obtained from matrices A, B and C matrices. In the derivation of these matrices, a sampling interval of 30 sec was assumed. The values of the initial gate openings for gate1, gate2, gate3, gate4 and gate5 were: u_1 = 1.4899 m, u_2 = 1.7258 m, u_3 = 1.2266 m, u_4 = 1.6875 m, u_5 = 2.4487 m, respectively. The analysis started by evaluating the system stability. All the eigenvalues of the system characteristic equation were positive and had values less than one. The controllability and observability matrices were calculated and the system was found to be both controllable and observable.

In order to evaluate the performance of the control algorithm, the canal dynamics was simulated for 15000 seconds with the feedback control algorithm and the Kalman filter in the loop. The simulation results of the control algorithm are discussed under three main categories. In the first category, the stability and robustness of the Linear Quadratic

Regulator (LQR) was analyzed for a constant-water level control in the system. In the second category, the stability and robustness of the Linear Quadratic Gaussian (LQG) controller in the control loop was compared with the LQR controller. In the third category, the stability of the robust control algorithm (LQG/LTR) was analyzed and compared with the stability of the LQR technique.

4.3. Analysis of Linear Quadratic Regulator (LQR)

The linear quadratic regulator for the multi-input and multi-output system minimized a quadratic objective function which included control penalties. Design of an optimal quadratic regulator for a linear system assumes full state feedback (i.e. assuming that values for all the state variables (water surface elevations, flow rates) were available) and a quadratic objective function. LQR control problem solution was an optimization problem in which the cost function to be minimized is quadratic in nature. The linear quadratic regulator (LQR) was designed to generate the control input, $\delta u(k)$, based upon the measured state-vector $\delta x(k)$.

4.3.1. Performance Results of Linear Quadratic Regulator Controller (LQR)

As first part of the optimal LQG controller, a Linear Quadratic controller was designed to regulate the five pool canal system using a constant-level control approach. The system response was simulated using the controller in the feedback loop. In the derivation of the feedback gain matrix K, the control cost weighting matrix, $R1$, of dimensions 5, was set equal to 100, whereas the state cost weighting matrix, $Q1$, was set equal to an identity matrix of dimensions 271. The matrix dimension 271 comes from the system dimension.

Since the irrigation canal is divided into 141 nodes and each node has a set of two equations, in other words the dimension of the system was 282. But the system has 6 gates and 5 turnouts; therefore, the system matrix dimensions was 271. The cost weighting matrix and the control cost matrix must be symmetric and positive definite (i.e. all eigenvalues of *R1* and *Q1* must be positive real numbers). A priori, we do not quite know what values of *Q1* and *R1* will produce the desired effect. In the absence of a well-defined procedure for selecting the elements of these matrices, these values were selected based upon trial and error. At first, we began by selecting both *Q1* and *R1* as identity matrices. By doing so, we were specifying that all state variables and control inputs were equally important in the objective function, i.e. it was equally important to bring all the deviations in the state variables (water surface elevations and flow rate) and the deviations in the control inputs to zero while minimizing their overshoots. Note that the existence of a unique, positive definite solution to the algebraic Riccati equation (Equation 2.100) is guaranteed if *Q1* and *R1* are positive semi-definite and positive definite, respectively, and the system is controllable. To test whether the system was controllable, the system controllability matrix was calculated and was found that the system was controllable. After defining *Q1* and *R1* matrices, the optimal feedback gain matrix, *K*, was calculated. Large components in gain matrix, K, could cause overtopping of the canals due to surge waves. Conversely, if the control is not of sufficient magnitude, the water level would return to the equilibrium condition very slowly, causing large deviations in depths of flow in the pools. Using the given initial values, the system response was simulated for 500 time increments or 15000 seconds. As shown in Figure 4.3, in all pools, the variations in flow depths returned to equilibrium. In pool5, the

variations in flow depth reached to approximately -0.1193 m at 15000 seconds, whereas in pool1, pool2, pool3 and pool4 the variations were small: -0.0128 m, -0.0313 m, -0.0472 m, and -0.0421 m, respectively, at 15000 seconds. The gates in the canal reached equilibrium position at 9000 seconds (Figure 4.4). Gate1 and gate2 had highest standard deviations of 0.0884 and 0.0814, respectively, and mean of cumulative changes in gate openings were approximately 0.1935 m, and 0.1730 m respectively. The deviations at gate1 are large because of highest discharge rate (74.4 m^3/sec) and downstream water requirements, whereas the deviations at gate2 were larger because of the high turnout rate (11.807 m^2/sec) adjacent to gate2. Gate3 and gate4 had almost the same amount of standard deviations, 0.053 m, for cumulative gate openings. At the beginning of the simulation, gate5 had a decrease in gate opening but later it reached a total of 0.03 m cumulative opening at 15000 seconds (Figure 4.5). Highest cumulative gate change was 0.2975 m at gate1 and lowest cumulative gate change was at gate5 0.0291 m. Finally, at the end of the simulation, the highest final gate opening at 15000 seconds was 2.4774 m at gate5 and lowest final gate opening was 1.4051 m at gate3 (Figure 4.6).

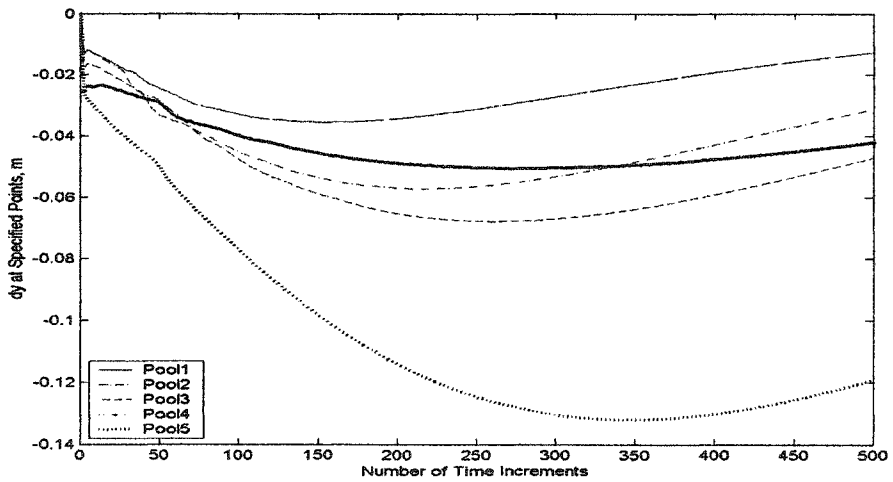

Figure 4.3. The Output of Final Depth Variations (dy) using LQR Controller.

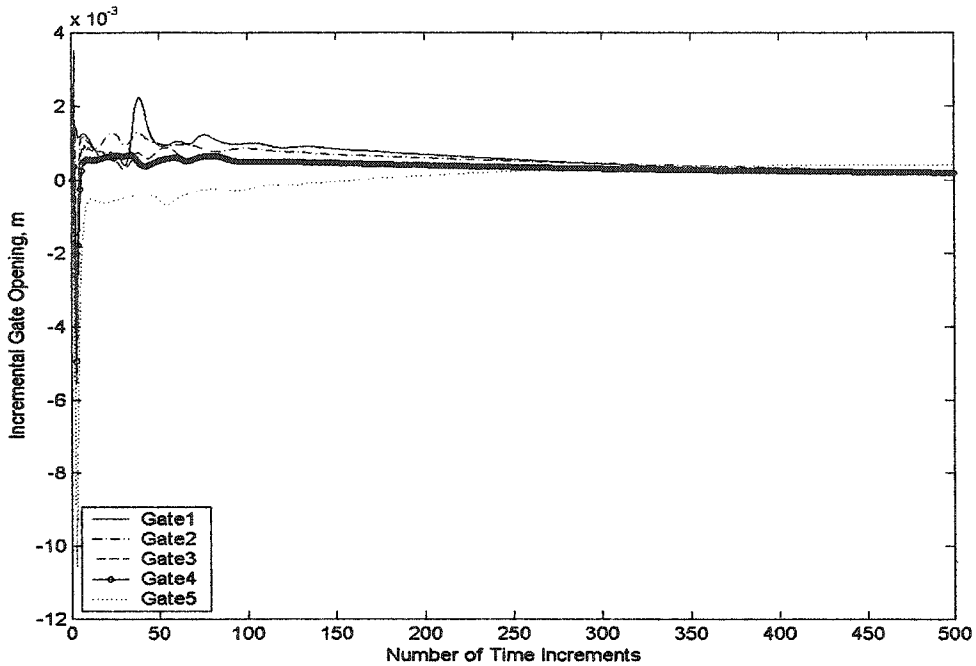

Figure 4.4. Incremental Gate Opening using LQR Controller.

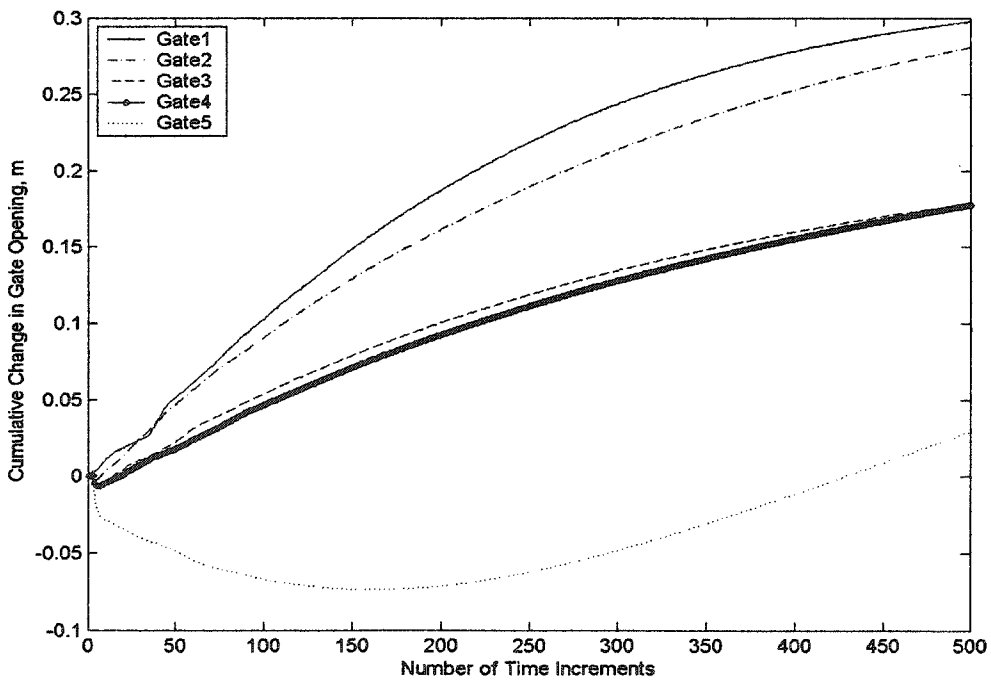

Figure 4.5. Cumulative Gate Opening using LQR Controller.

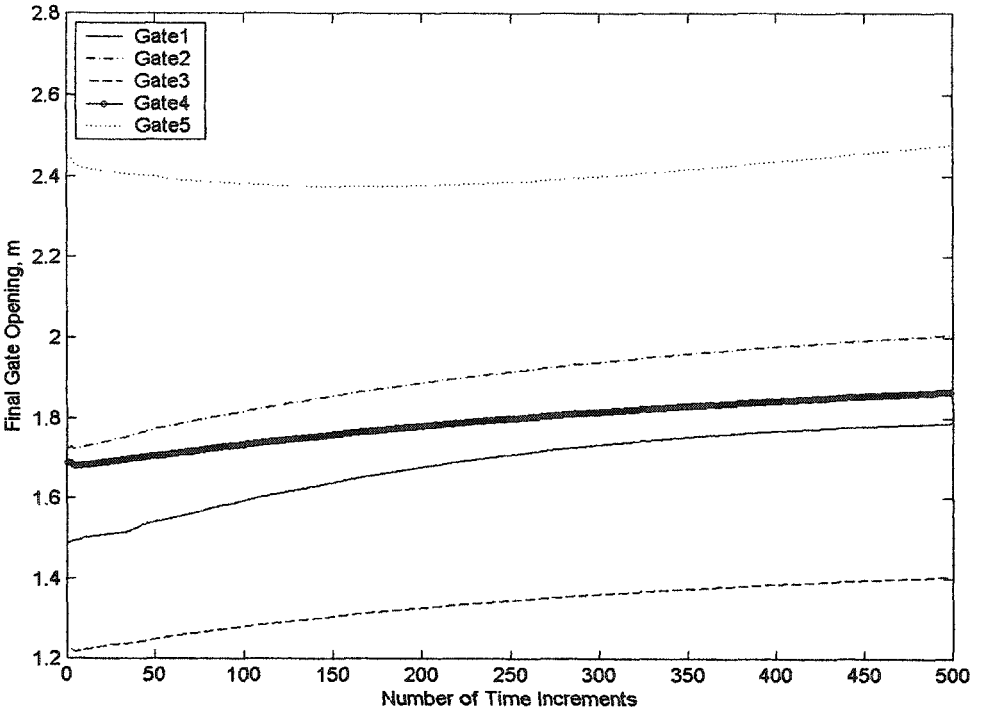

Figure 4.6. Final Gate Opening using LQR Controller.

4.3.2. Stability and Robustness Results of Linear Quadratic Regulator (LQR)

For stability and robustness analysis of the LQR controller, the frequency response methods were used to show the system's response to initial conditions at different frequency ranges (bandwidth). Singular values and Bode plot robustness and stability analysis were conducted for the system. As explained in Chapter 2, it is well known that if *R1* and *Q1* matrices are chosen right, LQR controller (i.e. assuming all the states are available and no stochastic inputs) will have prefect robustness properties. That is, the LQR controlled system will have a gain margin equal to infinity for each control input of the system. Then we can say that LQR singular values and LQR Bode diagrams will be target loop functions for the irrigation canal stability and robustness analysis.

The singular values (SV) of LQR controller help us analyze the stability and robustness properties of a multivariable feedback system. Singular value graphs show maximum and minimum singular values. In other words, one pool has two singular value curves. For analyzing robustness of LQG controller, the singular values of the LQR controller were used as a Target Loop Function (Figure 4.7). The singular values (SV) of LQR controller were graphed on a semi-log scale. The x-axis of the graph represents frequency, ω (rad/sec), and the y-axis represents the magnitude of the gain margin in decibel (dB). Figure 4.7 shows singular values (SV) of LQR regulator of the control algorithm.

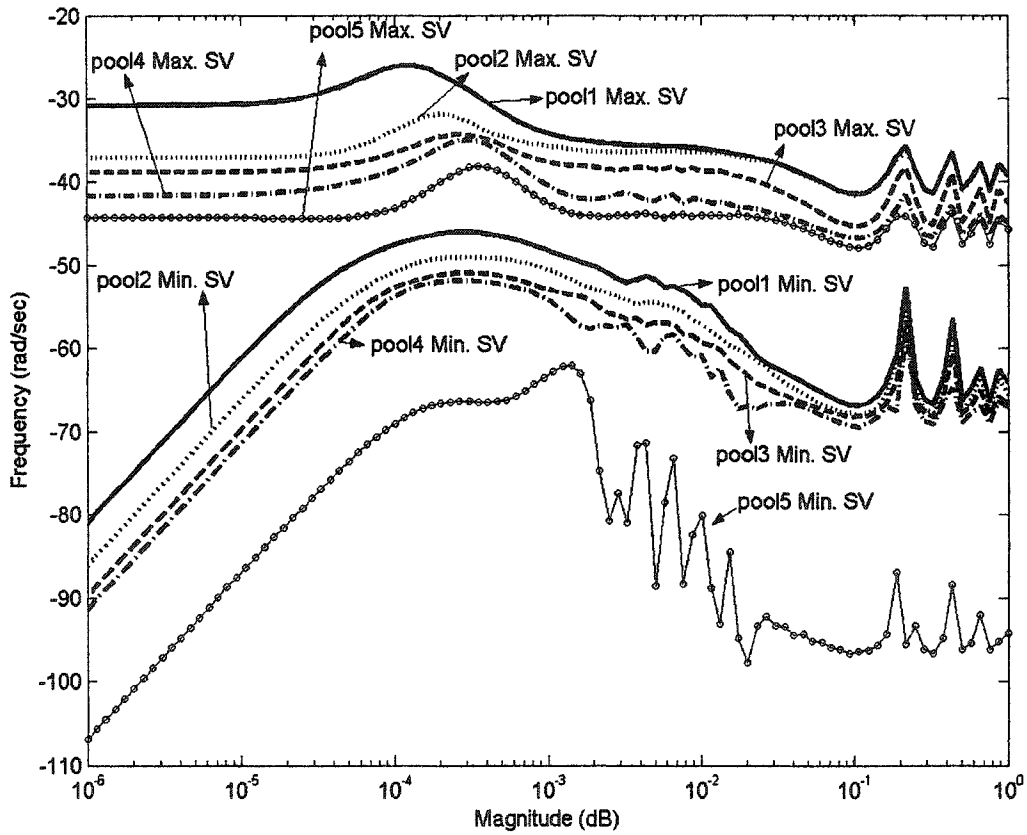

Figure 4.7. Singular Values using LQR Controller.

At low frequencies, the LQR controller was stable except Pool5. When the disturbance frequency, ω, reached 0.1 rad/sec, the system started having oscillatory behavior. Pool5 had oscillatory behavior when the frequency was equal to 0.001 rad/sec. Since the LQR controller has the best robustness properties, the control algorithm will use these singular value curves in loop shaping of the LQG controller.

As a second analysis, Bode diagrams were used to define gain margin and phase margins of the LQR controller for stability margins. Gain margin is the change in closed loop gain required to make the system unstable. Phase margin is the change in closed loop phase shift required to make a closed loop unstable. Figure 4.8 shows the Bode diagram for the irrigation canal control system and we had 10 sets of Bode diagrams for each pool. The reason for that is that the system has 10 external inputs (disturbance), two for each pool (one at the beginning of the sampling interval and the other at the end of the sampling interval). The Bode diagram has two different graphs which are gain and phase margins. The x-axes in both graphs represent the disturbance frequency, ω, whereas the y-axes represent the magnitude of the gain margin in decibel (dB) in gain graph and degrees of phase in phase graph. Since it was time consuming to analyze all Bode graphs in the system, a set of graphs was chosen from pool1 to see the stability properties of the LQR controller for the control system. Figure 4.9 shows that the robustness properties of the LQR controller in pool1 for initial conditions of the canal. The phase margin is the difference in phase between the phase curve and -180 degrees at the point corresponding to the frequency that gives a gain of 0 dB (the gain cross over frequency). Likewise, the gain margin is the difference between the magnitude curve and 0 dB at the point corresponding to the frequency that gives us a phase of -180 deg (the phase cross over

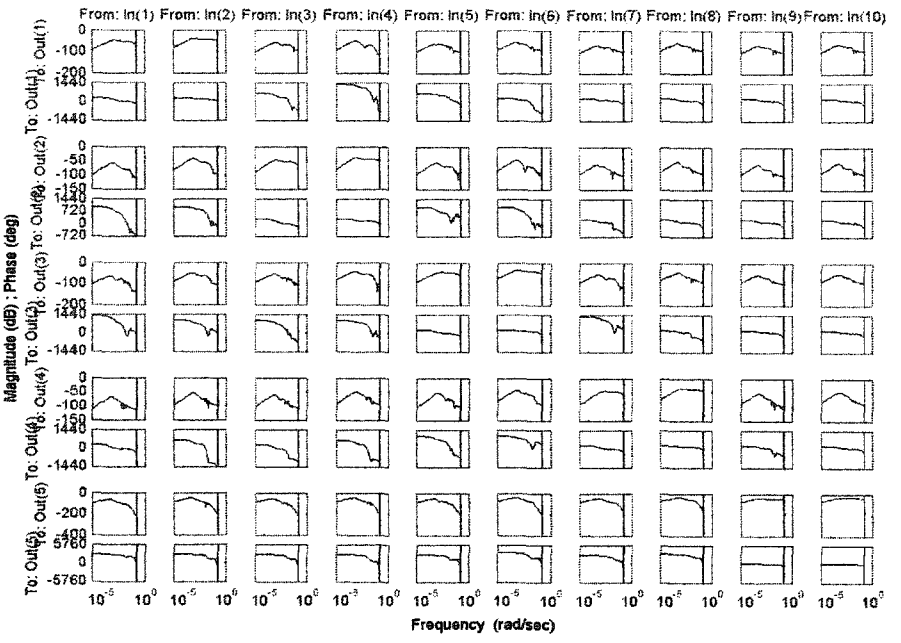

Figure 4.8. Bode Stability Diagram of All Pools using LQR Controller.

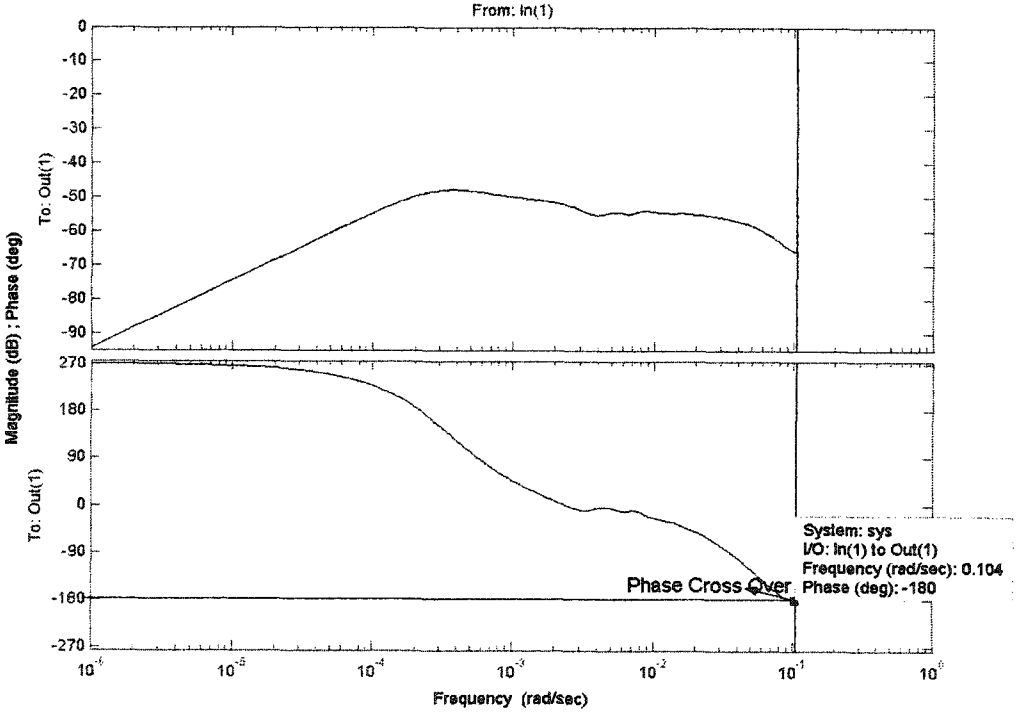

Figure 4.9. Bode Stability Diagram of Pool1 using LQR Controller.

frequency). It was obvious that phase reached -180 deg where frequency was 0.104 rad/sec. In other words, the phase cross-over point was at frequency 0.104 rad/sec. Since all gain margins at all frequencies were less than zero dB, then we can say that at all disturbance frequencies the control system was stable in pool1 for the LQR controller. This implied that the control system's LQR controller had good stability properties.

4.4. Analysis of Linear Quadratic Gaussian (LQG) Controller

The Linear Quadratic Regulator (LQR) was used to obtain the elements of the controller gain matrix (K) and the performance of the model with full-state feedback was found to be acceptable. However, in LQR design we assumed that measured values for all the state variables needed in the feedback loop were available. The stability of the control algorithm with full-state feedback was acceptable. However, the implementation of the LQR control algorithm would be very expensive because of the required number of measured values for the state-variables in a canal system. Usually, one or two flow depths per pool are measured in the regulation of irrigation canals. To minimize the cost of implementing the control algorithm, the number of flow depth measurements available per pool was assumed to be two, and the values for the rest of the variables needed in the feedback loop were estimated using an on-line observer. The control algorithm designed an observer using the Kalman filter technique to estimate the values for the state variables in the system. Kalman filter for the system used the control input $\delta u(k)$, generated by the LQR, measured water depths $\delta y(k)$ for each pool, and the disturbances $\delta q(k)$ and $\eta(k)$ with known power spectral densities, ρ. The Kalman filter is designed to provide an optimal estimate of the state variables vector, $\delta x(k)$. In the design of the Kalman filter, in

lieu of actual field data on withdrawal rates from the turnouts, the random disturbances were assumed to have some prespecified levels of variance. The actual time series of the demands was not used in the design of the filter; only the variance of the time-series was required in the design of the filter. Usually the sensors is used to measure flow depths in open-channel are reasonably accurate to a fraction of a centimeter; therefore, the variance of the measurement error is usually very small. The variances of the disturbances must be estimated from historical records on water withdrawals from the canal outlets. The control algorithm used a diagonal disturbance matrix, $Q_{esti,}$ along the diagonal. The variances of the disturbances were: $w_1=1^2$, $w_1=1.3^2$, $w_1=0.7^2$, $w_1=1.4^2$ and $w_1=1.3^2$. A value of 0.0005 was used for the variance of the measurement spectral density matrix (RC), and it was an identity matrix. The observer estimated the values for the intermediate state variables, given two flow depth measurements in each pool (upstream and downstream ends of a pool). Note that in the case of the steady state Kalman filter design, the selection of the value for the measurement spectral density covariance matrix was based upon a trial-and-error approach. However, since the same noise covariance was assumed for all the pools, the effort involved in the selection of a value for the covariance matrix was easy compared with the effort needed to select optimal locations for the poles in the case of a MIMO control system.

4.4.1. Performance of the Linear Quadratic Gaussian (LQG) Controller and its Comparison with the LQR Performance

After designing the Kalman filter, the control algorithm combined both the LQR controller and the Kalman filter to design an optimal Linear Quadratic Gaussian

controller (LQG) which generated the control input, $\delta u(k)$, based upon the estimated state-vector, $\delta\hat{x}(k)$, rather than the actual state-vector, $\delta x(k)$, and the measured output vector, $\delta y(k)$. Figure 4.10 shows the depth of flow variations for LQG and LQR design in each pool. The highest flow depth variation was in pool5 where LQR controller had highest flow depth variations. The final depth variations for LQG controller were -0.0139 m, -0.0308 m, -0.0433 m, -0.0369 m, and -0.0914 m, respectively, in pool1, pool2, pool3, pool4 and pool5, at 15000 seconds. There were no significant differences between the flow depth variations for LQR and LQG controller. Figure 4.11 compares the incremental gate opening for both LQG and LQR controllers. Incremental gate openings for the LQG controller was very close to LQR's gate openings. Final gate openings and cumulative gate openings had very close values to LQR controller's final and cumulative gate openings.

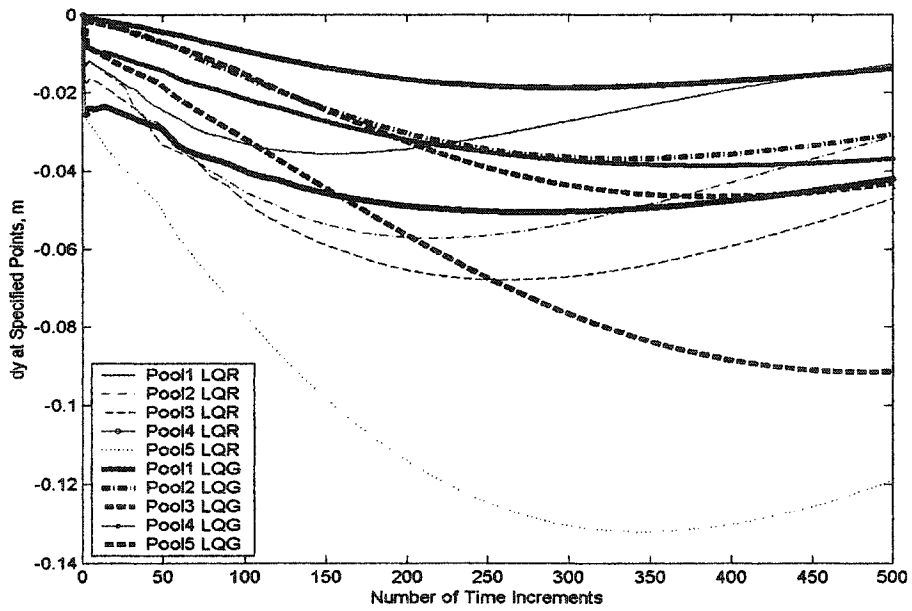

Figure 4.10. Comparison of Flow Depth Variations using LQR and LQG Controllers.

As shown in the Figures, LQG controller's flow depth variations and gate openings had no significant changes compared to LQR controller's gate openings and flow depth variations. This was because of the perfect selection of the optimal regulator's weighting matrices, *Q1* and *R1*, and the Kalman filter's spectral disturbance densities, *RC* and *Qesti*. Hence, the matrices *Q1*, *R1*, *RC*, *Qesti* and scale parameter, ρ, were the design parameters for the LQG controller. Note that a judicious choice of Kalman filter's spectral disturbance density matrix would yield the best recovery of the full state feedback (LQR) dynamics.

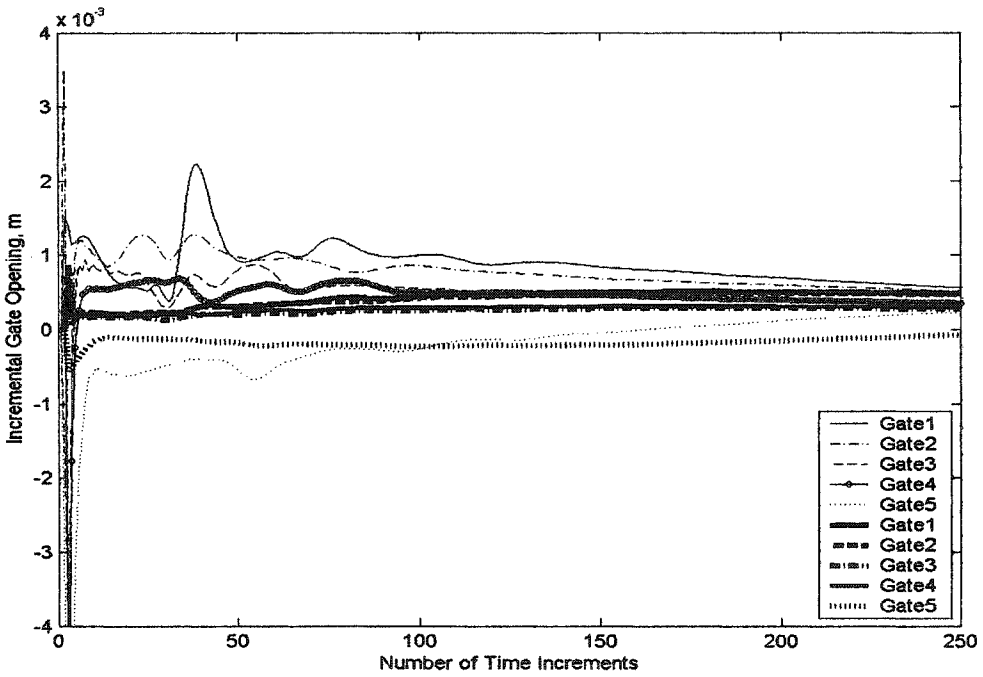

Figure 4.11. Comparison of Incremental Gate Openings using LQG and LQR Controllers.

4.4.2. Stability and Robustness Results of Linear Quadratic Gaussian (LQG) Controller and Comparison with LQR Controller

After achieving a stable LQG controller, the control algorithm examined the robustness and stability of the designed LQG compensated closed-loop controller with respect to the

unknown disturbances in comparison with the full-state feedback system. The LQG controller had good stability properties, but the robustness properties of LQG controller to the actual disturbance variations were not evaluated. Since LQR controller had the best robustness properties, the robustness analysis of the LQG controller uses the LQR robustness properties as a target. Bode diagram and singular value analysis were used in the study. As shown in Figure 4.12, for the sake of simplicity, we didn't show the maximum singular values of the LQG and the LQR controller. Figure 4.12 shows that

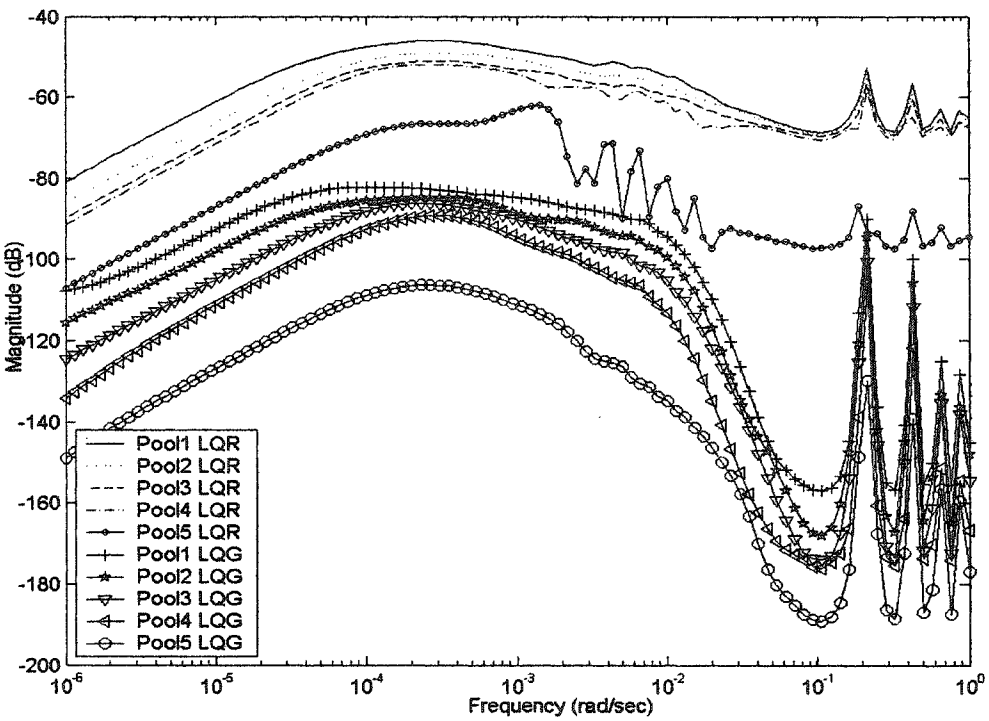

Figure 4.12. Minimum Singular Values Comparison of LQG and LQR Controllers.

there are some differences between the minimum singular values of the LQG compensated system and the full-state feedback system, indicating that even though LQG controller was stable, the LQG controlled system was much less robust than the full-state

feedback system (LQR). The y-axis of Figure 4.12 represents the magnitude of the singular values of the return ratio matrix in decibel and the x-axis of Figure 4.12 represents the frequency of the disturbances. As mentioned in Chapter 2, the function $H(z)G(z)$ is called the return ratio. $H(z)$ is the transfer function of the LQG controller and $G(z)$ is the transfer function of the system. For LQR controller, the return ratio, $H(z)G(z)$, is equal to $-K(zI-phi1)^{-1}\Gamma$. When the LQG compensated controller was designed, the singular values of the return ratio, $H(z)G(z)$, was targeted to approach the corresponding singular values of the LQR controller. To determine the stability of the LQG and the LQR controllers, in the analysis, we investigated how close the singular values of the return ratio were close to zero. Since the LQR was the target loop function, the investigation concentrated on adjusting the LQG's singular value curves as close as to the possible LQR's singular value curves. It is obvious from Figure 4.12 that the first 4 pools were stable at higher sinusoidal frequencies for LQR controller but pool5 has oscillation when the frequency was 0.001 rad/sec. However, for all 5 pools the LQG controller was more stable until a frequency of 0.01 rad/sec. But when the sinusoidal frequency increased, all pools started having higher oscillations than the LQR had. But as far as the robustness of LQG was concerned, the system was less robust than LQR. It was obvious that if the LQR and Kalman filter were combined together, there will be a loss of robustness for the new compensated controller (LQG) as compared to the full-state feedback LQR controller. Also, there are some differences in the flow depth variations. In pool5 the variation in flow depth was equal to 0.1193 m for LQR design, whereas, it was 0.0914 m for LQG design. This implies that the performance of the LQG controller is inferior to the performance of the LQR controller, at least in pool5.

Bode plots show the stability analysis of the LQG controller. Figure 4.13 shows all gain and phase margin diagrams for all the pools, in response to all the 10 external disturbances (inputs). From these graphs it is obvious that the LQG controller has a good stability like LQR. For clarity, the response of the first pool to the first disturbance is discussed for the purpose of stability analysis. Figure 4.14 represents the Bode diagram of pool1 for the first sinusoidal disturbance. The gain margin for both the LQG controller and the LQR controller was high. Because both curves are very far away from 0 dB. If the curves were close to or over the 0 dB, the system would be unstable. In other words, the gain margin would be small. In other words, the LQG and the LQR controllers are both stable but the phase diagram did not allow us to make that same statement about the robustness of the LQG controller. It was obvious that LQR curve had a cross over with -180 degrees around a disturbance frequency of 0.104 rad/sec and it had a large frequency range (bandwidth) for stability. The LQG curve has a phase crossover at a disturbance frequency of 0.000139 rad/sec. In other words, LQG controller could lose its stability if the frequency range of the disturbance was increased beyond 0.000139 rad/sec. A comparison of the LQR and the LQG stability bandwidths reveals that LQR is stable at all disturbance frequencies whereas LQG has less frequency range for stability.

4.5. Stability and Robustness Analysis of Linear Quadratic Gaussian/Loop Transfer Recovery (LQG/LTR) Controller

For recovering the full-state feedback robustness in LQG controllers, the control algorithm used a H_2-norm minimization loop shaping technique and redesigned the Kalman filter by adjusting the disturbance spectral density matrix with a scale parameter,

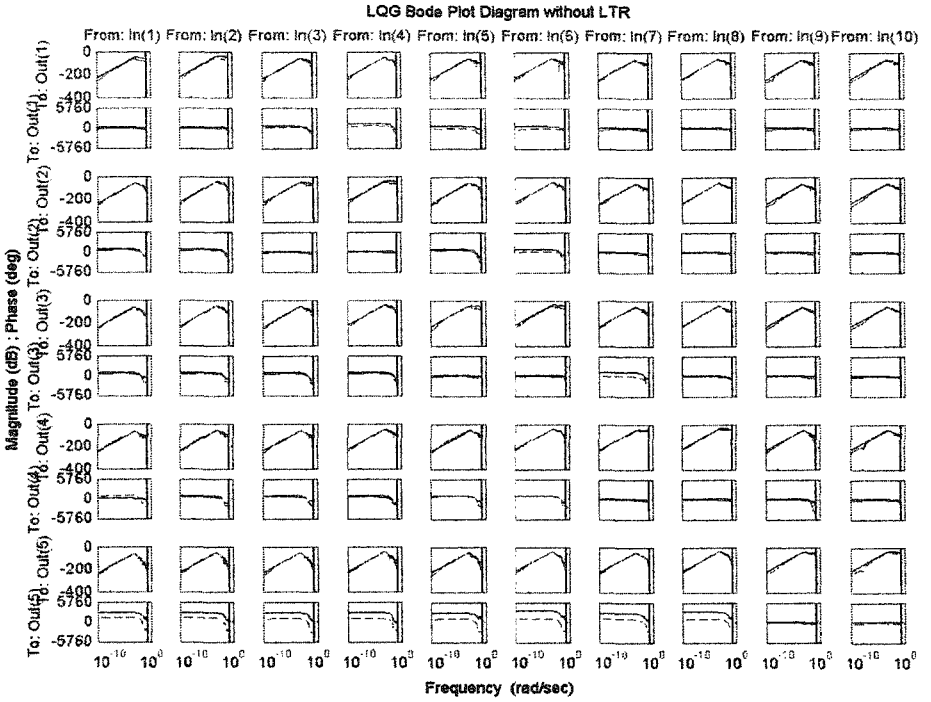

Figure 4.13. Comparison of Bode Diagrams of LQR and LQG Controllers.

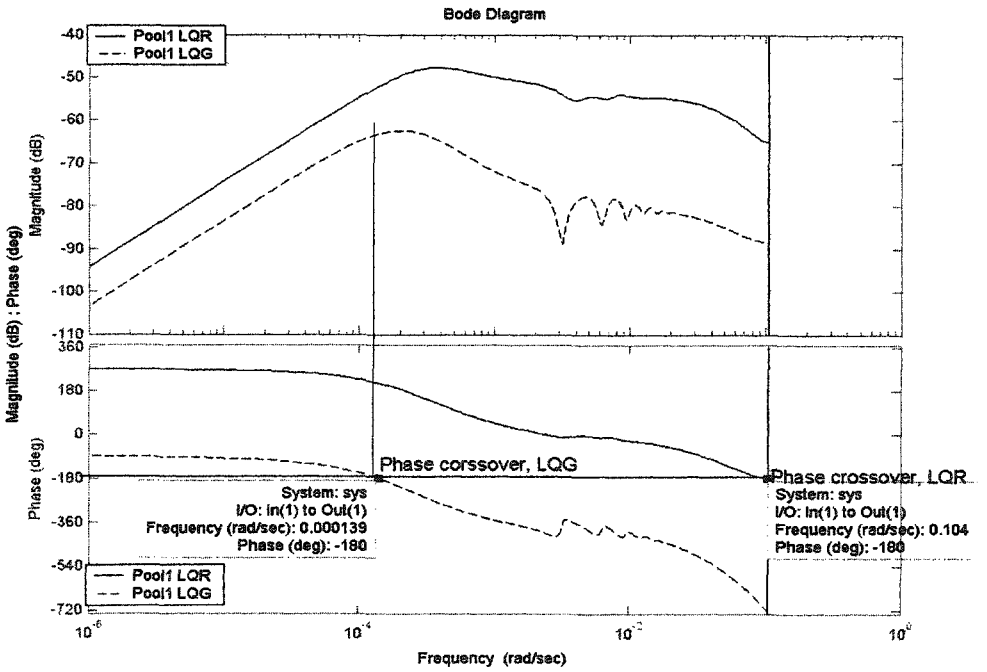

Figure 4.14. Comparison of Bode Diagrams of LQR and LQG in Pool 1.

ρ, to approach the full-state feedback LQR controller return ratio. The values used for the scale parameter were 25, 75, 260, 2500, 3000. The algorithm tuned the Kalman filter design by raising the level of input process noise until the sensitivity at the plant input for the state estimate feedback design was similar to that of the full-state feedback design in the frequency range of interest.

4.5.1. Simulation Results for LQG/LTR Controller: ρ = 25

The control algorithm started to tune the LQG compensator by setting the value of the scale parameter, ρ, at 25. As shown in Figure 4.15, there was no significant change on the variations in flow depth in the pools when the scale parameter was increased to 25 units. The variations in flow depth were very close to the ones that were obtained for LQR. The variations of final depth were -0.0147 m, -0.0348 m, -0.0510 m, -0.0425 m, and -0.1105 m in pool1, pool2, pool3, pool4 and pool5, respectively, at 15000 seconds.

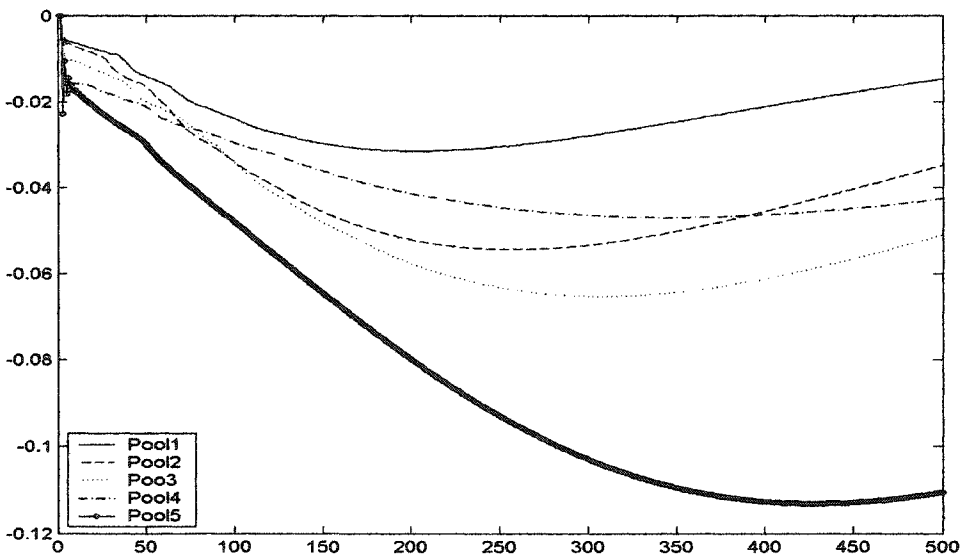

Figure 4.15. Variations of Flow Depth using LQG/LTR Controller with ρ= 25.

Also the results for the gate opening were very close to LQR controller. Figure 4.16 shows that there was not much change in incremental gate opening and the system reaches equilibrium at 12000 seconds. The final gate openings and cumulative gate openings were very close to the LQR and the LQG values. It was obvious that if the scale parameter was increased by 25 units, this increase would not have any significant effect on system equilibrium.

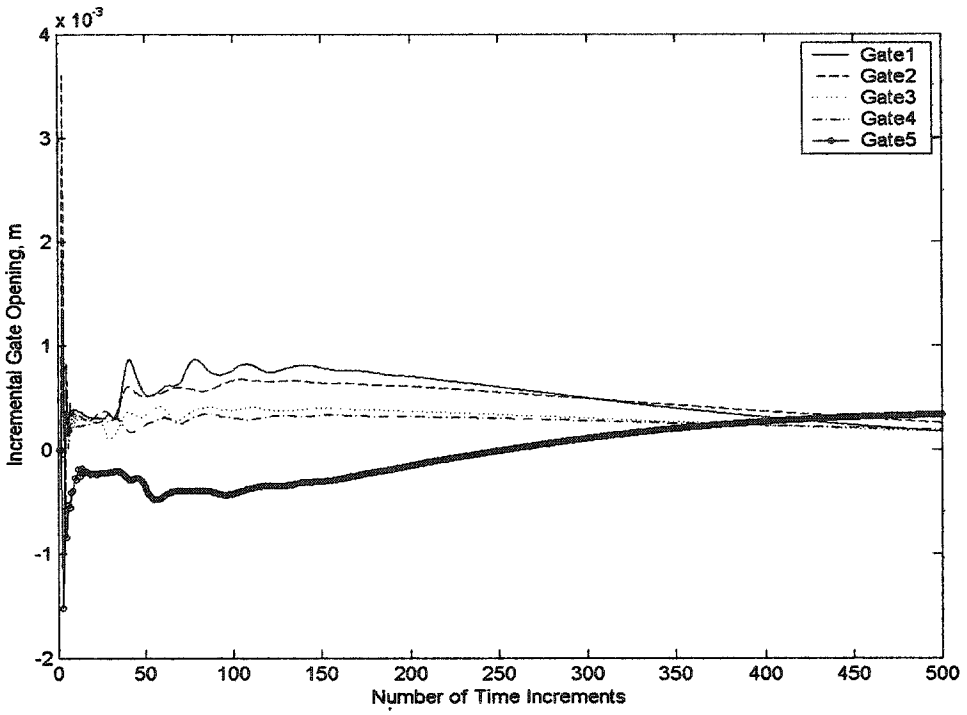

Figure 4.16. Incremental Gate Opening using LQG/LTR Controller with ρ = 25.

But as shown in Figure 4.17 there was some improvement in robustness properties of LQG design singular values with ρ=25 units. Figure 4.17 shows the singular values for each pool in different graphs. In pool1, there was a good robustness improvement with loop shaping and the return ratio of LQG/LTR approached that of the LQR controller. Again at high disturbance frequencies, ω=0.1 rad/sec, the LQG/LTR system was oscillating but the system was coming close to the target loop function of the LQR, i.e.,

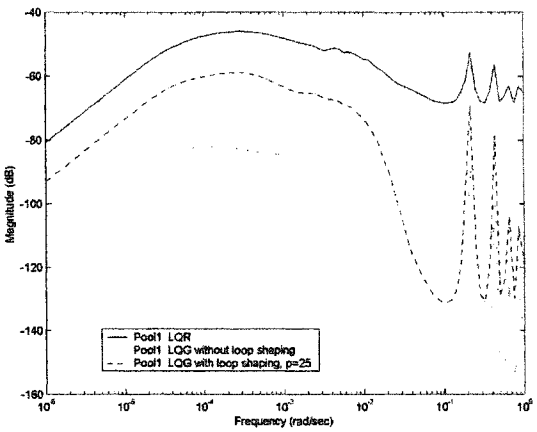

Pool1

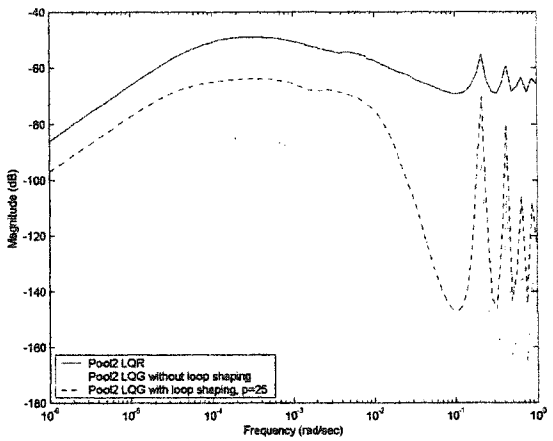

Pool2

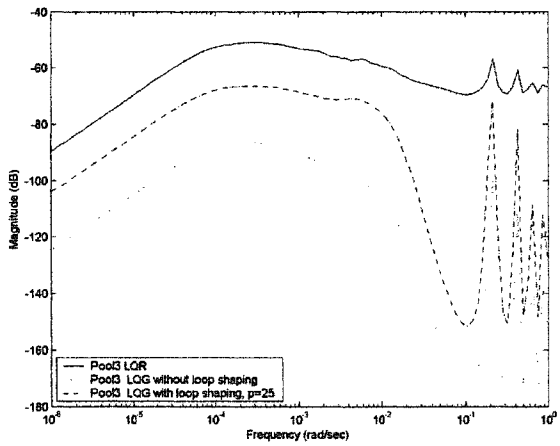

Pool3

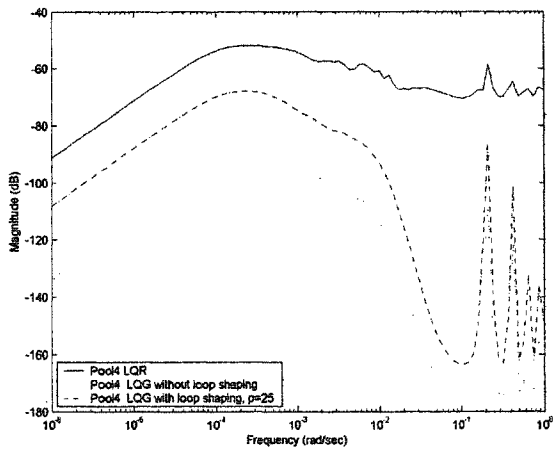

Pool4

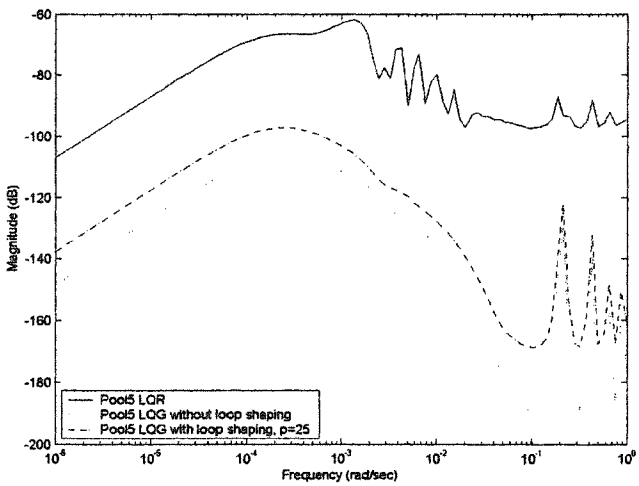

Pool5

Figure 4.17. Comparison of Singular Values of LQR, LQG and LQG/LTR Controllers with ρ=25.

the robustness of the system was increasing. In pool2, the LQG controller with or without loop shaping had oscillatory behavior at high frequencies, ω=0.01 rad/sec, but overall the system was stable and there was robustness improvement for the LQG/LTR controller. Pool3 had stability when the sinusoidal disturbance was increased and also the singular values shifted to the target loop function (LQR). Pool4 was stable and the robustness properties of pool4 improved when the frequency of the external disturbances was increased. Again pool4 had stability for sinusoidal disturbance frequency of less than 0.01 rad/sec. Pool5 had better stability in LQG/LTR design than that of LQR, because LQR target loop has oscillatory behavior at low disturbance frequencies, ω=0.001 rad/sec, whereas LQG does not have oscillatory until the disturbance frequency, ω=0.01 rad/sec. Increasing the disturbance frequency scale parameter value improved the robustness properties of the LQG/LTR design. With increased scale parameter values, the variations in flow depth approached LQR's variations in flow depth (0.1193 m at 15000 seconds). For example, in pool5 the variations in flow depth for ρ=25 was 0.1105 m at 15000 seconds. This means the LQG/LTR design with ρ=25 was approaching the performance of the LQR.

Gain and phase margin of the LQG/LTR controller was evaluated using Bode graphs. Figure 4.18 displays the Bode diagrams for all the pools with the LQG/LTR controller with the scale parameter ρ=25. All diagrams show that if the scale parameter was increased to 25 units to adjust the disturbance spectral density matrix, there will be no significant change in the stability of the system but there would be some improvement in robustness. To see the stability in pool1, the Bode diagrams for pool1 were analyzed in more detail. Figure 4.19 shows the gain and the phase margin for pool1. It is obvious that

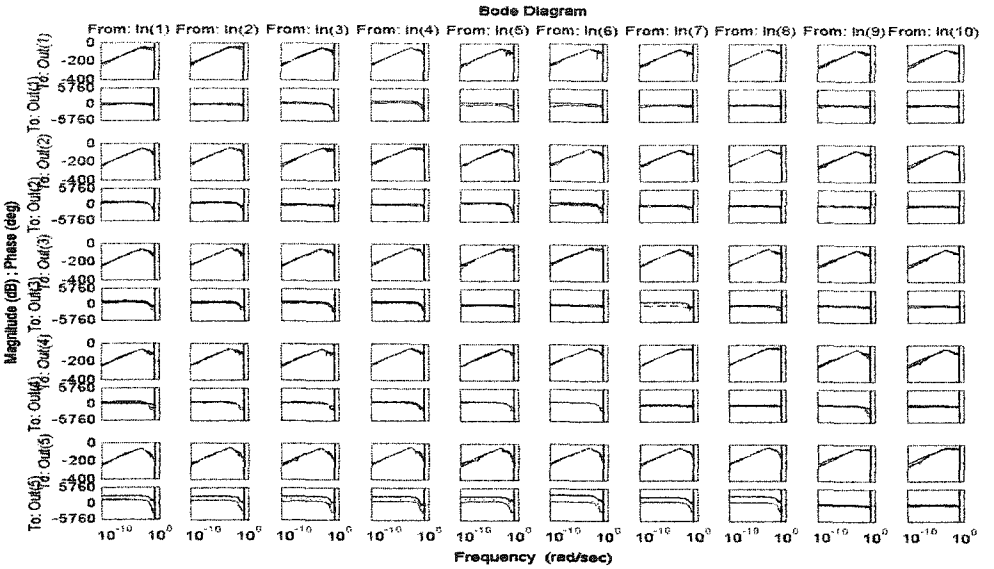

Figure 4.18. Comparison of Bode Diagrams of LQR, LQG and LQG/LTR Controllers with ρ=25.

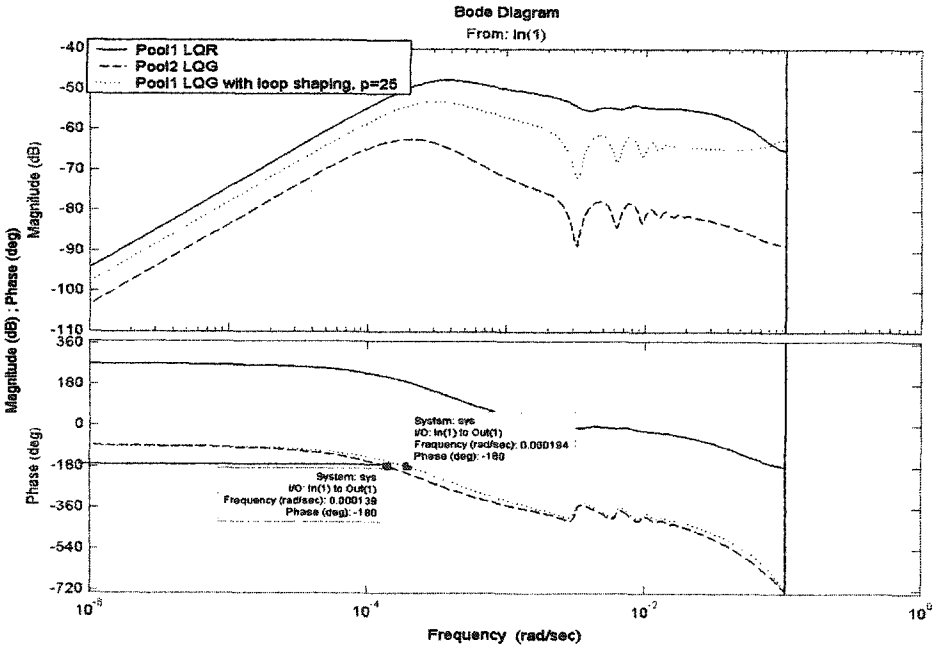

Figure 4.19. Comparison of Bode Diagram of LQR, LQG and LQG/LTR Controllers in Pool1 with ρ=25.

with loop shaping technique the system will improve its robustness properties. Since the LQG/LTR controller was stable, in other words the gain margin curve was under 0 dB, there was not a significant difference in the gain margin but the phase crossover point moved to the right. That means the system could lose its stability if the disturbance frequency was more than 0.000194 rad/sec.

4.5.2. Simulation Results for LQG/LTR Controller: $\rho = 75$

Since adjusting the disturbance density matrix with the scale parameter ρ increases the system robustness, the value of the scale parameter was increased to 75. A new LQG controller was designed with ρ=75, and the performance of the new controller was simulated. No significant changes in the variations of flow depth were observed (Figure 4.20). The variations in flow depth were: -0.0143 m, -0.0341 m, -0.0504 m, -0.0423 m, and -0.1114 m, respectively, in pool1, pool2, pool3, pool4 and pool5 at 15000 seconds. The gate openings of the LQG controller with and without loop shaping were very close (Figure 4.21). Final gate openings were 1.7873 m, 2.0062m, 1.4051 m, 1.8650 m and 2.4774 m in pool1, pool2, pool3, pool4 and pool5, respectively, at 15000 seconds. The control system reached equilibrium values at 12000 seconds when the scale parameter for disturbance spectral density matrix was increased to 75.

The singular values of the return ratio was analyzed to study the robustness properties of the LQG/LTR controller. Figure 4.22 shows the singular values of all the pools with the system disturbance matrix scale parameter ρ =75. Pool1 was still stable with the scale parameter value increased to 75. The oscillatory behavior starts at 0.1

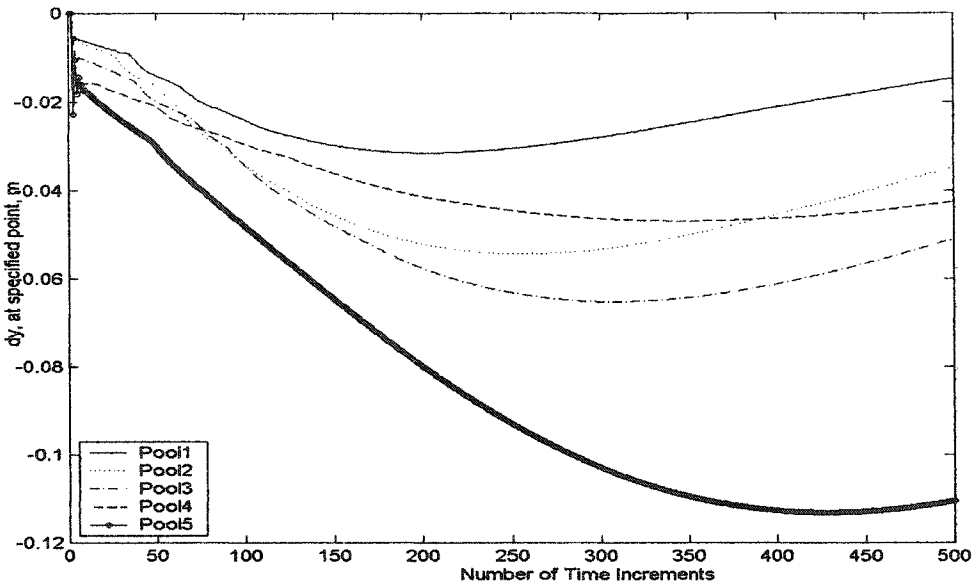

Figure 4.20. Variations of Flow Depth using LQG/LTR Controller with ρ = 75.

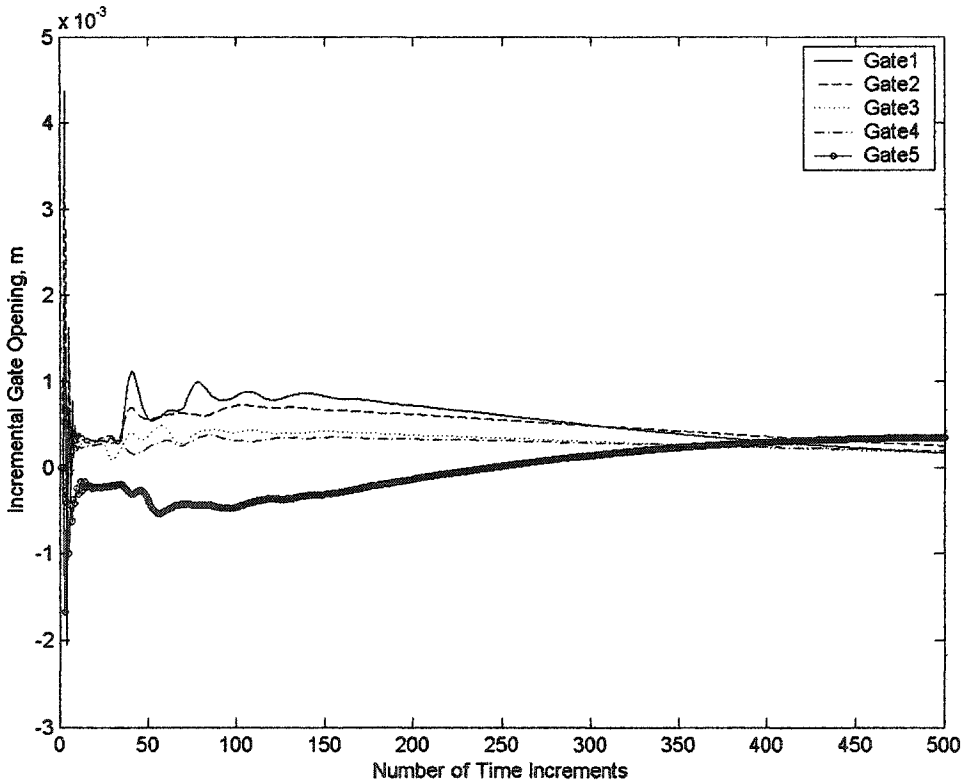

Figure 4.21. Incremental Gate Opening using LQG/LTR Controller with ρ = 75.

rad/sec disturbance frequency for all the four designs (LQR, LQG, LQG/LTR, LQG/LTR with ρ =75). However, when the scale parameter value, ρ, was increased from 25 to 75, there was some improvement in the robustness and the singular value curves shift closer to the LQR target loop curve. The system was stable in pool1 at a large disturbance frequency range. pool2 was stable but the singular values become oscillatory at high frequencies like 0.1 rad/sec. Increasing the scale parameter for disturbance spectral density matrix improved the robustness in pool2. The singular value curve was shifting towards the target loop, LQR. pool3 and pool4 are both stable like pool1 and pool2. The oscillations start at high disturbance frequencies (larger than 0.1 rad/sec). Also there was some improvement in robustness of the system in pool3 and pool4 because the singular value curves shifted upward and approached to the LQR target loop function. Pool5 was a little bit different than other pools as far as the stability was concerned. When the scale parameter for the disturbance matrix (or spectral density matrix) was increased and the disturbance frequency was high, the control system was more stable than that of LQR. Since LQR had better robustness properties, we tried to push this curve towards the LQR singular values curve. Especially in this pool, the LQR controller is less stable when the disturbance frequency range was over 0.001 rad/sec whereas the three different LQG designs were more stable until the disturbance frequencies reached to 0.1 rad/sec. Also the variation in flow depth was 0.1114 m in pool5 for ρ=75 at 15000 sec. When this value is compared with other two designs, LQG and LQG/LTR (ρ=25), it is obvious that this value is closer to LQR's value (0.1193 at 15000 second). In other words, with ρ=75, the control system performance was approaching the LQR performance in pool5.

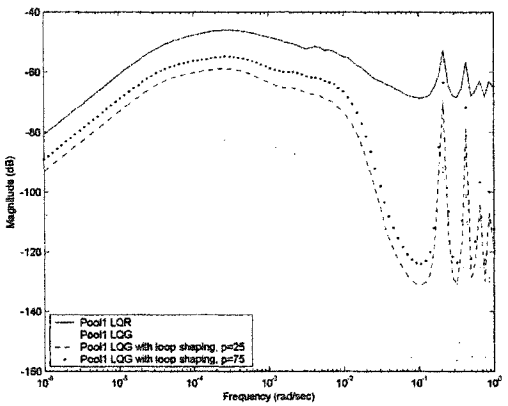

Pool 1

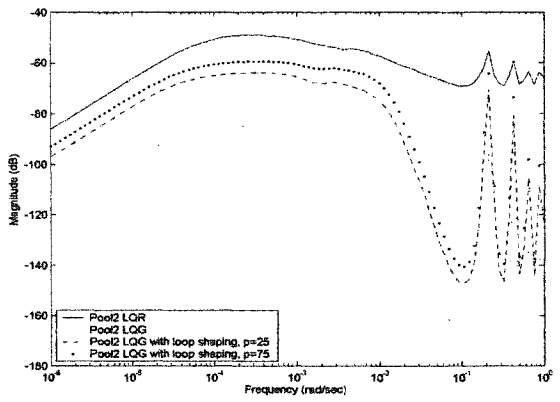

Pool 2

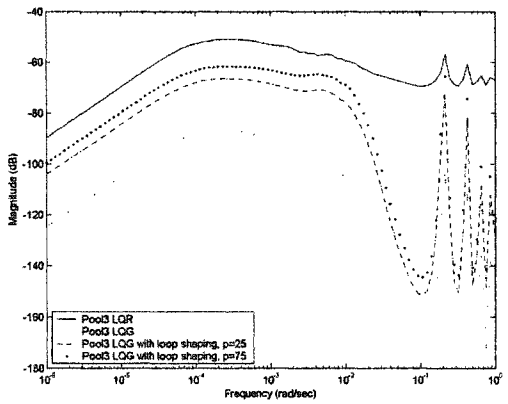

Pool 3

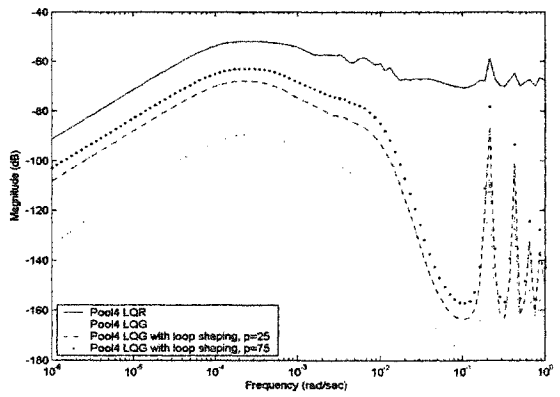

Pool 4

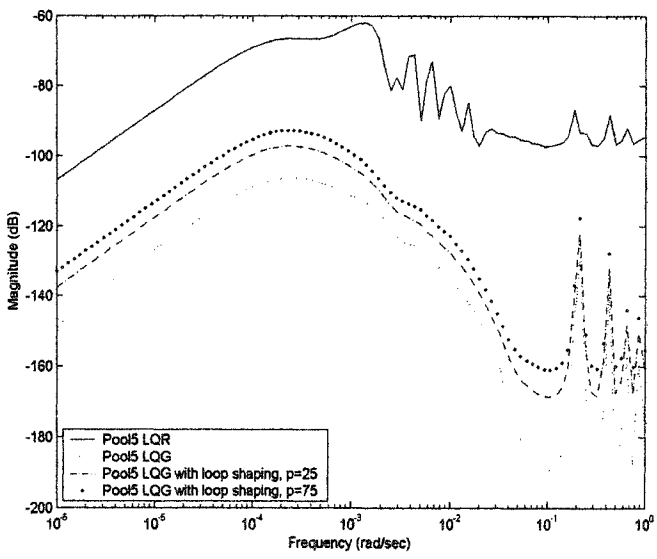

Pool 5

Figure 4.22. Comparison of Singular Values of LQR, LQG and LQG/LTR Controllers with ρ=75.

Figure 4.23 shows the Bode diagrams for all the five pools. Since the gain margin was under 0 dB, the control system for the irrigation canal had very good stability for all the pools where ρ=75. To explain this better and for simplicity, an individual Bode diagram for Pool1 was analyzed. As shown in Figure 4.24, the phase crossover of the control system was shifted to the right, in other words, the system can withstand higher disturbance frequencies. Since the system was stable both for the LQR and the LQG/LTR controller, no gain crossover was observed. When the disturbance density matrix scaling parameter, ρ, was increased, the system improved its robustness.

4.5.3. Simulation Results for LQG/LTR Controller: ρ = 260

To recover the robustness of the full-state feedback LQR controller, the scale parameter for the disturbance spectral density matrix was increased from 75 to 260. When the scale parameter was increased to 260, again there was no significant change in the stability of system. The variations in flow depths were close to the variations in flow depth obtained with the LQR controller. Figure 4.25 shows the variations in flow depth for the new LQG design with the scale parameter ρ = 260. The variation of flow depth were -0.0139 m, -0.0334 m, -0.0494 m, -0.0418 m and -0.1114 m in pool1, pool2, pool3, pool4 and pool5, respectively, at 15000 seconds. Figure 4.26 shows the gate openings for this particular LQG/LTR design. No significant changes in the incremental gate openings were observed with LQR and the other LQG/LTR designs. The final gate openings at 15000 seconds were 1.7873 m, 2.0062 m, 1.4051 m, 1.8650 m and 2.4774 m in pool1, pool2, pool3, pool4 and pool5, respectively. These final gate openings were very close to the

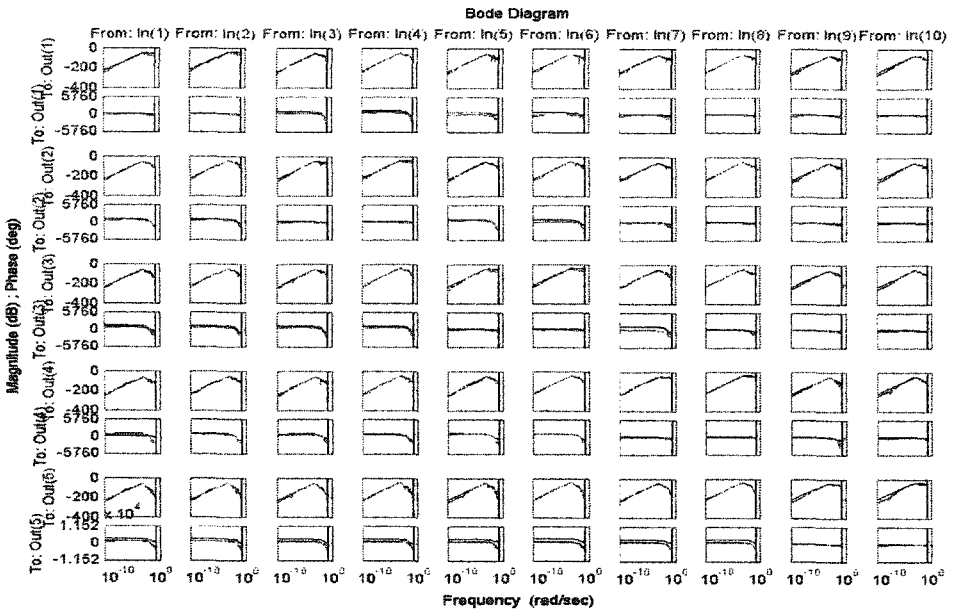

Figure 4.23. Comparison of Bode Diagrams of LQR, LQG and LQG/LTR Controllers with ρ=75.

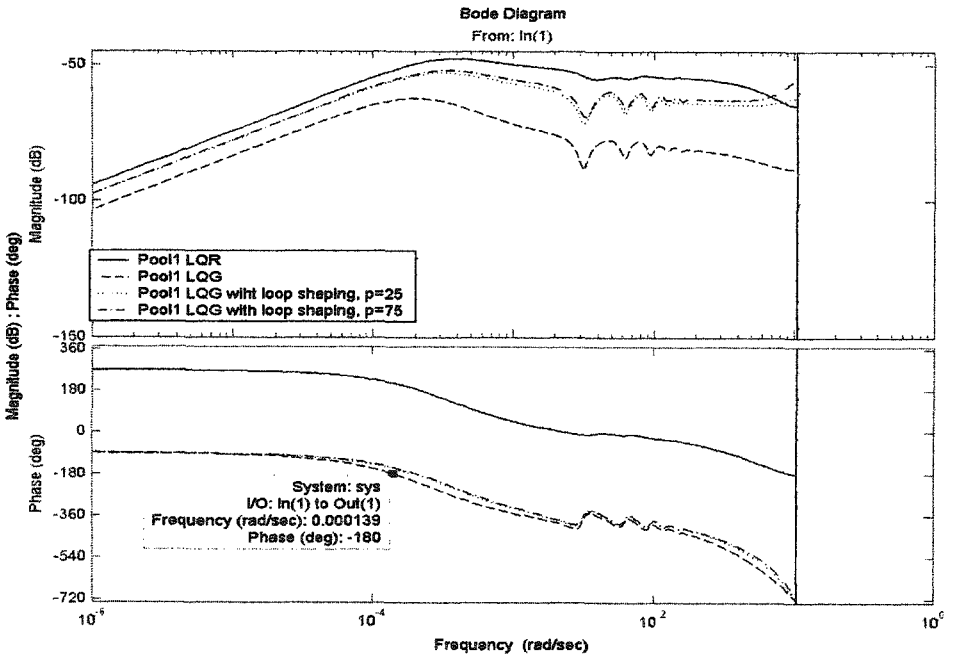

Figure 4.24. Comparison of Bode Diagram of LQR, LQG and LQG/LTR Controllers in Pool1 with ρ=75.

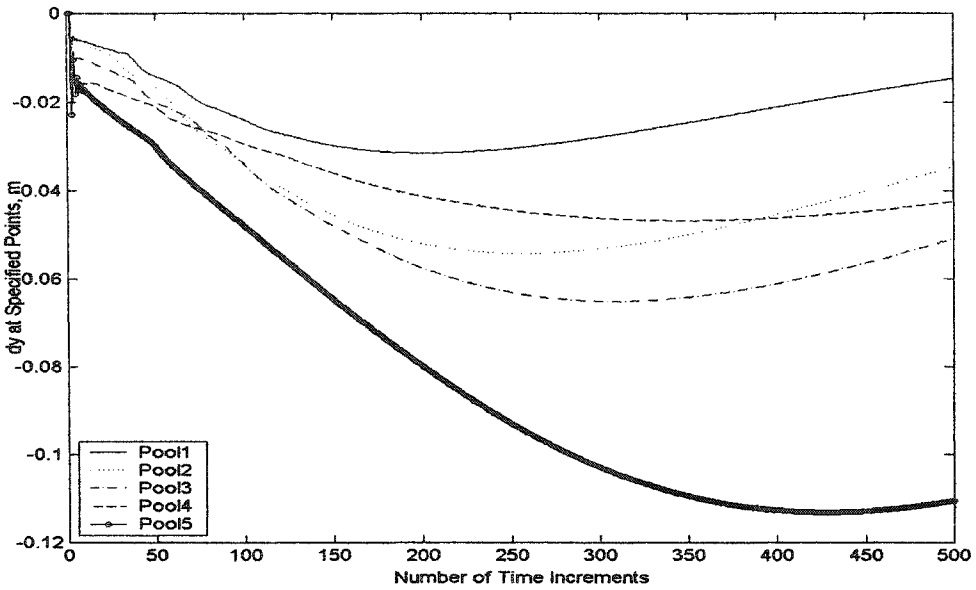

Figure 4.25. Variations of Flow Depth using LQG/LTR Controller with ρ=260.

LQR final gate openings. It was obvious that the system was stable when the scale parameter, ρ, was increased from 75 to 260. The improvements in robustness properties are presented in Figure 4.27 (singular value graph of the system). Pool1 has a good stability even though there was a large increase in the scale parameter. Some oscillation is noticeable at a disturbance frequency of 0.1 rad/sec. Also there is some improvement in robustness of the LQG/LTR controller for ρ=260. The singular value curves are shifted up and came close to the LQR target loop function. Water flow will be stable in pool1 and will be robust against unpredicted perturbations until a frequency range of 0.1 rad/sec. Pool2, Pool3 and Pool4 were also stable when the scale parameter for the disturbance spectral density matrix was increased. Large oscillations in singular values were observed after the disturbance frequency range of 0.1 rad/sec. The oscillatory waves are lager than that of the LQR controller. In these there pools, the robustness properties are improved and the singular value curves shifted upward and approached to the LQR

loop transfer function. Then it was obvious that the LQG/LTR design of irrigation canal for the different disturbance matrix scale parameter values was stable and the controller will increase robustness properties of the pool. The four pools (pool1, pool2, pool3, pool4) in the canal can withstand any unpredicted disturbances coming from farmers or water users. The pool5 had a good stability for the LQG/LTR controller and again there was some oscillatory behavior after 0.1 rad/sec. In other words, in the pool5, the system was stable when the frequency disturbances were less than 0.1 rad/sec. Also the robustness properties of the pool5 had improvement. The singular value curves shifted upward and more close to LQR design than the other three LQG/LTR designs.

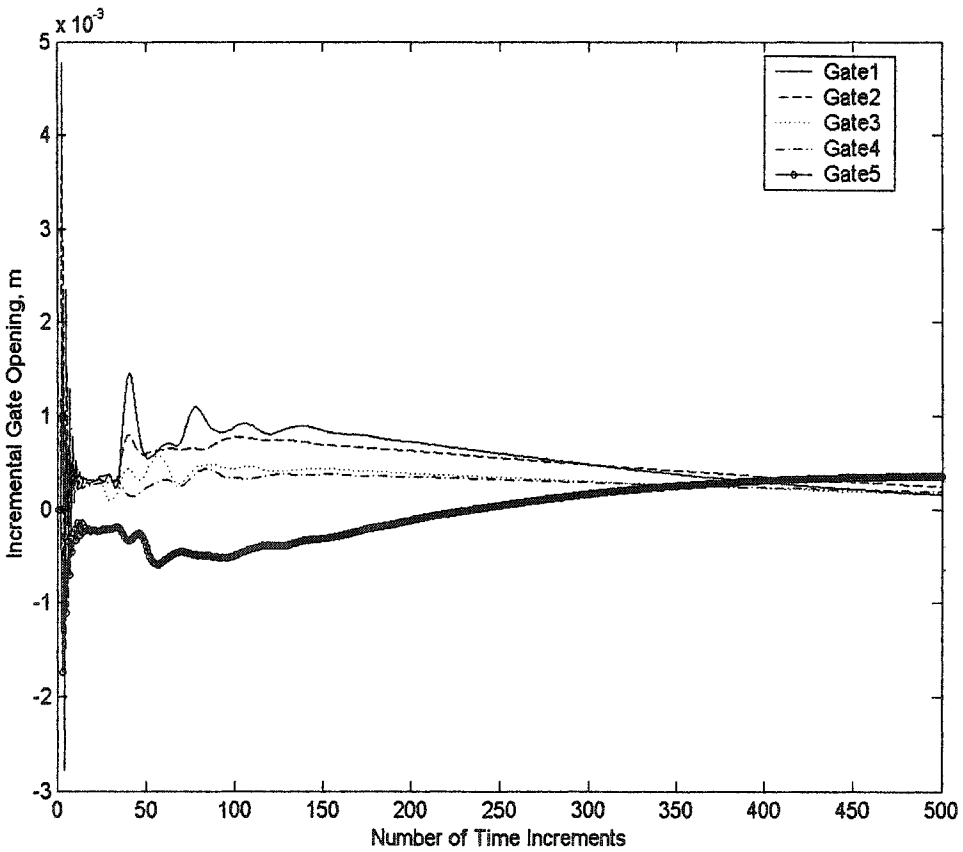

Figure 4.26. Incremental Gate Opening using LQG/LTR Controller with ρ = 260.

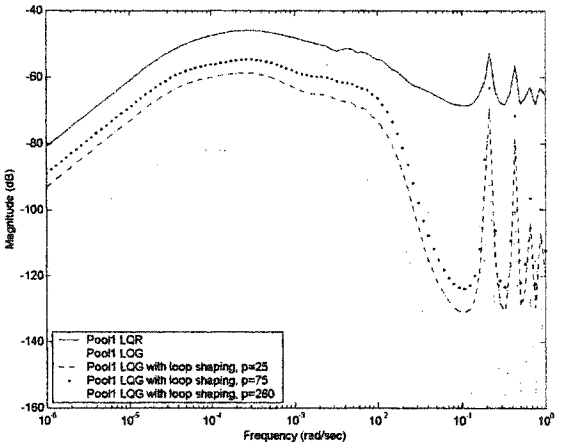

Pool 1

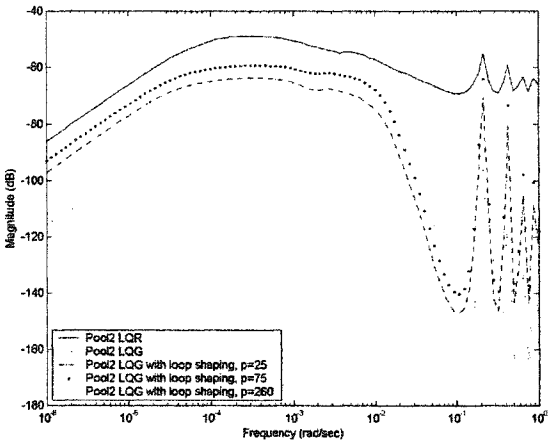

Pool 2

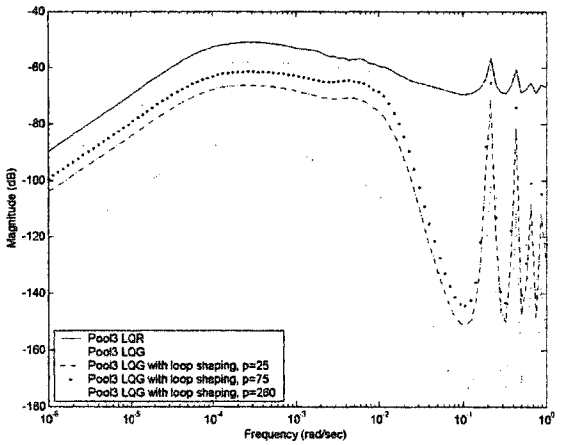

Pool 3

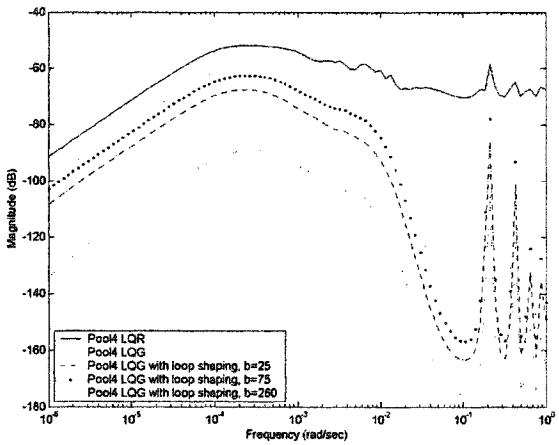

Pool 4

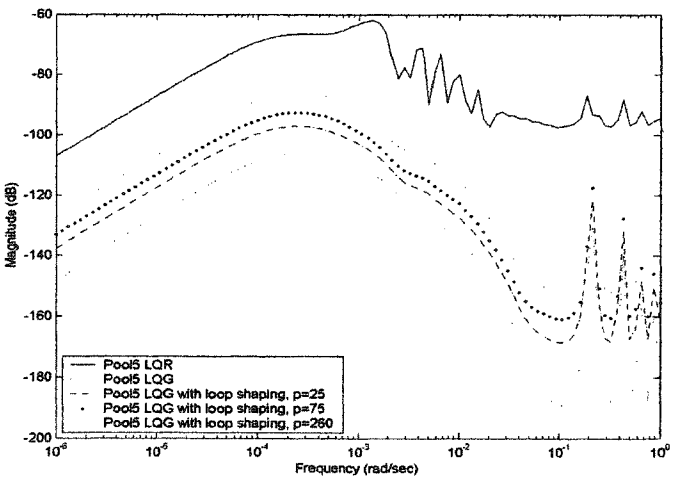

Pool 5

Figure 4.27. Comparison of Singular Values of LQR, LQG and LQG/LTR Controllers with ρ=260.

Figure 4.28 shows the Bode diagrams for all the pools. Gain margin values implied that the control system was still stable even when the scale parameter values was increased from 75 to 260. For better analysis of the stability and robustness, Bode diagram from pool1 was chosen. Figure 4.29 displays the gain and phase margin for pool1. Gain margin was under 0 dB level, in other words, the system was stable but phase crossover point shifted to the right and it reached a value of 0.000216 rad/sec. The system now had stability at higher disturbance frequencies than the other LQG/LTR designs. It was obvious that there was some improvement in robustness of the control system. The variation in flow depth did not change for pool5 at ρ=260. Again the variation in flow depth in pool5 was 0.1114 m. This value is the same as for the other LQG/LTR design with ρ=75.

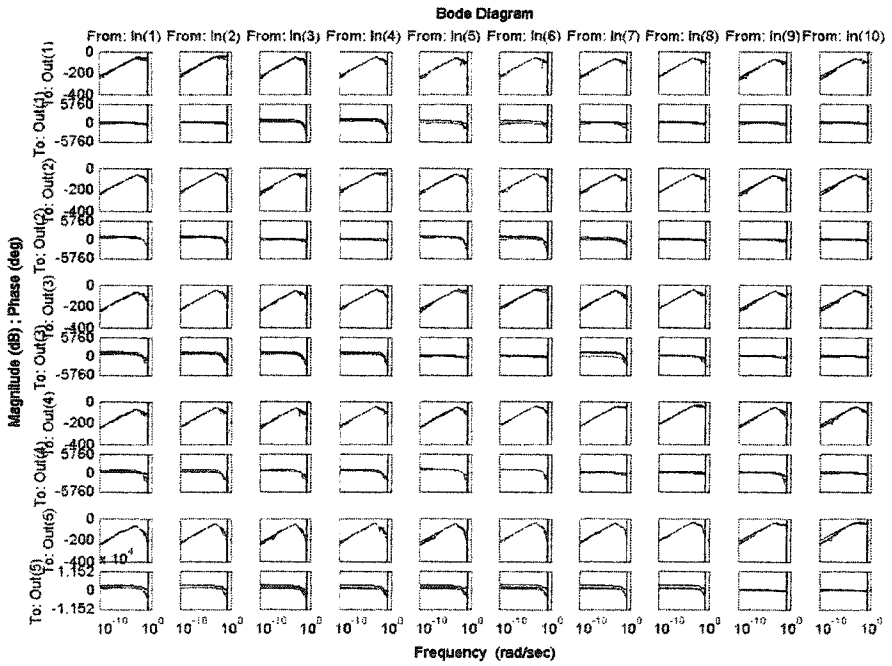

Figure 4.28. Comparison of Bode Diagrams of LQR, LQG and LQG/LTR Controllers with ρ=260.

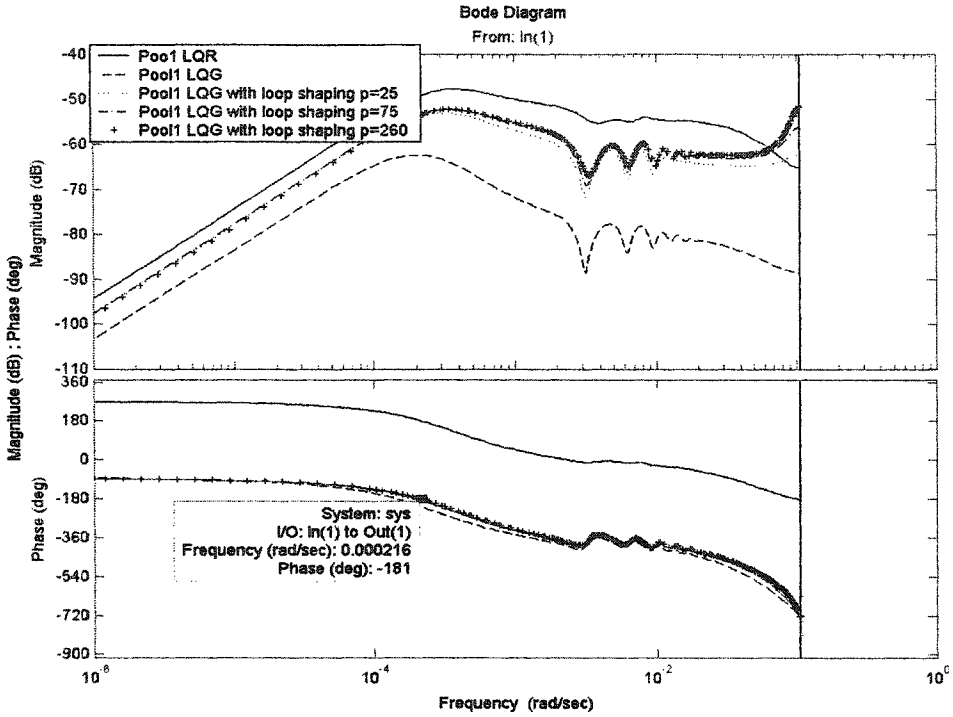

Figure 4.29. Comparison of Bode Diagram of LQR, LQG and LQG/LTR Controllers in Pool1 with ρ=260.

4.5.4. Simulation Results for LQG/LTR Controller: ρ = 2500 and higher

Since increasing the scale parameter for the disturbance density matrix improved the robustness of the irrigation control system, the scale parameter, ρ, value was increased further to 2500. There was no significant change in flow depth variations when the scale parameter was increased from 260 to 2500. As shown in Figure 4.30, the flow depth variations were stable, and the flow depth variations were -0.0137m, -0.0328 m, -0.0487 m, -0.0413 m, -0.1116 m, and 0.0323 m in pool1, pool2, pool3, pool4 and pool5, respectively, at 15000 seconds. These variations in flow depth were very close to LQR's depth variations. As shown in Figure 4.31, the gate openings were approaching equilibrium at 12000 seconds, and this time limit was the same as the LQR design. Final

gate openings were 1.7873 m, 2.0062 m, 1.4051 m, 1.8650 m, and 2.4774 m in pool1, pool2, pool3, pool4 and pool5, respectively.

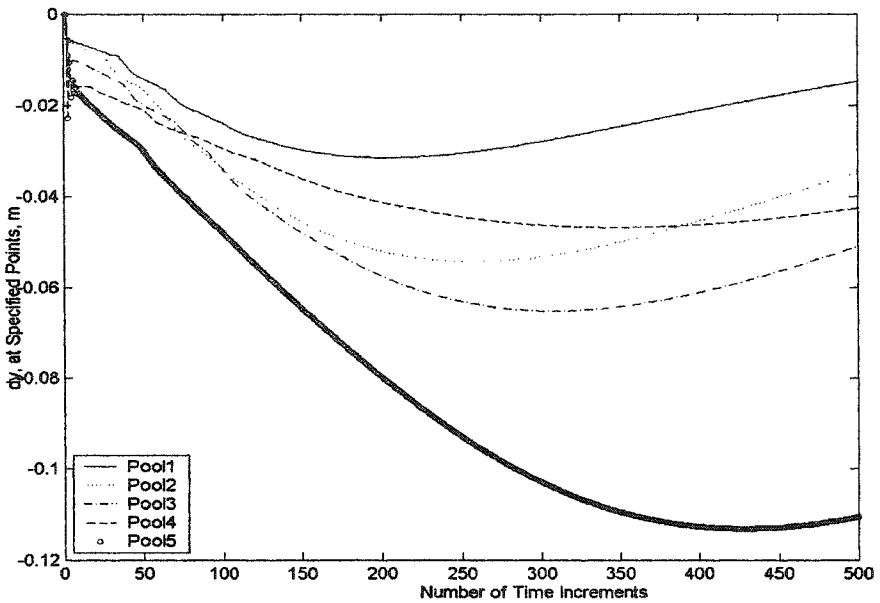

Figure 4.30. Flow Depth Variations using LQG/LTR Controller with ρ=2500.

Since the system was stable and the design results were very close to the LQR design outputs, the robustness analysis was applied to observe if there was some improvement in the robustness properties of the system. Figure 4.32 shows that if the scale parameter was increased from 260 to 2500, the robustness properties of the system were improving too. The singular values curves approached closer to the target loop function (LQR). In other words, the irrigation canal was more robust than the other LQG/LTR designs with different scale parameters. Pool1 had good stability for this disturbance density matrix scale parameter, and there was no oscillatory waves until the disturbance frequency reached a value of 0.01 rad/sec. The singular values curve for the new LQG/LTR design is the closest one among the others. That is, the first pool in irrigation canal had a good robustness properties when the disturbance spectral density

matrix scale parameter was 2500. Pool2 also was stable, and between the frequency ranges of 0.00012-0.01 rad/sec. There was an exact recovery of the robustness properties. That is, the system recovers the full-state feedback return ratio exactly but this does not happen all the time. After the disturbance reached a value of frequency 0.01 rad/sec, the system started to loose its robustness and stability. Pool3 is stable and again there is an overlap between the frequency range 0.0014-0.01 rad/sec. This means pool3 had an exact recovery between this frequency range. After this bandwidth, the controller started having oscillatory behavior. Pool4 was stable until the disturbance frequency reached a value of 0.1 rad/sec. There was some improvement in the robustness, and the singular

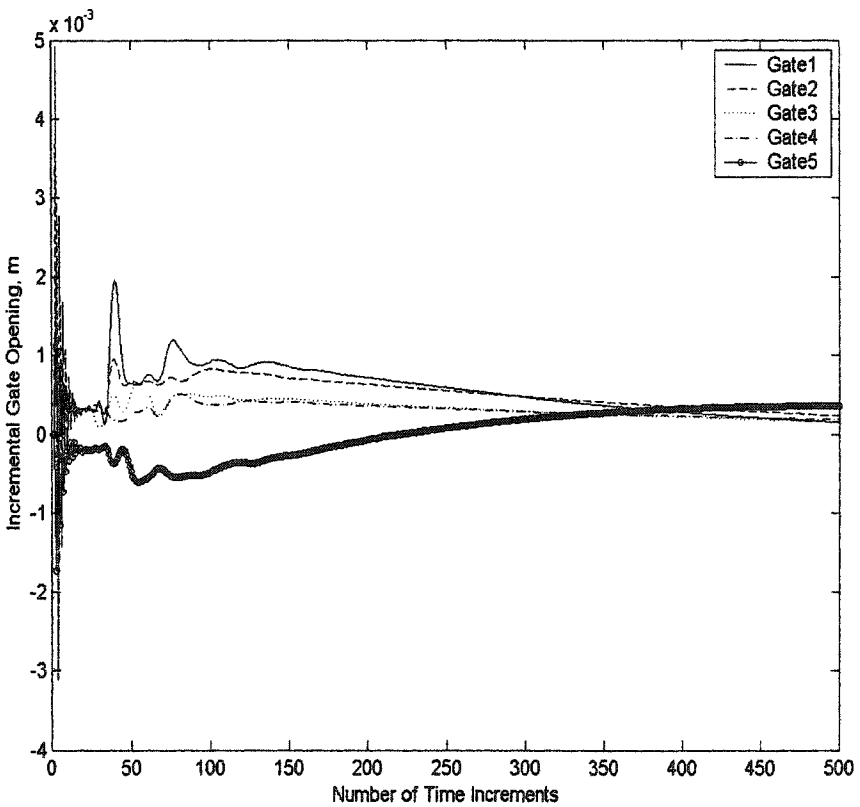

Figure 4.31. Incremental Gate Openings using LQG/LTR Controller with ρ=2500.

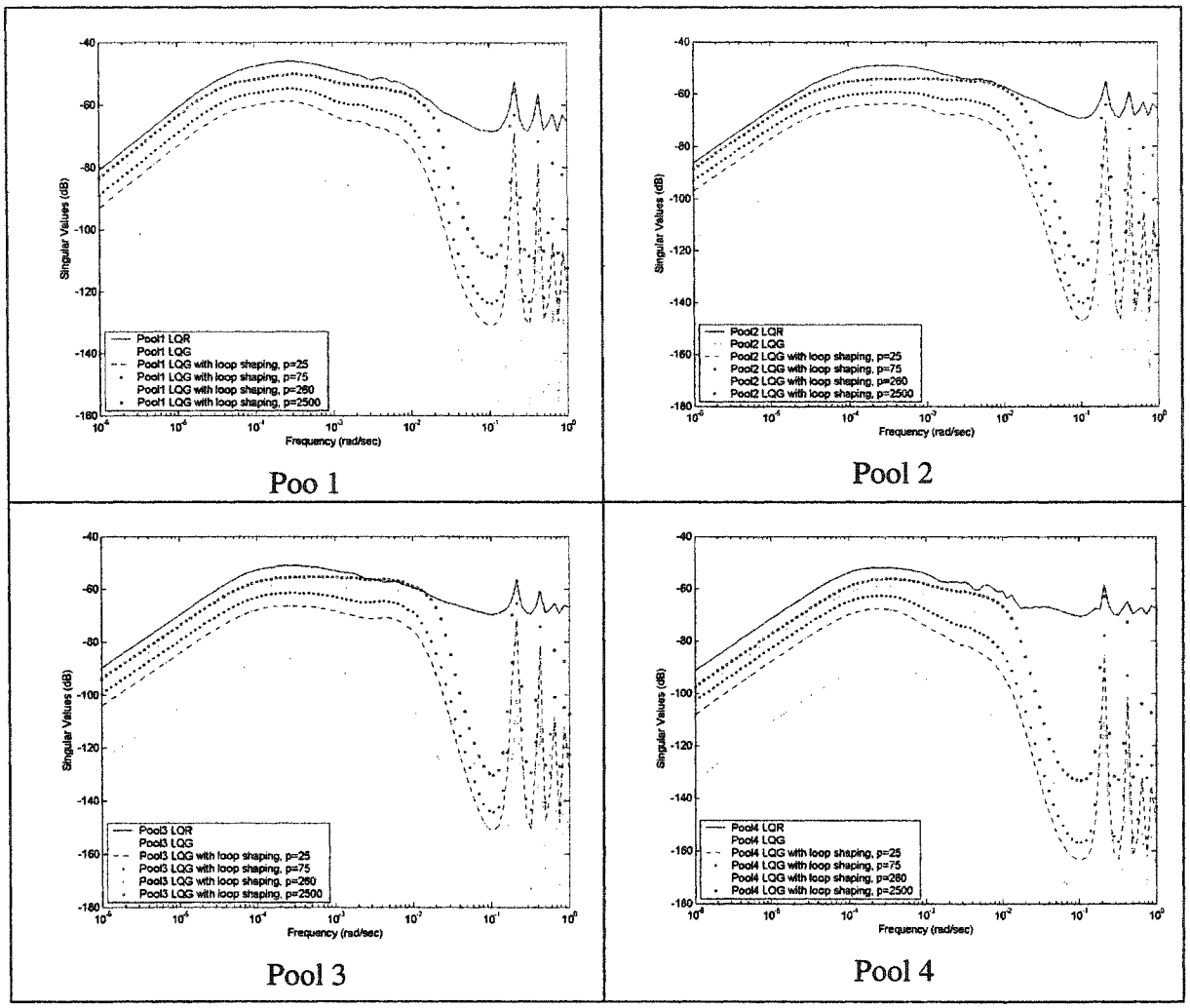

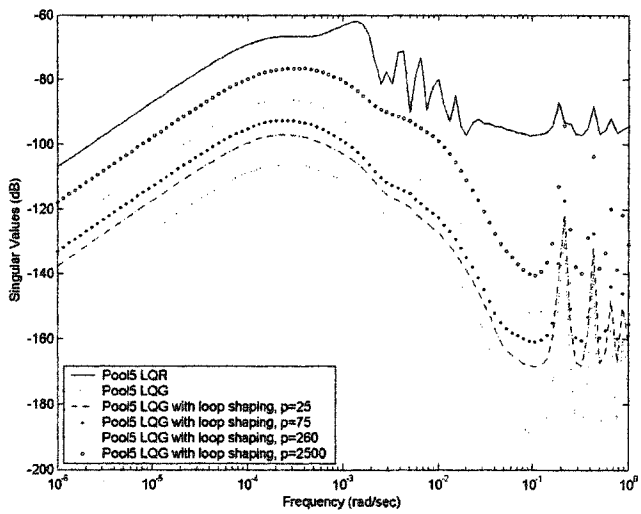

Pool 5

Figure 4.32. Comparison of Singular Values of LQR, LQG and LQG/LTR Controllers with ρ=2500.

value curves approached the target loop function (LQR). When the performance of pool5 was compared with the other pools, there was less stability and less robustness improvement in pool5, and the system was sensitive for higher disturbance frequencies. Even though the singular value curve was far from LQR target loop function, there was still some robustness improvement in this particular pool. Figure 4.33 shows the stability analysis of the all pools. The diagram shows that there was no significant effect on stability when the scale parameter was increased from 260 to 2500. To see this better, the Bode diagram for pool1 was analyzed in more detail as shown in Figure 4.34. Since the gain margin was under 0 dB level, the system was stable but at -180^0 the phase crossover had a significant movement to the right. In other words, there was little improvement in the robustness properties of the system. Also the variation in flow depth (0.1116 m) for this particular design was closer to the LQR than for LQG/LTR designs. This shows that the LQG/LTR design with ρ=2500 was approaching the LQR's variations in flow depth.

Making adjustments to the disturbance spectral density matrix does improve the robustness of the system but as mentioned in the pervious chapters, the design engineer will adjust the disturbance spectral density matrix spectral parameter until the irrigation canal maintain its stability and improves its robustness like in our case or the irrigation canal will gain stability and robustness at the same time. In some cases, however, when higher values are used for the scale parameter, the irrigation system may loose its stability and robustness properties. Figure 4.35 shows that increasing the scale parameter for disturbance spectral matrix did not have any effect on stability of the system until the parameter was equal to 2500. When the scale parameter value was increased from 2500 to 3000, the control system started to loose its robustness. Therefore, the value of the

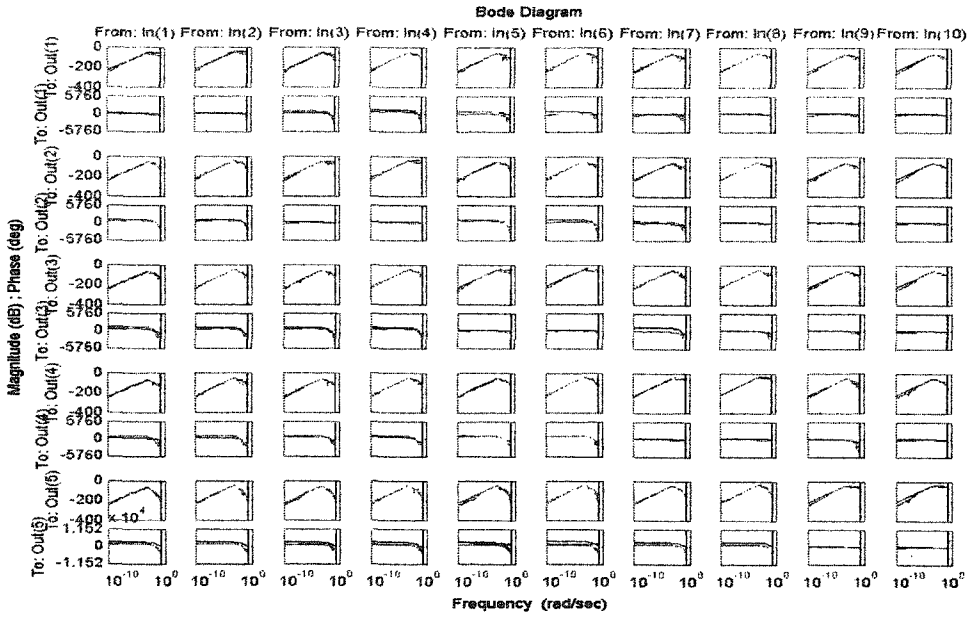

Figure 4.33. Comparison of Bode Diagrams of LQR, LQG and LQG/LTR Controllers with ρ=2500

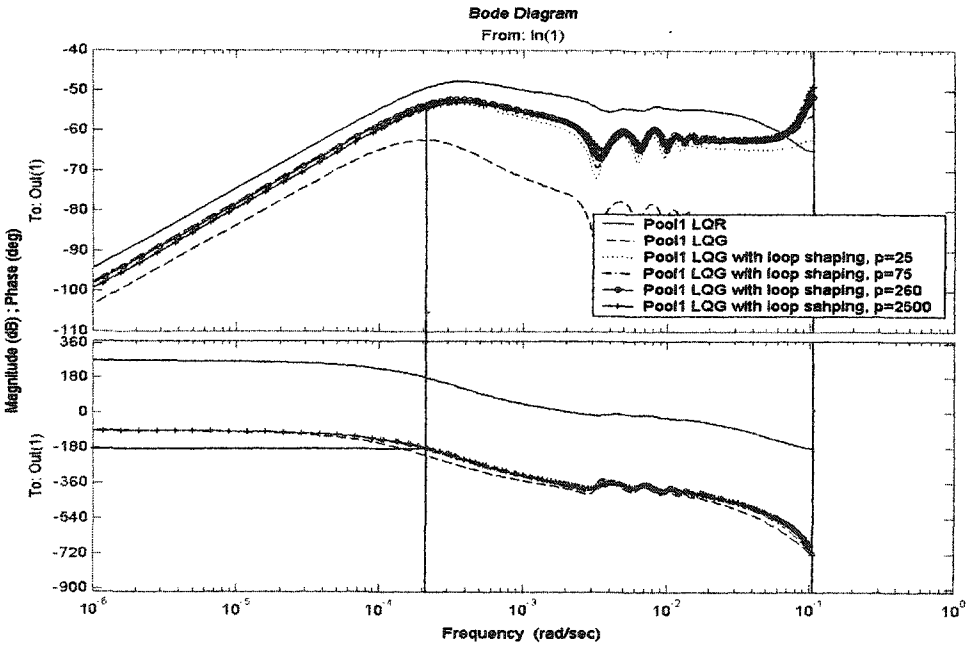

Figure 4.34. Comparison of Bode Diagram of LQR, LQG and LQG/LTR Controllers in Pool1 with ρ=2500.

scale parameter, ρ, must be selected sufficiently larger so that it approximately recovers the return ratio of the LQR over a specified range of frequencies. When the scale parameter was set equal to 3000, pool1 did not have any significant difference from the previous designs and there was no loss of robustness. But at low frequencies, the singular value curves moved upward and crossed the LQR singular value curve. Pool2 with this particular scale parameter had a good stability and robustness properties and there was an overlap between frequencies 0.0016 and 0.012 rad/sec. Also the singular value curve was very close to LQR loop target function's curve. In pool3, the system was not stable and there was loss of robustness of the system at low frequencies. The singular values curve was moving away from the LQR target loop function between frequencies 0.000001 and 0.0001 rad/sec. At higher frequencies the system again started having stability and there was some overlap between the frequency range of 0.0013 and 0.012 rad/sec. In pool4 and pool5 the singular values curve was moving away from the LQR target loop, that is, the system lost some of its robustness at low frequencies. Since we targeted a stable and robust irrigation canal at given range of frequencies, the chosen scale parameter, $\rho = 3000$, was not acceptable because of robustness issues. Bode diagrams will show the loss of robustness in the system in a better way. As shown in Figure 4.36, when the spectral density parameter was increased to 2500 in pool1, the system was stable until the frequency range approached 0.000218 rad/sec. As shown in Figure 4.37, when the scale parameter was increased to 3000 in pool1, the system is stable but for a small range of frequency (bandwidth). The system is robust just between the frequencies of 0.0000399 rad/sec and 0.00017 rad/sec. Also the variations in flow

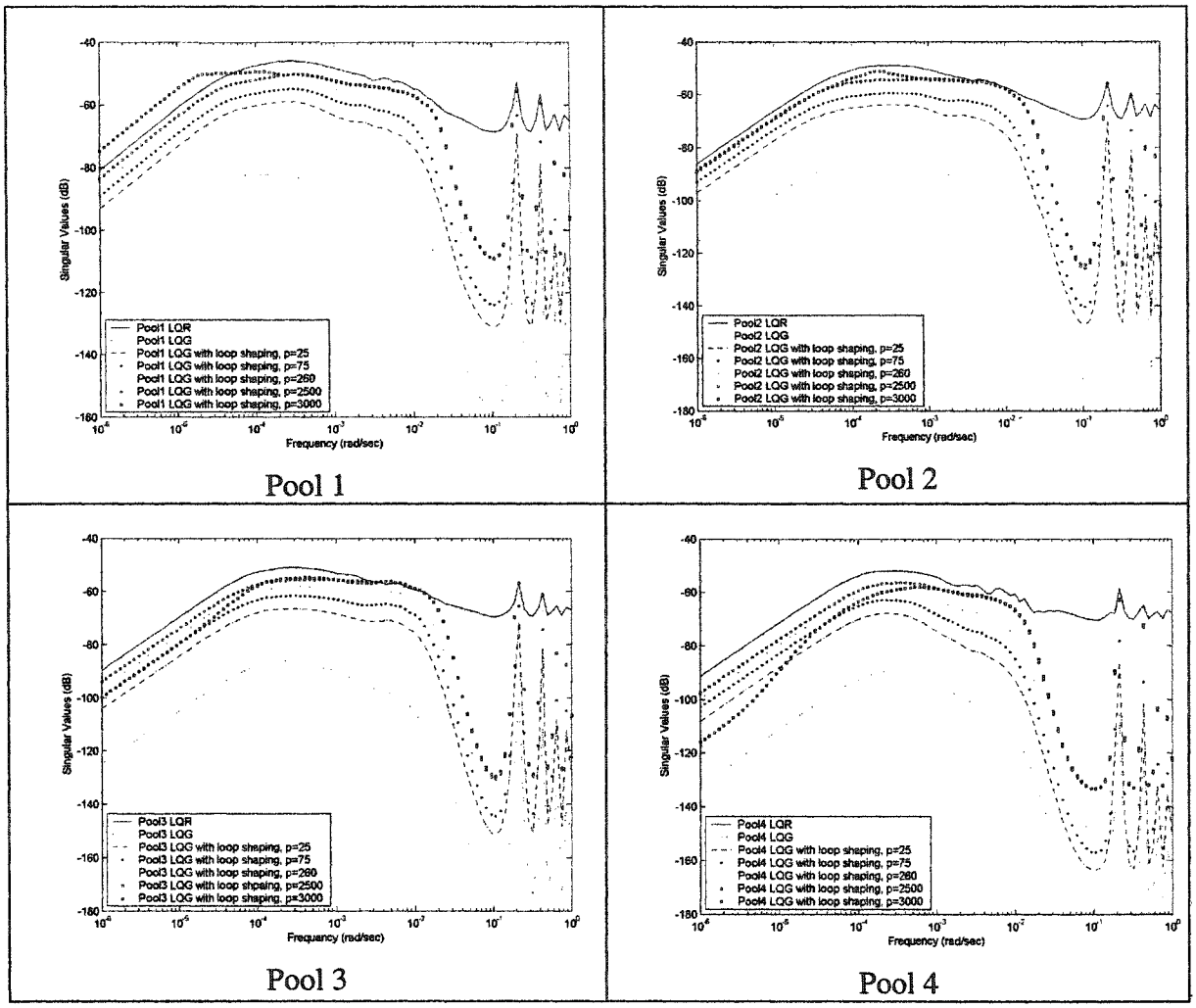

Figure 4.35. Comparison of Singular Values of LQR, LQG and LQG/LTR Controllers with ρ=3000.

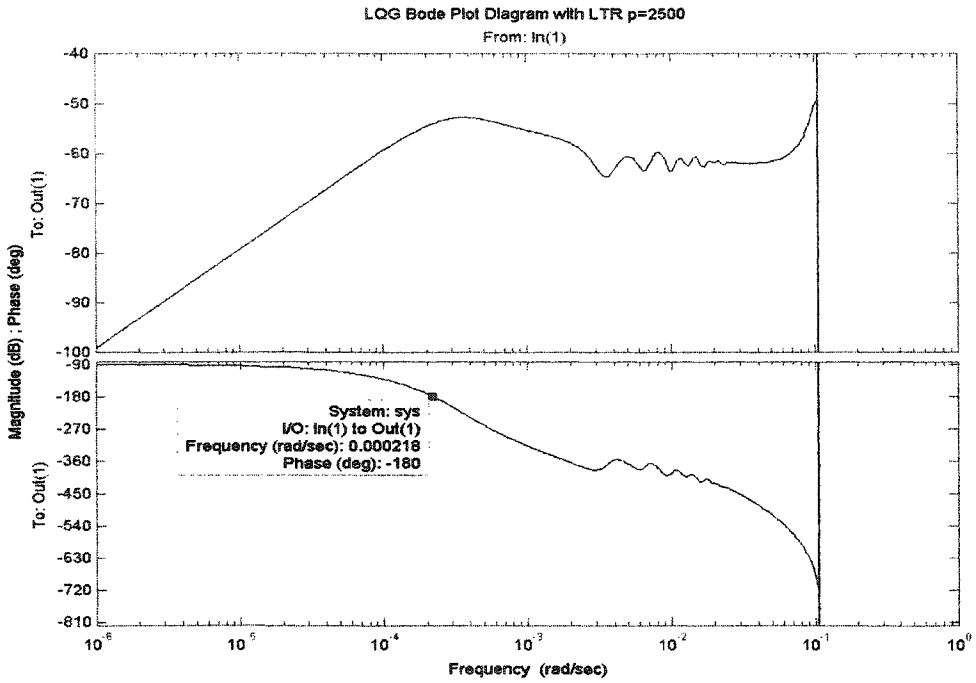

Figure 4.36. LQG/LTR Bode Diagram for Pool1 with ρ = 2500.

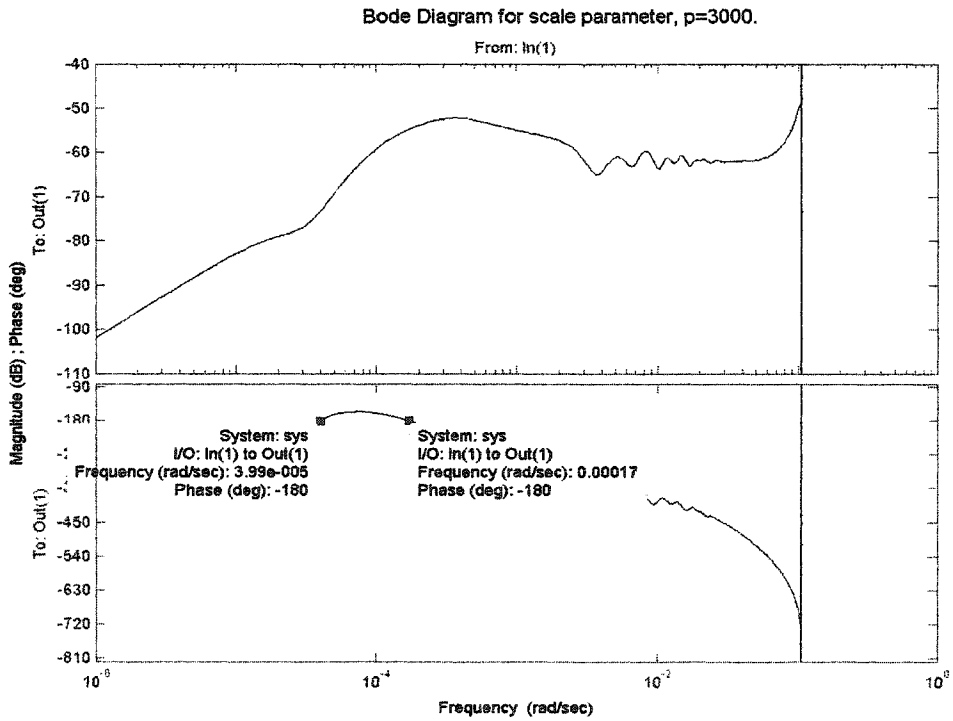

Figure 4.37. LQG/LTR Bode Diagram for Pool1 with ρ = 3000.

depth for ρ =3000 were -0.0121 m, -0.0298 m, -0.0474 m, -0.0406 m and -0.1022 m in pool1, pool2, pool3, pool4 and pool5, respectively. The variations in flow depth in pool5 (0.1022 m) was less than the former LQG/LTR's variations in flow depth (0.1116 m) in pool5 at 15000 second. In other words, if ρ was equal to 3000, the control system would be moving away from LQR's variations in flow depth. Therefore, the scale parameter, 2500, was found to be acceptable for a robust and stable irrigation canal system. At low and high disturbance frequencies the irrigation canal was always stable and there was no loss of robustness from the irrigation canal. But, as discussed above, it is difficult to get exact loop recovery for discrete-time control systems. Therefore, the design engineer has to choose the best value for the parameter ρ by trail and error in order to design a robust control system.

CHAPTER 5

SUMMARY, CONCLUSION AND RECOMMENDATIONS

5.1 Research Summary

The research presented herein, which culminated in the development of a computerized robust canal control algorithm, represents an original contribution to the fields of water resources operations and systems management by using Linear Quadratic Guassian (LQG)/Loop Transfer Recovery (LTR) techniques into a computerized control procedure for an open-channel water distribution system using the techniques of system modeling and system analysis. The purpose of the control algorithm is to allow an open-channel water distribution system to be operated on a demand basis at a high level efficiency under unknown external perturbations. This increased efficiency will result in the conservation of water through improved system efficiency and will reduce operating costs. Allowing the users to take water as their needs require, namely on a demand basis, can also lead to an increase in overall system efficiency. If the system provides irrigation water, allowing the users to take water on a demand basis, it can lead to not only a reduction in water requirements but also an increase in crop yields. As the world's demand for both water and food supplies continues to increase, it is essential that we search out and develop new techniques and procedures that will allow water to be conserved and crop yields to be improved.

The control algorithm, at the beginning, computes initial steady backwater profile for the system and then computes coefficients for continuity and dynamic equations. In order to apply the concepts of linear optimal control theory, the system equations must be transformed into a set of first-order, ordinary, differential equations. After applying Preissmann implicit-difference scheme and the Taylor series expansions to continuity and dynamic equations, a set of linear, ordinary differential equations are obtained. Once the coefficients of linear state variable description are calculated, the algorithm designs an optimal Linear Quadratic Gaussian (LQG) controller using Seperation Theorem for an irrigation canal. The LQG controller integrates the controller design and the states estimation into a single body of knowledge. Using the Separation Theorem, the algorithm first designs Linear Quadratic Regulator (LQR) to generate controller input *(u(k))* based upon the measured state vector (*x(k)*). And then designs a state estimator Kalman filter with known control input (*u(k)*), measured flow depth (*y(k)*), measurement error (*RC*) and disturbance spectral density matrix (Q_{esti}) to estimate optimal values for all the state variables that are not measured. An LQR controlled system has good stability margins at the system inputs, and a Kalman filter has good stability margins at the inputs to estimator gain (K_f). But for a LQG controlled system with a combined Kalman filter and LQR control law, there are no guaranteed stability margins. To recover the robustness of the LQG controller, the control algorithm redesign Kalman filter by selecting the measurement *(RC)* and process noise spectral densities (Q_{esti}) matrices, such that the singular values of the return ratio at the system's input, $H(z)G(z)$, approach the corresponding singular values with full-state feedback. The recovery condition is derived from the fact that if control variable *u(t)* had the same effect on the both actual state

variable $x(t)$ and reconstructed state variable $\hat{x}(k)$, then the LQG system would have the same transfer functions properties as the LQR system.

5.2 Conclusions

The purpose of this research has been to show that LQG/LTR controller techniques can be applied in the design of closed-loop control systems for an open canal with a multiple number of gates. To design the control theory, the basic nonlinear hydrodynamic partial differential equations for open channel flow were discertized and linearized about equilibrium conditions. The LQG/LTR control technique augmented with loop shaping is a very powerful design synthesis procedure to recover the robustness of the system. The technique is conducive to educated trial and error design iterations, and offers a well defined trade-off management perspective on controller synthesis. With LTR having obtained, we recovered a satisfactory return ratio for the Kalman filter.

To demonstrate its effectiveness, the LQG/LTR method was used to control a 39 km open-channel with 5 pools and 6 gates. The open-channel system represents a part of an irrigation system delivering water directly to on-farm users. As explained in Chapter 4, the irrigation canal has 5 pools and each pool has its canal geometry, gate and turnout properties. For convenience, each pool was divided into nodes and 5 pools have 141 nodes. First the control algorithm computed the steady state values. The analysis started by evaluating the system stability. All the eigenvalues of the feedback matrix were positive and had values less then one. The system was found to be both controllable and observable. The stability and robustness of control algorithm was simulated for 4 hours. The results of the control algorithm simulation were analyzed under three categories: 1)

the stability and robustness of the optimal state feedback (LQR), 2) the stability and robustenss of the state feedback with state estimator (LQG), 3) the stability and robustness of the LQG/LTR controller.

In the first category, Linear Quadratic Regulator (LQR) applied to regulate the five pool canal system using a constant-level control approach. In LQR design we assumed that all the state variables needed in the feedback loop were measured. Through the performance of control algorithm with full-state feedback was acceptable and system was stable. It was also observed that the robustness properties of LQR controller was acceptable. In the second category, full-state feedback applied to canal with the Kalman state estimator (LQG), because it would be very expensive measuring all the state variables. The results of LQG simulation showed that a good selection of measurement and disturbances spectral density matrices provided a good stability for LQG controller. There was no significant stability differences between LQR and LQG controller. Since it was expensive to implement the full-state feedback, a Kalman filter based up on two flow depth measurements per pool could be used to estimate the values for the state variables. The results of control algorithm showed that LQR controlled system had good stability margins and robustness at the system inputs , and a Kalman filter had good stability margins at the inputs to estimator gain (K_f). But for a LQG controlled system, a combined Kalman filter and LQR control law, there are no guaranteed robustness of the system. The result on incorporating a state estimator into the controller (LQR) was that the resulting controller (LQG) may no longer possess the desirable robustness presented in the original LQR design. Therefore, in third category, the control algorithm applied a loop shaping technique (LTR) to recover the robustness of the system and to catch the

robustness level of the LQR controller. The control algorithm achieved the loop shaping by selecting the measurement error spectral density as $RC=I$ and disturbance spectral density matrix, $Q_{esti} = Q_o + \rho I$, where ρ is a scaling parameter. To recover the robustness of LQR controller, the algorithm increased the scale parameter for disturbance spectral density matrix. For the scale parameter, the control algorithm used the values *25, 75, 260, 2500, 3000.* Finally the control algorithm had very close robustness properties like LQR control at ρ =*2500.* Therefore, we can say that the control algorithm has attractive robustness properties like LQR controller. However making ρ extremely large, such as ρ is equal to 3000, reduced the stability and robustness of the closed-loop transfer function, which is undesirable. Hence, instead of making ρ very large to achieve perfect loop transfer recovery at all frequencies, we should choose a value of ρ which is sufficiently large to approximately recover the return ratio over a given range of frequencies.

5.3 Recommendations

Based on the results from the research, robust feedback controllers for open channel systems can be designed using modern control theory. Various features make LQG/LTR technique a very effective design tool for linear multivariable feedback systems. However, many questions remain unanswered. The following are recommendations for further study: 1) The major weakness of LQG/LTR technique appears to be its restriction to design tradeoffs at only one loop-breaking point. That is the method can trade of sensitivity function *S(jw)* against closed loop transfer function *T(jw)* with both defined at the output or both defined at the input. However, it cannot easily trade off these functions when they are defined at different points. This means that the method currently obligates

designers to reflect all feedback design requirements to one of the two loop-breaking points. To overcome the limitations of the LQG/LTR control technique, H_∞ control theory should be studied for an open-channel flow. 2) In spite of the fact that all states were used in formulating both the regulator feedback gain matrix K and observer error gain matrix L, the effects of immediately adjacent pools were found to be dominant (distant pools made much smaller contributions). This needs further investigation. A possible approach might be employ a suboptimal controller and estimator where many of the elements in the K and L matrices are set to zero. 3) In practice there is need for accurate identification of the turnout demands in order to accurately calculate future equilibrium conditions. This can be achieved using modern filtering theory and should be a subject of future study. 4) Only the effects of disturbances caused by the withdrawal of water were considered in this study. Other parameter changes (e.g., wind, manning coefficients, etc.) might be important in some instances.

REFERENCES

Anderson, B.D.O., and Moore, J.B. (1990). *Optimal Control*, Prentice-Hall, New Jersey.

ASCE, (1993). *Unsteady-flow modeling of irrigation canals*, ASCE Task Committee on irrigation canal system hydraulic modeling, Journal of Irrigation and Drainage Engineering, Vol 119(4), pp. 615-630.

Aström, K., and Wittenmark, B. (1990). *Computer Controlled Systems; Theory and Design*, Prentice-Hall International Editions, London, 544p.

Athans, M. (1971). *The role and use of the stochastic linear-quadratic-gaussian problem in control system design*, IEEE Transactions on automatic control, Vol. AC-16(6), pp. 529-551.

Balogun, O.S. (1985). *Design of real-time feedback control for canal systems using linear quadratic regulator theory*, Ph.D thesis, Department of Mechanical Engineering, University of California at Davis, 230 p.

Balogun, O.S., Hubbard, M., and DeVries, J.J. (1988). *Automatic control of canal flow using linear quadratic regulator theory*, J. of Irrigation and Drainage Eng., 114 (1), pp. 75-101.

Baumann, W.T., and Rugh, W.J. (1986). *Feedback control of nonlinear systems by extended linearization,* IEEE Transactions on automatic control, Vol AC-31(1), pp. 40-46.

Black, H.S. (1934). *Stabilized feedback amplifiers*, Bell Syst. Tech. J., vol. 14, pp.1-18.

Bode, H.W. (1940). *Relations between attenuation and phase in feedback amplifier design*, Bell Syst. Tech. J., vol. 19, pp. 421-454.

Burt, C.M. (1983). *Regulation of sloping canals by automatic downstream control*, PhD, Utah State University, Logan, Utah.

Chevereau, G., and Schwartz-Benezeth, S. (1987). *BIVAL systems for downstream control*, Proc., ASCE Symp. On Plang., Operation, Rehabilitation, and Automation of Irrigation Water Delivery Systems, ASCE, New York, pp. 155-163.

Chalfen, M., and Niemiec, A. (1986). *Analytical and numerical solution of Saint Venant equations*, Journal of Hydrology, 1(13), pp. 1-12.

Chow, Ven Te. (1954). *Open-Channel Hydraulics,* McGraw-Hill Book Company, New York.

Corriga, G., Sanna, S., and Usai, G. (1982). *Sub-optimal level control of open-channels,* Proc. Int. AMSE Conf., Paris, France, July 1-3.

Dora, T., and Varga, I., (1982). *Design principles and dynamic problems of water distribution at the Kiskore irrigation projects*, ICID Bull. 31(2), pp. 60-78.

Doyle, J.C. (1979). *A truth maintenance system,* Artificial Intelligence, 12(3), pp. 231-272.

Doyle, J. C., and Stein G. (1981). *Multivariable Feedback Design: Concepts for a Classical/Modern Synthesis.*IEEE Transactions Automatic Control, AC-26, 4.

Dutton, K., Thompson, S., and Barraclough, B. (1997). *The Art of Control Engineering*, Addison-Wesley, Essex, England.

Garcia, A., Hubbard, M., and DeVries, J. J. (1992). *Open-channel transient flow control by discrete-time LQR methods,* Automatica, 28(2), pp. 255–264.

Goodman, G.J. (1984). *The LQG/LTR method and discrete-dime control systems,* M.S Thesis, MIT, Cambridge, Massachusetts.

Ishihara, T. (1995). *Discrete-time control systems design via loop transfer recovery*, Control and Dynamic Systems, 70, pp. 163-198, Academic Press.

Jacquot, R. G. (1995). *Modern Digital Control Systems*. Marcel Dekker, New York.

Kantorovich, V.K., and Kuchment, L. S. (1980). *Application of the finite element method to calculation of unsteady flow by Saint Venant Equations*, Institute of Water Problems, Report UDC. 556.013, pp. 45-53.

Kwakernaak, H., and Sivan, R. (1972). *Linear Optimal Control Systems*. Wiley, New York.

Liu, F., Malaterre, P.O., Baume, J.P., Kosuth, P., and Feyen, J. (1995). *Evaluation of a canal automation algorithm CLIS*, First International Conference on Water Resources Engineering, 14-18 August, San Antonio, USA.

Liu, F., Feyen, J., and Berlamont, J. (1992). *Computation method for regulating unsteady flow in open channels*, J. Irrig. and Drain. Engr., ASCE, 118(10), pp. 674-688.

Mahmood, K., and Yevjevich, V. (1975). *Unsteady Flow in Open Channels*, Volume I, Water Resources Publications, Fort Collins, CO, pp. 140-150.

Malaterre, P.O. (1997). *Multivariable Predictive Control of Irrigation Canals. Design and Evaluation on an a 2-pool Model*, In: International Workshop on Regulation of Irrigation Canals, pp. 230-238, Marroco.

Malaterre, P.O., Rogers D.C., and Schuurmans J. (1995c). *Classification of Canal Control Systems*, First International Conference on Water Resources Engineering, Irrigation and Drainage, San Antonio, Texas, USA, 14-18 August 1995.

Malaterre, P.O. (1995b). *Regulation of irrigation canals: characterization and classification*, International Journal of Irrigation and Drainage Systems, Vol. 9(4), November 1995, pp. 297-327.

Malaterre, P.O. (1995d). *PILOTE: optimal control of irrigation canals*, First International Conference on Water Resources Engineering, Irrigation and Drainage, San Antonio, Texas, USA, 14-18 August 1995.

Malaterre, P.O. (1998). *PILOTE: Linear quadratic optimal controller for irrigation Canals*, J. of Irrigation and Drainage Eng., Vol. 124(4), pp. 187-194.

Matlab & Simulink (1992). *A program for simulating dynamic systems*, MathWorks Inc.

Moore, J.B., and Xia L. (1987). *Loop recovery and robust state feedback designs*, IEEE Trans. Automat. Contr., AC-32, pp. 512-517.

Reddy, J.M. (1986). *Evaluation of optimal constant volume control for irrigation canals*, Journal of Applied Mathematical Modelling, 14 p.

Reddy, J.M. (1990). *Local optimal control of irrigation canals*, J. of Irrigation and Drainage Eng., 116 (5), pp. 616-631.

Reddy, J.M, Dia, A., and Oussou, A. (1992). *Design of control algorithm for operation of irrigation canals*, J. of Irrigation and Drainage Eng., 118 (6), pp. 852-867.

Reddy, J.M. (1992a). *Decentralized constant-volume control of irrigation canals*, Proceedings "Advances in Planning, Design and Management of Irrigation Systems as Related to Sustainable Land Use". Leuven, 14-17 September 1992, Feyen et al. (Ed), pp 889-898.

Reddy, J.M. (1995). *Kalman filtering in the control of irrigation canals*, Int. J. Appl. Math. Modeling, 19(4), pp. 201–209.

Reddy, J.M., and Jacquot R.G. (1999). *Stochastic optimal and suboptimal control of irrigation canals*, J. of Water Resources Pln. and Mgt., 125 (6), pp. 369-378.

Rhodes, D.G. (1995). *Newton-Raphson solution of gradually varied flow*, Journal of Hydraulic Research, Vol. 33(2), pp. 213-218.

Rodellar, J., Gomez, M., and Bonet, L. (1993). *Control method for an on-demand operation of irrigation canals*, J. Irrigation and Drainage Eng., ASCE, 118(6), pp. 852-867.
Saberi, A., Sannuti, P., and Chen, B.M. (1993). *Loop Transfer Recovery*, Springer-Verlag.

Safonov, M. G., and Athans, M., (1977). *Gain and phase margin for multiloop LQG regulators*, IEEE Transactions on Automatic Control, AC-22, 173-178.

Saleh, A., and Adeli, H. (1997). *Robust parallel algorithms for solution of riccati equation*, Journal of Aerospace Engineering, Vol. 10(3), pp. 161-178.

Savadogo, S., Malaterre, P.O., and Kosuth P. (1995). *Multivariable optimal control for on demand operation of irrigation canals*, International Journal of System Science, Vol. 26(1), pp. 126-133.

Skogestad, S., and Postlethwaite, I. (1996), *Multivariable Feedback Control*, Wiley, New York.

Stein, G., and Athans M. (1987). *The LQG/LTR procedure for multivariable feedback control design*, IEEE Trans. Automat. Contr. AC-32, pp.105-114.

Stengel, R. F. (1986). *Stochastic Optimal Control.* John Wiley and Sons, New York.

Stepien, I. (1984), *On the numerical solution of the Saint Venant equations*, Journal of Hydrology, 67(1), pp. 1-11.

Tewari, A. (2002), *Modern Control Design with Matlab and Simulink*, Wiley, New York.

Xavier, L. (2001). *Robust flow control of single input multiple outputs regulated rivers*, Journal of Irrigation and Drainage Engineering, Vol. 127(5), pp. 281-286.

Zhou, K., and Doyle, C.J. (1998), *Essentials of Robust Control,* Prentice Hall, Upper Saddle River, New Jersey.

Zimbelman, D.D. (1981). *Computerized control of an open-channel water distribution system*, PhD thesis, Arizona State University, Tempe, Arizona.

APPENDIX A

SOUTHERN ANATOLIA PROJECT AND HARRAN MAIN CANAL

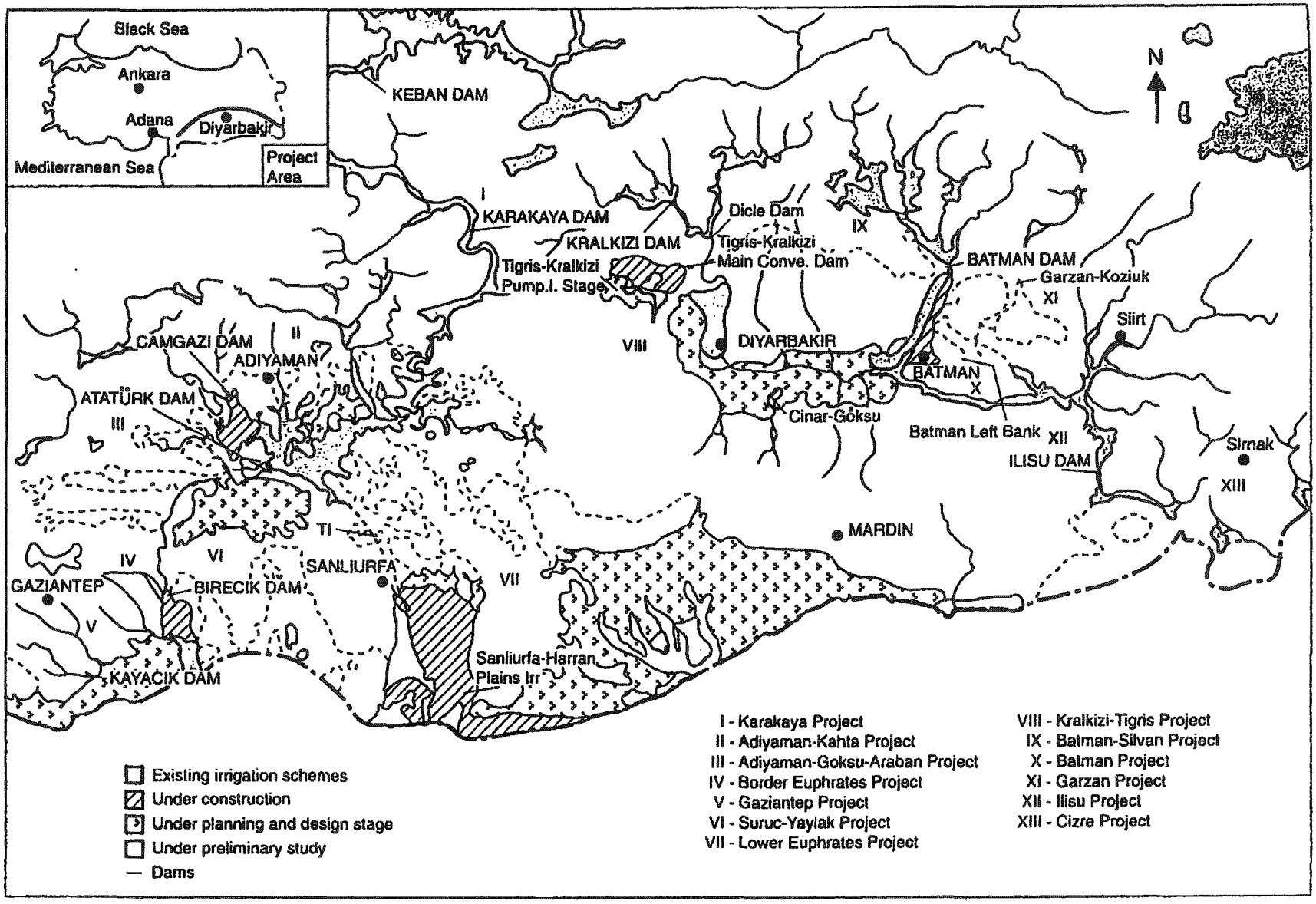

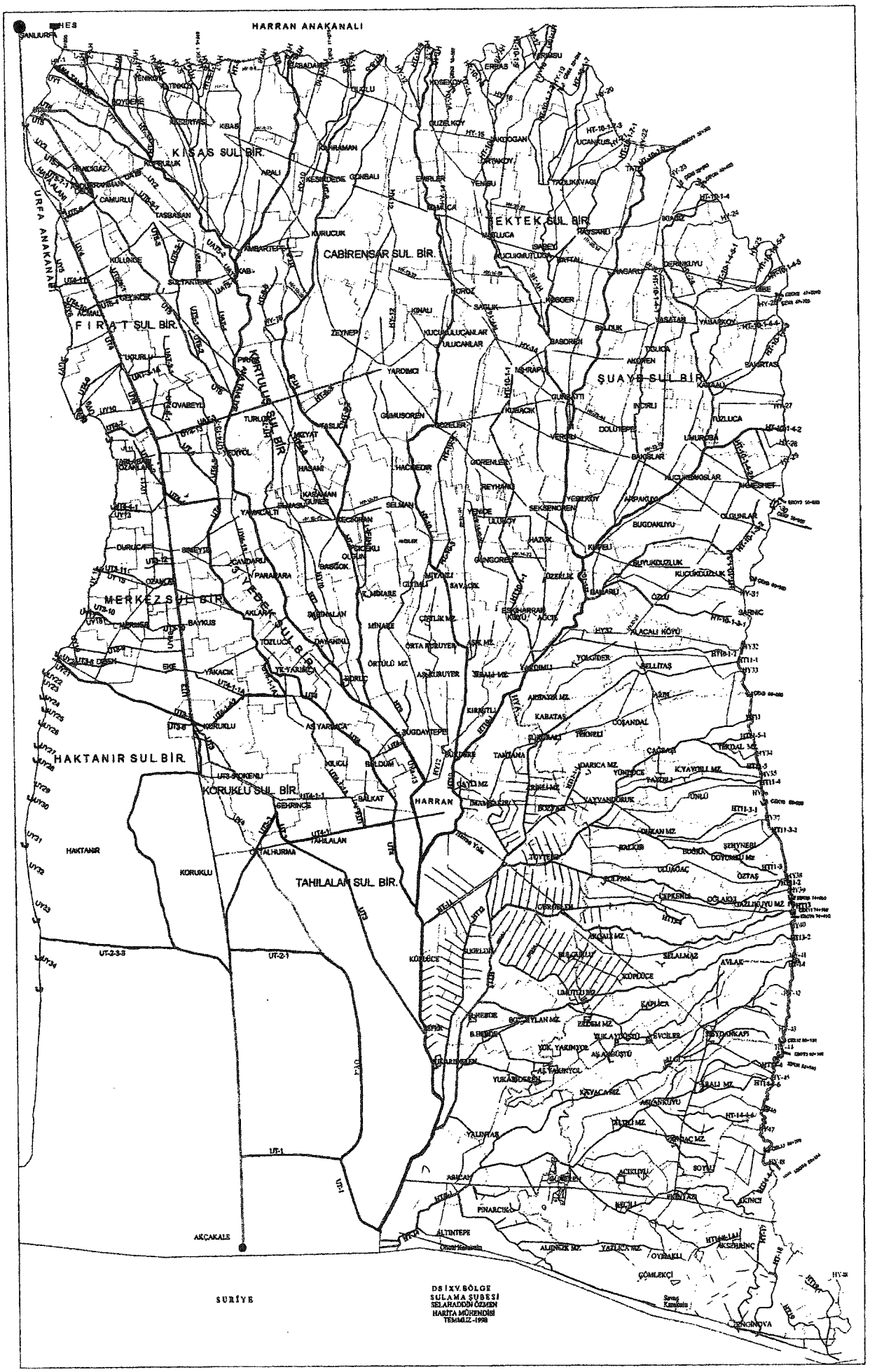

APPENDIX B

DATA USED FOR THE SIMULATION STUDY

POOL DATA							
Δx,m	Bottom Width(B),m	Side Slope(z)	Slope (So)	Roughness Coff.	Initial Turnout Flow(q),m^3/sec	Upstream depth(m)	Node Type
0	16	1.5	0.0001	0.016	0	5	2
259	16	1.5	0.0001	0.016	0	0	1
259	16	1.5	0.0001	0.016	0	0	1
259	16	1.5	0.0001	0.016	0	0	1
259	16	1.5	0.0001	0.016	0	0	1
259	16	1.5	0.0001	0.016	0	0	1
259	16	1.5	0.0001	0.016	0	0	1
259	16	1.5	0.0001	0.016	0	0	1
259	16	1.5	0.0001	0.016	0	0	1
259	16	1.5	0.0001	0.016	0	0	1
259	16	1.5	0.0001	0.016	0	0	1
259	16	1.5	0.0001	0.016	0	0	1
259	16	1.5	0.0001	0.016	0	0	1
259	16	1.5	0.0001	0.016	0	0	1
259	16	1.5	0.0001	0.016	0	0	1
259	16	1.5	0.0001	0.016	0	0	1
259	16	1.5	0.0001	0.016	0	0	1
259	16	1.5	0.0001	0.016	0	0	1
259	16	1.5	0.0001	0.016	0	0	1
259	16	1.5	0.0001	0.016	0	0	1
259	16	1.5	0.0001	0.016	0	0	1
259	16	1.5	0.0001	0.016	0	0	1
259	16	1.5	0.0001	0.016	0	0	1
259	16	1.5	0.0001	0.016	0	0	1
259	16	1.5	0.0001	0.016	0	0	1
259	16	1.5	0.0001	0.016	0	0	1
0	16	1.5	0.0001	0.016	2.398	0	3
0	16	1.5	0.0001	0.016	0	4.7	2
272	16	1.5	0.0001	0.016	0	0	1
272	16	1.5	0.0001	0.016	0	0	1
272	16	1.5	0.0001	0.016	0	0	1
272	16	1.5	0.0001	0.016	0	0	1
272	16	1.5	0.0001	0.016	0	0	1
272	16	1.5	0.0001	0.016	0	0	1
272	16	1.5	0.0001	0.016	0	0	1
272	16	1.5	0.0001	0.016	0	0	1
272	16	1.5	0.0001	0.016	0	0	1
272	16	1.5	0.0001	0.016	0	0	1
272	16	1.5	0.0001	0.016	0	0	1
272	16	1.5	0.0001	0.016	0	0	1
272	16	1.5	0.0001	0.016	0	0	1
272	16	1.5	0.0001	0.016	0	0	1
272	16	1.5	0.0001	0.016	0	0	1
272	16	1.5	0.0001	0.016	0	0	1
272	16	1.5	0.0001	0.016	0	0	1
272	16	1.5	0.0001	0.016	0	0	1

Δx,m	Bottom Width(B),m	Side Slope(z)	Slope (So)	Roughness Coff.	Initial Turnout Flow(q),m^3/sec	Upstream depth(m)	Node Type
272	16	1.5	0.0001	0.016	0	0	1
272	16	1.5	0.0001	0.016	0	0	1
272	16	1.5	0.0001	0.016	0	0	1
272	16	1.5	0.0001	0.016	0	0	1
0	16	1.5	0.0001	0.016	11.807	0	3
0	16	1.5	0.0001	0.016	0	4.6	2
360	14	1.5	0.0001	0.016	0	0	1
360	14	1.5	0.0001	0.016	0	0	1
360	14	1.5	0.0001	0.016	0	0	1
360	14	1.5	0.0001	0.016	0	0	1
360	14	1.5	0.0001	0.016	0	0	1
360	14	1.5	0.0001	0.016	0	0	1
360	14	1.5	0.0001	0.016	0	0	1
360	14	1.5	0.0001	0.016	0	0	1
360	14	1.5	0.0001	0.016	0	0	1
360	12.5	1.5	0.0001	0.016	0	0	1
360	12.5	1.5	0.0001	0.016	0	0	1
360	12.5	1.5	0.0001	0.016	0	0	1
360	12.5	1.5	0.0001	0.016	0	0	1
360	12.5	1.5	0.0001	0.016	0	0	1
360	12.5	1.5	0.0001	0.016	0	0	1
360	12.5	1.5	0.0001	0.016	0	0	1
360	12.5	1.5	0.0001	0.016	0	0	1
360	12.5	1.5	0.0001	0.016	0	0	1
360	12.5	1.5	0.0001	0.016	0	0	1
360	12.5	1.5	0.0001	0.016	0	0	1
360	12.5	1.5	0.0001	0.016	0	0	1
360	11	1.5	0.0001	0.016	0	0	1
0	11	1.5	0.0001	0.016	0.63	0	3
0	11	1.5	0.0001	0.016	0	4.4	2
303	11	1.5	0.0001	0.016	0	0	1
303	11	1.5	0.0001	0.016	0	0	1
303	11	1.5	0.0001	0.016	0	0	1
303	11	1.5	0.0001	0.016	0	0	1
303	11	1.5	0.0001	0.016	0	0	1
303	11	1.5	0.0001	0.016	0	0	1
303	11	1.5	0.0001	0.016	0	0	1
303	11	1.5	0.0001	0.016	0	0	1
303	11	1.5	0.0001	0.016	0	0	1
303	11	1.5	0.0001	0.016	0	0	1
303	11	1.5	0.0001	0.016	0	0	1
303	11	1.5	0.0001	0.016	0	0	1
303	11	1.5	0.0001	0.016	0	0	1
303	11	1.5	0.0001	0.016	0	0	1
303	11	1.5	0.0001	0.016	0	0	1

Δx,m	Bottom Width(B),m	Side Slope(z)	Slope (So)	Roughness Coff.	Initial Turnout Flow(q),m^3/sec	Upstream depth(m)	Node Type
303	11	1.5	0.0001	0.016	0	0	1
303	11	1.5	0.0001	0.016	0	0	1
303	11	1.5	0.0001	0.016	0	0	1
303	11	1.5	0.0001	0.016	0	0	1
303	11	1.5	0.0001	0.016	0	0	1
303	11	1.5	0.0001	0.016	0	0	1
303	11	1.5	0.0001	0.016	0	0	1
303	11	1.5	0.0001	0.016	0	0	1
303	11	1.5	0.0001	0.016	0	0	1
303	11	1.5	0.0001	0.016	0	0	1
303	11	1.5	0.0001	0.016	0	0	1
303	11	1.5	0.0001	0.016	0	0	1
303	11	1.5	0.0001	0.016	0	0	1
303	11	1.5	0.0001	0.016	0	0	1
303	11	1.5	0.00025	0.016	0	0	1
303	11	1.5	0.00025	0.016	0	0	1
303	6.5	1.5	0.00025	0.016	0	0	1
303	6.5	1.5	0.00025	0.016	0	0	1
0	6.5	1.5	0.00025	0.016	4.314	0	3
0	6.5	1.5	0.00025	0.016	0	4.1	2
302	6.5	1.5	0.00025	0.016	0	0	1
302	6.5	1.5	0.00025	0.016	0	0	1
302	6.5	1.5	0.00025	0.016	0	0	1
302	6.5	1.5	0.00025	0.016	0	0	1
302	6.5	1.5	0.00025	0.016	0	0	1
302	6.5	1.5	0.00025	0.016	0	0	1
302	6.5	1.5	0.00025	0.016	0	0	1
302	6.5	1.5	0.00025	0.016	0	0	1
302	6.5	1.5	0.00025	0.016	0	0	1
302	6.5	1.5	0.00025	0.016	0	0	1
302	6.5	1.5	0.00025	0.016	0	0	1
302	6.5	1.5	0.00025	0.016	0	0	1
302	6.5	1.5	0.00025	0.016	0	0	1
302	6.5	1.5	0.00025	0.016	0	0	1
302	6.5	1.5	0.00025	0.016	0	0	1
302	6.5	1.5	0.00025	0.016	0	0	1
302	6.5	1.5	0.00025	0.016	0	0	1
302	6.5	1.5	0.00025	0.016	0	0	1
302	6.5	1.5	0.00025	0.016	0	0	1
302	6.5	1.5	0.00025	0.016	0	0	1
302	6.5	1.5	0.00025	0.016	0	0	1
302	6.5	1.5	0.00025	0.016	0	0	1
302	6.5	1.5	0.00025	0.016	0	0	1
302	6.5	1.5	0.00025	0.016	0	0	1
302	6.5	1.5	0.00025	0.016	0	0	1
302	6.5	1.5	0.00025	0.016	0	0	1
302	6.5	1.5	0.00025	0.016	0	0	1
302	6.5	1.5	0.00025	0.016	0	0	1
302	6.5	1.5	0.00025	0.016	0	0	1
302	6.5	1.5	0.00025	0.016	0	0	1
302	6.5	1.5	0.00025	0.016	0	0	1
302	6.5	1.5	0.00025	0.016	0	0	1
302	6.5	1.5	0.00025	0.016	0	0	1

Δx,m	Bottom Width(B),m	Side Slope(z)	Slope (So)	Roughness Coff.	Initial Turnout Flow(q),m^3/sec	Upstream depth(m)	Node Type
302	6.5	1.5	0.00025	0.016	0	0	1
302	6.5	1.5	0.00025	0.016	0	0	1
302	6.5	1.5	0.00025	0.016	0	0	1
302	6.5	1.5	0.00025	0.016	0	0	1
302	6.5	1.5	0.00025	0.016	0	0	1
302	6.5	1.5	0.00025	0.016	0	0	1
0	6.5	1.5	0.00025	0.016	11.097	0	3
0	6.5	1.5	0.00025	0.016	0	3.8	2

GATE DATA				
Gate Width	Gate Coefficient	Sill Height	Drop at Gate	Target Depth,m
16	0.83	0	0	4.7
16	0.83	0	0	4.6
11	0.83	0	0	4.4
6.5	0.83	0	0	4.1
6.5	0.83	0	0	3.8

TURNOUT DATA			
Turnout flow rate(q), m^3/sec	Turnout gate width(m)	Turnout initial flow rate, m^2/sec	Turnout gate discharge coefficient
2.398	0.201389116	0.65	0.5
11.807	0.292751008	0.65	0.5
4.314	0.43716174	0.65	0.5
11.097	0.943090496	0.65	0.5
3.67	0.481369107	0.65	0.5
0	0.15226982	0.65	0.5
11.348	1.295767046	0.65	0.5
1.513	2.042380356	0.65	0.5